AN ABSTRACT OF THE DISSERTATION OF

David J. Mildrexler for the degree of Doctor of Philosophy in Forest Ecosystems and Society presented on June 9, 2017.

Title: Satellite Monitoring of Earth's Surface Temperature: Effects of Land Cover, Disturbance, and a Changing Climate

Abstract approved:

_____

Warren B. Cohen

The Earth's surface is experiencing unprecedented change. Humanity's growing population, expanding land-use footprint, and increasing global emissions of atmospheric greenhouse gases affect a vast number of species on Earth and the functioning of virtually all ecosystems. Given the vital interactions and feedbacks between the Earth's land surface and climate, measurements that link surface conditions and climate can provide crucial information on biospheric change. Land surface temperature (LST) is one of the most important parameters in the physical processes of surface energy and water balances at local through global scales. Interactions between the land surface and the atmosphere and the resulting exchanges of energy and water have a substantial impact on climate. This dissertation presents new methodologies developed using satellite-derived LST in conjunction with other biophysical datasets to monitor, quantify, map and understand critical Earth system changes from global to ecoregional scales.

It has long been known that temperature is one of the key environmental controls and stressors to which an organism may be subjected. Its influence is fundamental, ranging from controls on chemical reactions that drive key processes on Earth, such as photosynthesis and respiration, to its role in defining large-scale species distributions and biome patterns. Climatological data can be developed for two kinds of surface temperatures: near-surface air temperature and the skin temperature, or LST. Although

correlated with air temperature, LST differs from air temperature in its physical meaning, magnitude, and measurement techniques. LST can be estimated from measurements of thermal radiance coming from the land surface, retrieved from satellite, and mapped globally. In vegetated areas, satellite-derived LST measures the canopy surface temperature, and is more closely connected to the biophysical characteristics of the land surface, such as the land cover type, vegetation density, and water and energy fluxes of a specific area. LST provides important insights into high temperature extremes associated with droughts and heat waves, and the thermal tolerances and exposures for species and ecosystems. The Moderate Resolution Imaging Spectroradiometer (MODIS) LST product is measured across every 1-km^2 pixel of the Earth's surface. This is an important distinction from air temperature measurements from weather stations that have an inequitable global distribution including few stations across remote areas of the Earth's surface, and cannot give detailed spatial patterns.

We describe a new global change indicator based on an annual global measure of the Earth's maximum land surface temperature (LSTmax) and demonstrate its value to examine critical Earth system functions (Chapter 2). LSTmax provides a unique integrated measure of the ecosystems thermal condition that is especially powerful at minimizing synoptic and seasonal variability and highlighting changes associated with extreme climatic events and significant land cover changes. We questioned whether maximum thermal anomalies could be indicative of heat waves and droughts, a melting cryosphere, and tropical forest disturbance from 2003 to 2014. The 1-km^2 LSTmax anomalies detected complex spatial patterns associated with heat waves and droughts across the Earth's surface, peaking in 2010 and 2012 with 5% (16%) of the Earth's surface experiencing anomalies greater than 4°C (2°C). Our findings show that entire biomes are experiencing shifts in their maximum surface temperature distributions in association with extreme climatic events and large-scale land surface changes. These directional shifts in components of the Earth's integrated LSTmax histograms are associated with melting of ice sheets, severe droughts in tropical rainforests, and with the incremental effects of forest loss in tropical forests. We conclude that with continued

warming, the Earth's integrated maximum temperatures will experience greater and more frequent directional shifts, increasing the likelihood that critical thresholds will be surpassed resulting in regional scale transitions that are tipping points in the global climate system.

In a regional assessment responding to the acute concern about increasing forest stress and tree mortality and its direct link to combinations of drought and high temperatures (Chapter 3), we developed and applied a new forest vulnerability index (FVI) that identifies when and where forests have been experiencing increasingly high surface temperatures and greater growing season water deficits across the Pacific Northwest region (PNW: Oregon and Washington) of the USA during the MODIS Aqua era (since 2003). Our technique incorporates the alterations to canopy water and energy exchange processes caused by drought and high temperatures with MODIS LST and evapotranspiration (ET) data, and with Parameter-elevation Relationships on Independent Slopes Model (PRISM) precipitation (P) data. The FVI's monthly assessment over the growing season revealed a possible trajectory toward more extreme conditions indicated by a trend toward cooler and wetter conditions in the spring, followed by a rapid transition to widespread warmer and drier trends in August and September. Area of increased vulnerability was concentrated in the months of August and September, with peak vulnerability occurring at separate times for different forest types. Overall, increased vulnerability rates were highest in drier forest type groups, such as Ponderosa Pine, Juniper, and Lodgepole Pine. Western Larch and Fir/Spruce/Mountain Hemlock groups occupy moister sites but also had relatively high proportion of increased vulnerability. The Douglas-fir group had the second largest total area of increased vulnerability due to its large areal extent in the study area. Based on an analysis using imagery viewed in Google Earth, we found that areas with increased vulnerability are associated with greater amounts of visible health decline and mortality. The FVI is a new way to conceptualize and monitor forest vulnerability based on first-order principles and has the potential to be generalized to other geographical areas.

In Chapter 4 we utilize the FVI and its intermediary datasets on canopy energy and water exchange trends to investigate the Swiss needle cast (SNC) epidemic in the Oregon Coast Range. SNC is caused by an ascomycete fungus endemic to the PNW, and is having important consequences on the region's coastal Douglas-fir forests. Seasonal changes in temperature and/or precipitation regimes, such as we detected in Chapter 3 of this dissertation, have the potential to shift conditions in favor of pathogens, resulting in widespread epidemics. Foliar fungi diseases such as SNC are thought to be especially responsive to climate changes. Previous research has verified that spring and early summer leaf wetness is a key factor in SNC disease epidemiology. In this study, we investigate the relationship between climatic trends detected during the spring and early summer months (May – August) along the Pacific Coast of Oregon from 2003 to 2012, and the distribution of forests with visible symptoms of SNC in 2012. Our objectives were to: 1) Calculate the relationship between LST and water balance (WB) trends and pixel-level presence/absence of SNC symptoms. 2) Compare the relationship between private and public forest lands to make inferences about the effects of forestry practices on forest vulnerability to SNC intensification. We find evidence that recent short-term directional climate changes may have contributed to the recent increases in SNC symptoms in Douglas-fir forests, and that this influence was stronger on private lands. The LST trends had greater explanatory power than WB trends, and the interactions between monthly LST trends increased the explanatory power of LST, whereas this effect was minimal for WB. The trends of the May and August LST together explained 7% of the deviance in SNC symptom distribution on private land, and 2% on public land. When combined with proximity to coast (strongest explanatory variable), May and August LST explained 14% of the deviance in SNC symptom expression on private land, and 8.7% on public land. Adding the WB factor did not improve the deviance explained in presence of SNC symptoms. This study indicates that early spring and mid-summer LST contains valuable information on leaf wetness, possibly contrasting both early season wetness and late season dryness, both of which are important to the epidemiology of SNC.

The results from this dissertation highlight the immense value of the LST measurement in tracking critical changes in the Earth system. While questions remain regarding upper temperature thresholds that may trigger biome shifts or widespread forest die-offs, our results help to fill the knowledge gap about how these temperature changes are impacting the Earth's ecosystems. The methodologies and tools developed here offer new and important opportunities for long-term monitoring that will continue to increase our understanding of these key land surface-climate interactions.

Satellite Monitoring of Earth's Surface Temperature: Effects of Land Cover, Disturbance, and a Changing Climate

by
David J. Mildrexler

A DISSERTATION

submitted to

Oregon State University

in partial fulfillment of
the requirements for the
degree of

Doctor of Philosophy

Presented June 9, 2017
Commencement June 2018

Doctor of Philosophy dissertation of David J. Mildrexler presented on June 9, 2017.

APPROVED:

_____

Major Professor, representing Forest Ecosystems and Society

_____

Head of the Department of Forest Ecosystems and Society

_____

Dean of the Graduate School

I understand that my dissertation will become part of the permanent collection of Oregon State University libraries. My signature below authorizes release of my dissertation to any reader upon request.

_____

David J. Mildrexler, Author

ACKNOWLEDGEMENTS

I would first like to thank my major professor, Dr. Warren Cohen, for the opportunity to pursue a PhD at Oregon State University (OSU), and for his persistent support throughout my studies and research. Warren gave me the latitude to choose my own destiny in this dissertation, and yet remained fully engaged and interested in every aspect of my research. As a scientist, I am much stronger thanks to learning from Dr. Cohen's thorough approach to his own exceptional scientific research.

I express my sincere appreciation to Drs. Tom Spies, Chris Still, David Shaw, Todd Einhorn, Jim Kiser, and the late Thomas Hilker for serving as members of my graduate committee. Their experience, insight, and knowledge played an important role in shaping this dissertation. Special thanks to Dr. Richard Waring for sharing his wealth of knowledge with me. Thanks to Drs. Zhiqiang Yang, David Bell, and Matt Gregory, and Erik Haunreiter for helpful conversations, suggestions, and technical assistance. It was remarkable to interact with such experienced and world-class scientists at OSU.

I am extremely grateful to be a Wilburforce Fellow in Conservation Science. It was a powerful experience and I thank the other Fellows for their support and encouragement.

I thank my family, especially my lovely wife Andrea for her love, constant support, and encouragement, and my two beautiful children, Aden and Selah, for lighting up with joy when I walk in the door. May this work and where it leads help to make your futures a little brighter. Thanks to my parents for your unyielding belief in me to achieve my goals.

This research was funded primarily by the USDA Forest Service, Pacific Northwest Research Station and OSU. I have been fortunate to receive funding support from the OSU Graduate School, the College of Forestry, and the Department of Forest Ecosystems and Society. I am also very grateful for the generous financial support of Duncan and Cindy Campbell through the Achievement Rewards for College Scientist's Foundation.

CONTRIBUTION OF AUTHORS

Chapter 2: Maosheng Zhao, Steve W. Running and Warren B. Cohen assisted with study design, data processing, and with development and refining of the manuscript. Xiao-Peng Song helped with data processing and manuscript edits. Matthew O. Jones contributed to interpreting the results, and refining the manuscript.

Chapter 3: Warren B. Cohen and Zhiqiang Yang assisted with the algorithm development, study design, data analysis, and drafting and revising the manuscript. David M. Bell assisted with interpretation of results, statistical analysis and manuscript refinements.

Chapter 4: David C. Shaw and Warren B. Cohen provided guidance and contributed to drafting the paper.

TABLE OF CONTENTS

LIST OF FIGURES

LIST OF FIGURES (CONTINUED)

Figure Page

LIST OF TABLES

LIST OF APPENDIX FIGURES

Figure Page

LIST OF APPENDIX TABLES

Chapter 1: Introduction

The Aqua spacecraft was launched on May 4, 2002, just a few months before I entered the Masters of Science Program at The University of Montana's College of Forestry and Conservation. Aqua is a major satellite mission of the National Aeronautics and Space Administration (NASA) Earth Observing System (EOS), and part of a coordinated series of polar orbiting and low inclination satellites for long-term global observations to improve understanding of the Earth as an integrated system (King et al. 1999). The satellite is in a near-polar, sun synchronous orbit at an altitude of 705 km, crossing the equator going north at 1:30 in the afternoon and south at 1:30 in the morning, local time (Parkinson 2003). Aqua's afternoon overpass time has critical implications for my own research. The Moderate Resolution Imaging Spectroradiometer (MODIS) instrument is one of six Earth-observing instruments onboard the Aqua spacecraft. Among the suite of measurements the MODIS instrument provides across every 1-km^2 pixel of the Earth's surface is the radiometric surface temperature, also called land surface temperature (LST), or land skin temperature (Norman and Becker 1995). This unique form of temperature measured from the Aqua MODIS instrument is the key dataset used in this dissertation.

When we check the weather forecast, or hear the daily temperature reported on the news, we are given the air temperature, also called "near-surface" air temperature. Air temperature is a very specific type of temperature, measured 1.5 to 2.0 meters above the ground level at official weather stations with sensors protected from radiation and adequately ventilated. This common standard ensures the intercomparability between the measurements recorded at disparate locations across the Earth's surface. However, these stations often experience relocations, changes in instrumentation and/or exposure, effects of land-use changes such as urbanization, and changing observing practices, all of which can introduce biases that are often undocumented (Karl et al. 2006). Nonetheless, with more than a century of instrumental data, air temperature is a popular and useful metric for summarizing the state of global climate (Hansen et al. 2006; Pielke 2007). MODIS measures something different: land surface temperature. As described in detail in this

dissertation (Chapters 2 and 3), LST differs fundamentally from air temperature in its physical meaning, magnitude, and measurement techniques (Jin and Dickinson 2010). LST is defined as the radiation emitted by the top of the land surface, hence the term "skin temperature," or the temperature you would feel if you touched the land surface. "Land surface" refers to the canopy surface in vegetated areas, or soil surface in bare areas (Wan et al. 2004). Because air is such a poor heat conductor, LST in mid-summer can be 30ºC - 40ºC higher than air temperature (Mildrexler et al. 2011a). We interact with LST constantly in our daily lives. Imagine the searing heat of beach sand (i.e. LST) on a hot summer day, when running from shade patch to water is the only way to avoid burning your feet, compared to the air temperature 1.5 m (nearly 5 feet) above the sand. Or imagine returning to your car in a parking lot on an especially sweltering summer day and finding that the handle is too hot to touch (i.e. LST). And the expression that it's "hot enough to fry an egg on the sidewalk." These are examples of LST.

Early on in my Master's studies my Advisor, Dr. Steven Running, told me about the new high quality LST product available from the Aqua satellite. This new LST product was developed under the direction of Dr. Zhengming Wan, and incorporated some of the most rigorous studies of the emissivity of land surface materials at that time (Wan and Li 1997). However, no one was yet using this promising new LST product for ecological research. Dr. Running told me to have a look at this LST data, with one very important caveat. He suggested I start by looking at the annual maximum surface temperatures to remove the large synoptic variability that affects surface temperature at daily to seasonal time scales (Prata et al. 1995). This suggestion stemmed from years of experience using LST to help understand energy and moisture fluxes at the Earth's surface (Nemani and Running 1989; Nemani et al. 1993; Nemani and Running 1997).

At the time, climatic extremes and extreme events were beginning to emerge as one of the most important facets of climate change (Easterling et al. 2000; Smith 2011). For decades, most climate impact studies had been on the mean climate variables, such as mean temperature (Mearns et al. 1984). Minimum and maximum temperatures were viewed as short-term deviations and regarded as extraordinary and non-representative

measurements (Jentsch et al. 2007). In a changing climate, however, the increasing variability is more important than averages in driving extreme events, and the relative importance of variability as a driver increases as the events become more extreme (Katz and Brown 1992). For example, consider a typical distribution of a climate variable that is normally distributed, such as the daily maximum temperature. The extremes are represented by the tails of the distribution that occur infrequently (i.e., values that are far from the mean or median value of the distribution) (Meehl et al. 2000). As future climate change shifts the distribution, there will be an increase in extreme events on one end and a decrease at the other (Meehl et al. 2000; Peterson et al. 2008). Moreover, the frequency of extremes changes nonlinearly with the change in the mean of a distribution, such that a slight change in the mean can result in a large change in the frequency of extremes (Mearns et al. 1984). Additionally, other aspects of the distribution may change, such as an increase in the standard deviation in a future warmer climate, causing more extreme events on both ends of the frequency distribution (Meehl et al. 2000).

Annual maximum LST (LSTmax) focuses on the high temperature extreme over an annual period at each pixel across the Earth's surface (Chapter 2). Thus the LSTmax measurement is constantly tracking conditions that fall within the upper tail of the overall annual surface temperature distribution. This is a powerful focus, as some of the most relevant climate change impacts are related to climatic extremes, rather than the mean climate values. Moreover, amplification of extreme temperatures can occur even when the global mean shows no such trend (Seneviratne et al. 2014). Annual maximum value compositing of the Aqua LST data results in operational (e.g. Aqua's afternoon overpass is near the peak of diurnal fluctuation), and ecological (e.g. the relationship between vegetation density and LSTmax is strongly coupled) advantages that together provide a unique and informative annual monitoring metric for integrating the biophysical influence of land cover and the consequences of changes across the Earth's land surface (Mildrexler et al. 2011b).

Concurrent with the emergence of climatic and weather extremes in climate change research was the increased recognition of the ecological impacts of extreme

events on ecosystem dynamics, such as phenological cycles of plants (Peñuelas and Filella 2001; Rich et al 2008), population dynamics in a variety of species (Sunday et al. 2012; Kerr et. al 2015), and effects on ecosystem structure, function, and carbon stocks (Turner 2010; Running 2008). Extreme events (i.e. severe drought and heavy rain) caused phenological shifts in plants of the same magnitude as one decade of gradual warming (Jentsch et al. 2009), and a large mountain pine beetle outbreak in Canada switched the entire nations forests from a carbon sink to a carbon source (Kurz et al. 2008). Additionally, weather extremes such as heat waves, droughts, heavy downpours, floods, hurricanes, and changing storm patterns have tremendous and increasing socio-economic consequences, necessitating improved understanding, predictability, and management responses to such events (Melillo et al. 2014). Extreme events are forecasted to increase in magnitude and frequency along with ongoing climate warming, potentially having far-reaching consequences for society, ecology and evolution (Jentsch et al. 2009; Allen et al. 2015; McDowell and Allen 2015).

Early examination of the Aqua MODIS LSTmax data led me to perform a pixel specific differencing between the first two full years of data (i.e. 2004 minus 2003). This revealed significant increased LSTmax values in remarkably close association with forested areas burned by wildfire in 2003. I brought a hardcopy image to Steve Running's office to see what he thought of this discovery. It was an exciting moment and I remember leaving the office with directions to couple LSTmax with a vegetation index product for disturbance detection. This was the conception of the MODIS Global Disturbance Index, possibly the first disturbance detection algorithm to use changes in extreme maximum surface temperatures to map abrupt disturbances at 1-km spatial resolution (Mildrexler et al. 2007). Although somewhat coarse for a disturbance detection methodology, our approach successfully detected a variety of large-scale ecological disturbances including impacts from wildfires, hurricanes, droughts, and large-scale logging (Mildrexler et al. 2009; Joyce et al. 2014). It was applied successfully by others to detect the impacts of wildfires, insect infestations and change information associated with agricultural outputs in Canada (Coops et. al 2009), wildfire in China (Tao et al.

2013), and applied globally at 500 m resolution (McDowell et al. 2015). Not only did this research confirm that annual maximum value composting removed the synoptic variability associated with seasonal to daily LST, it showed that significant changes in LSTmax were closely associated with verified ecological disturbances.

Furthering this research, we applied annual maximum value compositing to the Aqua MODIS 8-day LST Climate Model Grid data (0.05° spatial resolution) to address a long-standing curiosity about climate: where is the hottest spot on Earth? To achieve this, we created the first global maps of the highest surface temperatures experienced at every pixel across Earth's surface over an annual period, and then analyzed each pixel to identify the hottest spot on Earth (Mildrexler et al. 2006; Mildrexler et al. 20011b). Iran's Lut Desert dominated the highest land skin temperatures during our analysis, but we also revealed that the highest LSTmax on Earth was not always in the same place (Mildrexler et al. 2011b). This research also provided an outstanding opportunity to educate people about the difference between satellite-derived skin temperature and air temperature. Still, we knew that the bigger science challenge was in using the global, wall-to-wall LSTmax data to study the heterogeneity of the Earth's maximum thermal state.

Chapter 2 of this dissertation represents the completion of many years of key research based on the Earth's LSTmax from the MODIS sensor onboard NASA's Aqua spacecraft (Mildrexler et al. 2006; Mildrexler et al. 2011b; Parkinson 2013). For the first time my coauthors and I have applied annual maximum value composite to the entire Earth's surface using the 1-km^2 resolution LST Aqua MODIS data and present a new global indicator of integrated Earth system change. Our understanding of change detection using LSTmax includes the effects of abrupt disturbances due to human or natural causes, critical thermal thresholds such as phase change driven temperature shifts due to ice melt, and forest stress expressed via anomalously high temperatures experienced during droughts and heat waves. We apply our indicator to three key topics in Earth system science; vegetation disturbance, cryosphere melt, and heat waves.

Forest ecosystems have always been my greatest passion and research focus. Thus, when my PhD advisor, Dr. Warren Cohen, approached me with the opportunity to

develop an index of forest vulnerability to rising temperatures and increasing drought, I seized the opportunity. While many research papers had implicated increasing temperatures in forest stress and die-off events globally (Adams et al. 2009; Allen et al. 2015; Williams et al. 2013), few were using LST to track where these increasing temperature patterns were occurring on the landscape (see Toomey et al. 2011 for an exception). Chapter 3 of my dissertation describes the development and application of a new forest vulnerability index (FVI) associated with drought and high temperatures across the Pacific Northwest (PNW) region. While applied to the PNW region, the formulation is robust across one of the largest hydrological gradients in North America indicating that the metrics may be transferable to different ecosystems and larger areas, especially those characterized by a summer seasonal drought cycle.

The final study (Chapter 4) examines the relationship between the intensification of Swiss needle cast in the Douglas-fir forests of the Oregon Coast Range, and the unexpected discovery of the prevalence of wetter and cooler conditions we found in the spring and early summer with our forest vulnerability analysis. This chapter links the FVI to on the ground forest changes relevant to forest management in the PNW. Specifically, we quantified the relationship between Swiss needle cast symptoms and the FVI and its input variables (LST, water balance) within the region's most vulnerable forest areas. This analysis displays how the FVI and input variables have enormous potential to evaluate a variety of ecosystem changes associated with changing temperature and precipitation regimes.

The global, regional, and ecoregional research presented in this dissertation reflects my interest in ecology across spatial scales, ranging from pressing Earth science research needs to local-scale applied forest management issues. This dissertation develops new methodologies for utilizing a key Earth science dataset (i.e. LST) to address a variety of important research needs, providing information that will support management decisions and help predict the response of ecosystems to future changes.

Chapter 2: Thermal anomalies detect critical global land surface changes

Authors

D. J. Mildrexler[1,*], M. Zhao[2], W. B. Cohen[3], S. W. Running[4], X. P. Song[2], M. O. Jones[4,5]

Affiliations

[1]Department of Forest Ecosystems and Society, Oregon State University, Corvallis, OR 97331, USA.

[2]Science Systems and Applications INC., NASA GSFC, Greenbelt, MD 20771, USA.

[3]Pacific Northwest Research Station, USDA Forest Service, Corvallis, OR 97331, USA.

[4]Numerical Terradynamic Simulation Group, Department of Ecosystem and Conservation Sciences, University of Montana, Missoula, MT 59812, USA.

[5]Deptartment of Forest Management, University of Montana, Missoula, MT 59812, USA.

*Corresponding Author:

David Mildrexler

Email: david.mildrexler@oregonstate.edu

Telephone: 541-786-9354

Abstract

Measurements that link surface conditions and climate can provide critical information on important biospheric changes occurring in the Earth system. As the direct driving force of energy and water fluxes at the surface-atmosphere interface, land surface temperature (LST) provides information on physical processes of land cover change and energy balance changes that air temperature cannot provide. Annual maximum land surface temperature (LSTmax) is especially powerful at minimizing synoptic and seasonal variability and highlighting changes associated with extreme climatic events and significant land cover changes. We questioned whether maximum thermal anomalies from satellite observations could detect heat waves and droughts, a melting cryosphere, and tropical forest disturbance from 2003 to 2014. The 1-km^2 LSTmax anomalies detected complex spatial patterns associated with heat waves and droughts across the Earth's surface, peaking in 2010 and 2012 with 5% (16%) of the Earth's surface experiencing anomalies greater than 4°C (2°C). Our findings show that entire biomes are experiencing shifts in their LSTmax distributions driven by extreme climatic events and large-scale land surface changes. These directional shifts in components of the Earth's LSTmax histograms are associated with melting of ice sheets, severe droughts in tropical rainforests, and with the incremental effects of forest loss in tropical forests. As climate warming and land cover changes continue, it is likely that the Earth's maximum temperatures will experience greater and more frequent directional shifts, increasing the possibility that critical thresholds in the Earth's ecosystems and climate system will be surpassed resulting in profound and irreversible changes.

Introduction

The Earth's ecosystems are experiencing change that is unprecedented in human history (Steffen et al. 2007; IPCC 2013). These changes, primarily driven by humanity's expanding land-use footprint and increasing global emissions of atmospheric greenhouse gases threaten to initiate potentially irreversible changes in the Earth system (Rockström et al. 2009; Hansen et al. 2012). For example, investigations into the effects of climate change on the cryosphere have implicated increasing temperatures in the melting of glaciers and thinning of ice sheets, and the Greenland Ice Sheet (GrIS) has been one of the largest contributors to global sea-level rise over the past 20 years (Lenaerts et al. 2013; Khan et al. 2014; Yin et al. 2011; McMillan et al. 2016). In tropical forests the persistent effects of increasingly severe droughts, decreases in rainfall, and the interactions with ongoing forest loss, suggest the potential for large-scale degradation of these forests (Malhi et al. 2008; Marengo et al. 2011; Saatchi et al. 2013; Hilker et al. 2014; Zhou et al. 2014). An urgent goal of Earth science research today is the development of indicators to measure global changes and their consequences on climate that are relevant and communicable to society and decision-makers (Janetos et al. 2012). Land Surface Temperature (LST) is one of the most important parameters in the physical processes of surface energy and water balances at local through global scales (Mannstein 1987; Li et al. 2013; Wan et al. 2004). Its retrieval from remotely sensed thermal infrared data provides spatially continuous LST measurements with global coverage to examine the thermal heterogeneity of the Earth's surface, and the impact on surface temperatures resulting from natural and human-induced changes (Jin and Dickinson 2010; Li et al. 2015). Here we present a new global change indicator based on an annual global measure of the Earth's maximum land surface temperature (LSTmax) and demonstrate its value to examine critical Earth system functions. We questioned whether maximum thermal anomalies could be indicative of heat waves and droughts, a melting cryosphere, and tropical forest disturbance.

Most global temperature analyses are based on station air temperatures. Although correlated with air temperature, LST differs fundamentally in its physical meaning,

magnitude, and measurement techniques (Jin and Dickinson 2010). LST measures the emission of thermal radiance from the actual land surface where the incoming solar energy interacts with and heats the ground, or the surface of the canopy in vegetated areas. This quality makes LST a good indicator of energy partitioning at the land surface-atmosphere boundary and sensitive to changing surface conditions (Li et al. 2013; Mildrexler et al. 2009). By comparison, standard weather station air temperature is measured 1.5 m above the ground level with sensors protected from radiation and adequately ventilated. Because air is such a poor heat conductor, as midsummer temperature goes up, and more thermal energy is concentrated at the Earth's surface, LSTmax increases more rapidly than the corresponding maximum air temperature (Mildrexler et al. 2011a). LST is more closely connected to the biophysical characteristics of the land surface, such as the land cover type, vegetation density, and water and energy fluxes of a specific area compared with air temperature (Oyler et al. 2016). Moreover weather stations have an inequitable global distribution including few stations across remote areas of the Earth's land surface, and cannot give detailed spatial patterns (Kogan 1997; Daly et al. 2008; Mu et al. 2013; Li et al. 2015). For example, in this study we examine ice sheets and rainforests due to their importance in the global climate system. With the Moderate Resolution Imaging Spectroradiometer (MODIS) sensor onboard the Aqua satellite, LST is measured at every 1-km pixel across the 1.7 million km^2 Greenland ice sheet. By comparison, the Greenland Climate network consists of 18 weather stations where air temperature is recorded, about 1 station for every 94,000 km^2. Such a small number of monitoring stations limits our ability to understand what is happening across the entire area. The same is true for other remote regions of the Earth such as the Amazon and Congo rainforests, where sparse weather station coverage limits monitoring capability (see Fig. 1 in Mildrexler et al. 2011a), whereas remotely sensed LST provides spatially exhaustive coverage. These differences allow LST to magnify the land surface dynamics in a way that air temperatures cannot, offering a new and unique measure of biospheric change.

In recent decades an increase in the frequency and the total land area affected by extreme high temperature events such as droughts combined with heat waves have been linked to global warming (Seneviratne et al. 2014; Perkins et al. 2012). Extremely hot summertime outliers that once covered 1% of the Earth's land area, now cover about 10% of the land area (Hansen et al. 2012). Such extremes amplify moisture deficit, heat stress, and result in an increase in tree mortality and wildfire (Allen et al. 2015; Mitchell et al. 2014; Teskey et al. 2014). The frequency and severity of extreme droughts and heat waves are predicted to increase in the future (Cook et al. 2014; IPCC 2013; Jentsch et al. 2007; Mitchell et al. 2014; Moritz et al. 2012; Fischer and Schär 2010). The global increase in high-temperature related extreme events portends the potential for regional-scale transitions in land cover once physical and/or physiological thresholds are surpassed, some of which are critical thresholds in the global climate system (Grimm et al. 2013; Chapin et al. 2008; Christidis et al. 2015). For instance, the cryosphere's ice and snow-covered surfaces have extremely cold LSTmax values, and play an important role as a climate buffer through the physics of phase change (Kenney et al. 2014). As ice sheets are exposed to warmer conditions, increased surface melt lowers the albedo, resulting in increased absorption of solar radiation and a positive feedback with further temperature increase and more surface melt (Tedesco et al. 2011; He et al. 2013). Tropical forest ecosystems are critical in cooling the Earth's surface temperatures, contain large stores of carbon, support tremendous biological diversity, and in this century face the dual threats of forest clearing and stress from climate change (Lee et al. 2011; Li et al. 2015; Malhi et al. 2008; Marengo et al. 2011). Climate model predictions indicate that extreme dry events may increase with climate change, pushing tropical forests toward a climatically induced tipping point and possible biome level degradation (Cox et al. 2008; Malhi et al. 2009). Here we utilize the high resolution and spatially continuous global coverage of the LST data to: 1) examine LSTmax anomalies and their association with verified heat waves from 2003 to 2014; 2) monitor large-scale ice warming and phase change driven temperature shifts in the cryosphere; and 3) investigate

changes in surface temperatures in evergreen broadleaf forests (EBF) in accordance with the 2005 and 2010 droughts, and in response to forest loss.

The uniqueness of annual maximum land surface temperatures

Multiple lines of research have found that the daytime LSTmax from the Aqua MODIS sensor is a unique and informative annual monitoring metric for integrating the biophysical influence of land cover and the consequences of changes across the Earth's land surface. The Aqua satellite's equatorial afternoon overpass time of approximately 13:30 allows for near ideal retrievals of maximum daily LST as it is temporally coincident with the maximum daily temperature of the land surface (Sinclair 1922; Wan et al. 2004). Measurements close to the peak of diurnal fluctuation better reflect the thermal response of rising leaf temperatures due to decreased latent heat flux as stomata close, and soil litter surfaces dry, accentuating differences in LST among vegetation cover types (Mildrexler et al. 2007). Focusing on the Earth's maximum surface temperatures provides important insights into high temperature extremes associated with droughts and heat waves, and the thermal tolerances and exposures for different biomes and species.

Satellite-derived LST is influenced by synoptic weather variability (wind-speed, cloud cover, humidity, radiation loading, etc.) on a continual basis, and has high natural variability (Friedl and Davis 1994; Nemani and Running 1997). While temperatures over land surfaces generally vary strongly in space and time (Prata et al. 1995; Li et al. 2013), annual maximum value compositing removes the natural synoptic variability associated with daily to seasonal LST while focusing on the maximum temperature in a given area. For a specific location and in the absence of change, the LSTmax metric has relatively low interannual variability. Moreover, the timing of LSTmax generally occurs during the year's driest clear sky conditions. This, in turn, imposes a strong limitation on the partitioning among the sensible and latent heat fluxes (H and LE respectively) that largely control the surface temperature in the surface energy balance (Bateni and Entekhabi 2012; Sandholt et al. 2002). Thus, LSTmax measurements provide unique

information on how the partitioning between H and LE varies and affects the expression of LSTmax across the Earth's surface in this moisture-limited condition. Since plants are the primary site for the exchange of water, energy, and momentum between the land and the atmosphere, the vegetated fraction of the Earth's surface has important effects on the magnitude and relative partitioning of the turbulent fluxes (H + LE). Indeed, a strong relationship has been observed between LSTmax and vegetation density over a wide range of land cover types (Mildrexler et al. 2007; Nemani et al. 1993; Goward et al. 1985; Smith and Choudhury 1990; Sandholt et al. 2002). The variations in land surface properties and vegetation densities across the Earth's surface give LSTmax a unique biogeographic influence. For example, forests, with their relatively deep root systems, can tap groundwater even during dry conditions and through transpiration, partition a larger proportion of incoming solar radiation to LE, cooling their surface temperature compared to other land cover types (Mildrexler et al. 2011a).

The complete global coverage and 1-km^2 resolution of the LST data provides detailed spatial information that can be examined at local (Zhou et al. 2012), regional (Jin and Mullens 2012; Van De Kerchove et al. 2013), as well as global scales (Mildrexler et al. 2011b; Li et al. 2015). Spatially continuous global LSTmax maps provide the means to visually assess the patterns of the highest temperatures across both large-scale natural vegetation density and type gradients (Fig. 2.1A and 2.1B)—such as the transition from the tropical rainforests of the Congo to the Sahara Desert—and relatively small-scale land cover changes due to irrigation and urban development (Fig. 2.1C). This scalability facilitates focusing on different regions of the Earth's land surface to explore the driving factors that contribute to changes in the higher-level global measurement (Fig. 2.1D). Thus, LSTmax has the potential to indicate large-scale shifts in the Earth's biosphere, while also retaining its physical meaning and significance across every 1-km^2 pixel of the Earth's land surface.

The annual LSTmax histograms include every 1-km^2 pixel across the global land surface and display a distinctive multimodal distribution influenced by the biophysical and biogeographic factors of the Earth's ecosystems (Fig. 2.1D). Barren deserts,

shrublands and grasslands in hot dry environments are reflected in the high temperature mode (~ 50° - 65°C) of the global histogram (Fig. 2.1D). Ice/Snow areas account for the low temperature mode (~ −30° - 0°C) including the high kurtosis at 0°C, the ice melt point. The central mode of the global histogram (~ 20° - 35°C) is driven by forest cover types. These annual histograms illustrate that the Earth has a unique maximum thermal signature with relatively low interannual variability across 12 years of LSTmax data, reflecting two important global-scale land surface dynamics. First, in any given year, the vast majority of the Earth's land surface is undisturbed (Potter et al. 2003; Mildrexler et al. 2009; Goward et al. 2008). Second, the aggregate effects of natural disturbances globally on the surface energy balance, such as from the loss of vegetation to fire and the regrowth from natural succession, act to average each other out (Bowman et al. 2009). By starting from this integrated global perspective, we have developed an understanding that bulk shifts in any component of the histogram signal potential major climate or human-induced changes in the Earth's system. Using the MODIS land cover as a mask, LSTmax data can be extracted for specific cover types and land cover specific histograms analyzed for change.

Data and Methods

The key datasets used in this study are global satellite-derived LST and land cover data from the MODIS sensor from 2003 to 2014. We also used Landsat derived forest loss data and continental perimeter maps for classification and comparison of the LST data. Our approach involves several key steps. 1) Annual maximum value compositing of the 1-km^2 LST data and calculation of LSTmax annual histograms. 2) Calculation and spatial analysis of the global LSTmax pixel-specific anomalies and their association with verified heat waves and droughts. 3) Calculation of Ice/Snow LSTmax histograms and examination of interannual variations and spatial patterns related to ice melt in Greenland and Antarctica. 4) Calculation of EBF LSTmax histograms and examination of interannual shifts and anomalies associated with drought and forest loss in South America

and Africa, where the EBF forest area is predominantly within the Amazon and Congo rainforests respectively.

MODIS Aqua LST data

We used the collection 5 MODIS 8-day Aqua daytime LST (MYD11A2) from 2003 to 2014 at 1-km^2 spatial resolution. The MODIS LST products have been validated within 1 K at multiple sites in relatively wide ranges of surface and atmospheric conditions (Wan et al. 2004; Wan 2008). Refinements to the collection 5 LST product have minimized the main sources of uncertainty caused by cloud contamination and in accurately estimating the surface emissivity, and significantly improved the accuracy and stability of the MODIS LST products (Wan 2008). Annual maximum value compositing was applied to the LST data, selecting independently for each pixel the maximum 8-day LST over a one-year period from all 8-day composites labeled as reliable by the MODIS quality control and combined into one seamless image representing the highest LST recorded at every 1-km^2 pixel on the Earth's surface for a given year. LSTmax has been used to pinpoint global hot spots (Mildrexler et al. 2011b), map large-scale ecological disturbances and human induced land cover change at regional and continental scales (Lambin and Ehrlich 1995; Li et al. 2015; Mildrexler et al. 2007; Mildrexler et al. 2009), examine the degree to which different land cover types regulate LSTmax and how it varies compared with air temperature globally (Mildrexler et al. 2011a), and to better understand the maximum thermal characteristics of the global land surface (Mildrexler et al. 2011b).

LSTmax anomaly maps

Biophysical data such as LST are easily interpreted as a relative anomaly, or departure from a baseline condition (Janetos et al. 2012). The LSTmax anomaly is calculated on an annual basis as pixel-wise anomalies from each pixel's long-term data record mean (2003-2014).

$$\text{LSTmaxAnomaly}_{\text{annual}} = \text{LSTmax}_{\text{current year}} - \text{LSTmax}_{\text{data record mean}} \quad (1)$$

The LSTmax anomalies are calculated relative to the 2003-2014 average where normal is the 0 point and departures are mapped in 2°C increments.

MODIS Land Cover data

The MODIS collection 5.1 Land Cover product (MCD12Q1) provides annually updated land cover maps with a spatial resolution of 1-km^2 (Cai et al. 2014). The primary objective of the MODIS Land Cover product is to facilitate the inference of biophysical information for use in regional and global modeling studies and therefore must be discernible with high accuracy and directly related to physical characteristics of the surface, especially vegetation (Friedl et al. 2002). A classification scheme developed by the International Geosphere-Biosphere Programme (IGBP) groups the Earth's surface into 17 major classes. This provided a consistent grouping method to compute the land cover specific LSTmax statistics and provide biophysical interpretation. We used land cover specific masks to extract the annual LSTmax and anomaly data for specific cover types and develop cover specific histograms. To reduce uncertainties related to annual changes in the land cover map, we used the land cover data from 2003 to match with our first full year of MODIS Aqua LST data and held this layer constant for all other years (2003-2014).

Forest loss data

Forest loss was derived from 30-m^2 spatial resolution Landsat-based annual forest change data (Hansen et al. 2013). Forest loss from 2000 to 2012 were aggregated from 30-m to 1-km in sinusoidal projection and mosaicked to global geotiff files. Each change layer gives the percentage of Landsat change pixels that experienced forest loss during each year within a 1-km grid. Cumulative losses were computed as the total percentage of forest cover loss that occurred between 2000 and 2012. To examine the effects of significant large-scale forest loss on LST in the EBF cover type, we used a threshold of 30% forest loss, indicating that at least 30% of the MODIS 1-km pixel had experienced forest loss during the study period. While more subtle temperature responses are likely at

lower thresholds, the 30% threshold is effective for our purpose of demonstrating the generalized broad-scale temperature response from significant forest loss (Sulla-Menashe et al. 2014). To examine the effect of forest loss on LSTmax we utilized two approaches. First, to determine if persistent increases in the LSTmax of EBF were associated with areas that experienced forest loss, we computed the mean temperature change between the first (2003 - 2008) and second half (2009 - 2014) of the study period (globally and for South America) at each pixel, and then compared the changes with areas that experienced greater than 30% forest loss from 2002 to 2012. Second, we compared the temperature change for pixels that experienced greater than 30% forest loss to those that experienced less than 30% forest loss between the first year (2003) and the last year (2014) of our study period. Because forest loss has such persistent effects on LSTmax change, we found a very strong spatial correspondence between our LSTmax and forest loss datasets despite their minor temporal offset.

Results

Global heat waves

We used the spatially continuous1-km^2 annual LSTmax anomaly data to monitor for extreme heat events from 2003 to 2014 (Fig. 2.2). We found that positive anomalies with temperatures ranging from 2°C to over 8°C above the mean LSTmax correspond with major droughts and heat waves across the global land surface (Table 2.1). Area affected by positive anomalies peaked in 2010 and 2012 with 5% (16%) of the Earth's surface experiencing anomalies greater than 4°C (2°C) for both years (Table 2.2). The 2010 peak coincides with widespread and severe heat waves in Russia, Kazakhstan, Mongolia, and China (Sun et al. 2014), and the Amazon and Congo rainforests (Marengo et al. 2011; Zhou et al. 2014). In 2012 positive LSTmax anomalies stretched across the northern hemisphere in accordance with widespread summer heat waves in North America (Wang et al. 2014; Cattiaux and Yiou 2013; Karl et al. 2012) and northern Eurasia (Schubert et al. 2014). The 2012 positive anomaly over Greenland was the most

extreme melt year ever recorded across the GrIS with satellite monitoring (Nghiem et al. 2012).

Focusing on several high profile heat waves reveals complex spatial patterns detected across a variety of ecosystems (Fig. 2.3; boxes in Fig. 2.4 give locations of heat waves). The LSTmax anomalies associated with extreme heat waves generally display a core area of intense positive anomalies surrounded by anomalies of decreasing intensity grading out into the landscape (Fig. 2.3). For example, the most intense anomalies (>6°C) of the 2003 European heat wave were concentrated in France with smaller patches in Germany (Fig. 2.3A). Surrounding these areas were anomalies ranging between 4 - 6°C that connect the higher intensity patches together, and spread into Spain, England, across Germany and into eastern Europe. These areas were further surrounded by anomalies ranging between 2 - 4°C. Together these positive anomalies give a spatially defined footprint of the 2003 European heat waves most extreme surface temperatures. In 2007 heat waves affected both western and southern/eastern North America (Fig. 2.3B). Interestingly, a cold summer anomaly also occurred in Texas during 2007. As a result the 2007 LSTmax anomaly map for North America displays the juxtaposition of negative (cool) and positive (hot) anomalies. The Siberian heat wave (Fig. 2.3C), the 2011 Texas and Oklahoma heat wave (D), and the 2012 Greenland heat wave (E) each show a similar general pattern of a core area of the most intense positive anomalies surrounded and connected by less intense positive anomalies. These heat waves were associated with continent-wide reductions in ecosystem productivity (Ciais et al. 2005; Zhao and Running 2010; Schwalm et al. 2012), heat stress-induced damages to natural and agricultural systems (Cattiaux and Yiou 2013; Bréda et al. 2006; Long et al. 2013), unusually large and intense wildfires and air pollution (Wendler et al. 2011; Shaposhnikov et al. 2014), die-offs of plants and animals (Bréda et al. 2006; McKechnie et al. 2012; Allen et al. 2015), spread of infections (Baker-Austin et al. 2016), and widespread loss of human life (Bouchama 2004; Sun et al. 2014; Fouillet et al. 2008; Elliot et al. 2014). Low maximum temperature anomalies generally imply cooler summer conditions that are less notable from a meteorological point of view. Nonetheless the

LSTmax negative anomalies are associated with verified climatic events, such as the cool summers of 2004 and 2009 in much of the central portion of the U.S., the cool spring and summer of 2007 in Texas (Fig. 2.3B), and Australia's wet, cool summer in 2011.

Recent extreme heat events, such as those shown in Figure 2.3, are redrawing the temperature records of the planet, breaking records on daily to seasonal timescales (Barriopedro et al. 2011; Lewis and Karoly 2013). To visualize the footprint of increasingly extreme heat waves on the planet's highest temperatures, we extracted the year during which the highest LSTmax occurred from 2003 to 2014 across the global land surface. The resulting map shows the temporal juxtaposition of large, overlapping severe heat waves, particularly in the northern hemisphere, such as the 2003 European heat wave (light pink), and the 2010 Siberian heat wave (light green) superimposed on other major heat waves from 2006 and 2012 (Fig. 2.4). The 2012 positive anomaly in Greenland dominated the highest LSTmax over large areas of the ice sheet. North America shows the footprint of numerous extreme events such as the 2003 heat wave in western North America, and the 2004 heat wave in southeast Alaska (Fig. 2.4). The highest LSTmax values in the central and southeastern U.S. occurred during the heat waves in 2006, 2011, and 2012. In Australia, record-breaking heat waves in 2009 and 2013 dominate the timing of highest LSTmax over large areas of the continent. The 2005 drought had a strong footprint in Africa. In South America, the 2009 heat wave in La Plata Basin (green) and the 2013 heat wave in Argentina (orange) dominated the timing of the highest LSTmax in those areas. While patterns in tropical rainforests are generally more mixed, the 2010 heat wave was the dominant year during our study period for highest LSTmax in these forests.

Cryosphere melt

To isolate the Earth's year round ice and snow-covered lands for melt detection, we extracted the 1-km^2 LSTmax data from 2003 to 2014 for all pixels classified as Ice/Snow by the MODIS land cover map of 2003. The global Ice/Snow LSTmax histogram accounts entirely for the low temperature mode in the global histogram (Fig. 2.1D), including the sharp spike at 0°C (32°F), the ice melting point (Fig. 2.5). During

the melt phase change process, considerable energy is spent in the physical process of breaking hydrogen bonds rather than increasing the surface temperature, resulting in a convergence of surface temperatures around the ice melt temperature range. Close examination of the melting point peak reveals large shifts between years (2011-2014 shown on Fig. 2.5 inset graph). In 2012 the peak reached its highest level, representing about 32,000 km^2 of the ice and snow covered land surface, higher than any other year by over 10,000 km^2. Interestingly, once melt occurs, surface temperatures warm rapidly indicated by the relatively tiny fraction of the Earth's surface with LSTmax between 0° and 10°C (Figs. 2.5 and 2.1D). This suggests that the phase change acts as a climatic buffer that once overcome, results in a rapid surface temperature increase.

To examine the location of ice melt, we mapped the temperature range associated with the ice melt peak (~ −1.0° - 0.5°C) for 2011 – 2014 and compared Greenland and Antarctica, which together contain 99% of the freshwater ice on Earth. The maps show ice melt concentrated in the northern hemisphere, and especially on the GrIS where large areas around the coastal margin show LSTmax values within the ice melt range each year (Fig. 2.6). The increased surface melt during 2012 is clearly visible, indicating that the LSTmax histogram shifts are tracking major melt changes in the cryosphere. In comparison, Antarctica's LSTmax stayed mostly below the ice melt range (Fig. 2.6).

The LSTmax histogram plotted specifically for Greenland verifies that melt on the GrIS drove the observed shifts in the global Ice/Snow melt peak, including the 2012 maximum that corresponds to the year of record melt and a widespread positive LSTmax anomaly (Fig. 2.7). Spatial patterns reveal that the 2012 LSTmax positive anomalies were most intense in the northern interior part of the GrIS (Fig. 2.7A), which includes the cold polar areas at high altitudes where historical melt has been very rare (Clausen et al. 1988; Nghiem et al. 2012). However, in 2012 the pronounced positive anomalies resulted in surface temperatures that crossed the melt point in the cold polar areas. Also of importance is the shift toward warmer temperatures in 2012 for the entire LSTmax distribution of the GrIS relative to the other years, with the coldest temperatures rising to around −10°C, and a substantial increase in area of ice within the −5° to 0°C temperature

range (Fig. 2.7B). In comparison, much of Antarctica's Ice/Snow environment maintained cooler annual maximum surface temperatures in the −30° to −5°C range, and a much smaller peak at the melt point.

Tropical forest droughts

We isolated the LSTmax data for all EBF globally using the 2003 MODIS land cover. These tropical forests account for a portion of the central mode in the global LSTmax histogram and consistently regulate LSTmax between about 25° and 35°C (Fig. 2.8). The LSTmax histograms reveal a biome-level shift toward higher temperatures in 2010 (Fig. 2.8), the year Amazonia experienced a widespread and severe drought (Marengo et al. 2011). Severe drought also affected the Amazon rainforest in 2005 (Marengo et al. 2008). While these recent Amazonian droughts are well documented, in situ observations of drought effects are more limited in the central African rainforests. However, recent studies have presented observational evidence for widespread decline in vegetation greenness in Congolese forests in the past decade (Zhou et al. 2014). Our data indicates the potential of a whole biome-level extreme maximum temperature shift in 2010. We investigated the LSTmax anomalies and distributions for South America (Amazon rainforest) and Africa (Congo rainforest), which contain the two largest rainforests on Earth.

We found that positive LSTmax anomalies affected both the Amazon and Congo rainforests during the major droughts of 2005 and 2010 (Fig. 2.9). In the Amazon in 2005, positive anomalies were concentrated in the southwestern region (Fig. 2.9A), where patterns of drought impact on the forest canopy were most severe (Saatchi et al. 2013). In 2010 the positive LSTmax anomalies were much more widespread and intense (4° - 8°C) throughout the Amazon (Fig. 2.9B), driving a bulk shift in the 2010 LSTmax histogram for South America's EBF (Fig. 2.9C). The Congolese rainforests experienced positive anomalies during 2005, especially in their central, and more intense in their eastern extent (Fig. 2.9D). The 2010 positive anomalies in the Congo were also widespread, but generally less intense than in the Amazon (Fig. 2.9E). These widespread

anomalies drove directional shifts toward higher temperatures in Africa's EBF in 2005 and 2010 (Fig. 2.9F).

Tropical forest loss

It is well established that forest loss increases the LSTmax in tropical forests (Mildrexler et al. 2011a; Li et al. 2015). Thus, the cumulative effect of deforestation on LSTmax should over time shift the annual histograms toward higher temperatures. We found a shift toward higher LSTmax values between the first half (2003 - 2008) and the second half (2009 - 2014) of the study period for all EBF globally, and for the EBF in South America (Fig. 2.10A and 2.10B). In the Amazon, the area of forest loss between 2002 and 2012 was largely concentrated in the "arc of deforestation" along the southern edge of the Amazon forest (Fig. 2.10C). The significant mean temperature changes (>2.5°C) showed strong spatial association with areas of forest loss, and were nearly uniform toward higher temperatures (Fig. 2.10D). This indicates that the cumulative effects of forest loss over time are driving shifts in the EBF LSTmax histograms toward higher temperatures.

We also isolated EBF that experienced greater than 30% forest loss during our study period, and plotted their temperature change against areas that experienced less than 30% forest loss. The areas of 30% or greater forest loss experienced a much greater shift toward higher temperatures (Fig. 2.11A and 2.11B). A typical forest loss scene in the Amazon reveals the tight spatial coupling between forest loss and LSTmax increases of more than 5°C at the local scale (Fig. 2.11C). Zooming in closer reveals the temperature changes in areas of visible forest loss (Fig. 2.11D). Compared to the area of increased temperature, very little area shows a reduction in LSTmax that would indicate recovery from previous forest loss.

Summary and Discussion

Our results document that the Earth's maximum surface temperatures are experiencing biome-scale bulk shifts toward anomalously high temperatures in association with large-scale extreme climatic events, and land use change. Large-scale

directional shifts in maximum temperatures indicate important changes in the surface energy balance that push ecosystems and biomes toward critical thresholds. We found these shifts in the cryosphere in conjunction with the extreme melt of the GrIS, and in tropical rainforests caused by widespread and severe drought and the cumulative effects of forest loss. Interestingly, the peak years with positive LSTmax anomalies (2010 and 2012) were the same years we detected bulk shifts in the temperature distribution for entire biomes. This highlights the need to improve our understanding of the teleconnections within the Earth's global environment that manifest such widespread and extreme global heat waves that are projected to become more common in a future warmer world (Wang et al. 2014; Schubert et al. 2014; Hansen et al 2012).

Biome-level bulk shifts in the LSTmax distribution indicates the potential for thermal stress thresholds to be crossed for large areas, resulting in profound and irreversible changes. For example, 98.6% of the GrIS was under melt in 2012 (Nghiem et al. 2012) in conjunction with widespread positive LSTmax anomalies and a large increase in the ice melt peak of Greenland's histogram (Fig. 2.7). Melt occurred in the high polar altitudes of the GrIS in some areas where the last significant melt event is recorded in the 1889 ice layer (Claussen et al. 1988). Ice loss from the GrIS has rapidly accelerated during the last four years of our study period (2011-2014) accounting for an increasing proportion of global sea level rise, and the greatest ice loss occurred during the exceptionally warm summer of 2012 (McMillan et al. 2016). The 2012 LSTmax distribution for the GrIS provides a glimpse into how future ice summer temperature distributions will look under a melt regime characterized by 100% summer surface melt extent, a threshold reaching condition that will likely trigger tipping points in the ice sheet melt regime (Box et al. 2012). The unique phase change driven component to the Ice/Snow histogram will also provide valuable insights into future ice melt changes in Antarctica.

Demonstrating the importance of wall-to-wall global LST coverage, we found that the Amazon and Congo rainforests experienced widespread LSTmax anomalies and large-scale directional shifts toward higher temperatures in 2010, and to a lesser extent in

2005. The 2010 LSTmax anomalies show how large, severe droughts can rapidly shift an entire forest biome toward a condition of increased thermal stress (Fig. 2.9). Given that the 2010 drought caused a widespread reduction in vegetation greenness, increased mortality, and reduced growth that may have shut down the entire Amazon rainforest carbon sink (Lewis et al. 2011; Xu et al. 2011; Feldpausch et al. 2016), the effects of the 2010 LSTmax anomalies on the Congolese forests were most likely also severe. This is consistent with the gradual decline in photosynthetic capacity and moisture content observed in the Congolese forests over a similar time period (Zhou et al. 2014). It is not surprising that in comparison with 2005, the 2010 drought had a much stronger effect on shifting the LSTmax distribution in the Amazon rainforest. While both Amazonian droughts were severe, the 2010 drought caused declines in greenness spanning an area that was nearly five times greater compared to 2005 (Xu et al. 2011). Research into the effects of recent sub-continental hotter droughts on tree mortality have found that consecutive multi-year events cause progressive drying of the forest canopy and reductions in soil moisture that can result in widespread mortality of dominant trees species (Breshears et al. 2005; Asner et al. 2016). Extreme drought events have legacy effects on forest ecosystems that can last for several years, potentially reducing the resiliency of ecosystems to subsequent drought events (Anderegg et al. 2015; Saatchi et al. 2013). As the area affected by extreme high temperatures increases (Hansen et al. 2012), so will the exposure of ecosystems to anomalously high temperatures, reducing recovery time, and pushing ecosystems closer to resilience limits across scales potentially not yet witnessed before.

Forest cover changes are a key driver of anthropogenic climate change (Bonan 2008). Thus, the ability to detect human-induced forest loss is a critical aspect of the LSTmax global indicator. The shift in the mean LSTmax toward higher temperatures between the first half and the second half of our study period demonstrates how the temperature effects of annual forest cover changes accrue over time (Fig. 2.10). While the changes detected here are from a 2003 land cover baseline, by 2003 over 837,000 km^2 of Amazonian forests had already been lost (Malhi et al. 2008). Given the increases in

LSTmax we detected from 2003 to 2014 in association with forest loss, the historic forest loss has driven much more widespread increases in LSTmax with commensurate impacts on regional climate. Together, the effects of forest loss and climate change amplify one another, and our analysis provides a new integrated way to examine these critical changes.

This study has shown the immense value of a single, unique measurement in tracking critical changes in the Earth system. The focus on changing thermal regimes has the potential to detect the shifts of ecosystems toward thresholds of profound change (Mildrexler et al. 2016) and our global, semi-automated annual analysis is easily repeatable for continuous monitoring of the entire Earth's land surface. These are important distinctions from disturbance detection approaches that employ complex algorithms to provide detailed information on abrupt disturbances and land cover change, but are rarely applied annually over the entire Earth's land surface. As part of a global disturbance monitoring system, our efficient global analysis could identify areas for further examination with higher spatial resolution imagery, such as the 30-m Landsat product (McDowell et al. 2015). Moreover, given the trade-offs regarding disturbance detection accuracy with coarse resolution imagery (McDowell et al. 2015), and the link between warming temperatures and increasing rates of disturbance (Allen et al. 2015), we contend that our methodologies focus on large-scale directional shifts in surface temperatures provides a more informative first-look global change indicator in comparison with coarse-scale disturbance detection information alone.

A 12-year period is insufficient to attribute the LSTmax changes to anthropogenic climate change or establish long-term trends. Nonetheless, our results show a clear response of the cryosphere and tropical forests to changes in maximum temperature. Over time, extreme temperature events, especially heat waves and droughts, play an important role in redefining the Earth's surface thermal maxima (Fig. 2.4), and ultimately the global LSTmax histograms. We conclude that with continued warming, the Earth's integrated maximum temperatures will experience greater and more frequent directional shifts. This will increase the likelihood that critical thresholds will be surpassed resulting in regional

scale transitions that are tipping points in the global climate system (Chapin et al. 2008; Hilker et al. 2014). Given the unique qualities of the LSTmax measurement, and the importance of continuing this annual analysis for future trend detection, data continuity in satellite-derived LST is imperative. Subsequent research will investigate the ability of the LSTmax indicator to detect slower biome shifts, such as changes in woody plant cover in the Arctic that are altering the surface energy balance, and the ongoing land degradation in the Sahel of Africa.

Acknowledgments

Funding: This study was supported by the USDA Forest Service, Pacific Northwest Research Station and Oregon State University. **Author contributions:** D.M. designed the study with the help of M.Z. and S.R. D.M. analyzed data, interpreted results, and wrote the manuscript. M.Z. and W.C. helped write the manuscript. M.Z. and X.S. processed data. All authors contributed to interpreting the results, and refining the manuscript. **Competing interests:** The authors declare that they have no competing interests. **Data and materials availability:** All data needed to evaluate the conclusions in the paper are present in the paper. Additional data related to this paper may be requested from the authors. MODIS data used in this work are available from Land Processes Distributed Active Archive Center (https://lpdaac.usgs.gov/dataset_discovery/modis/modis_products_table).

Figures and Tables

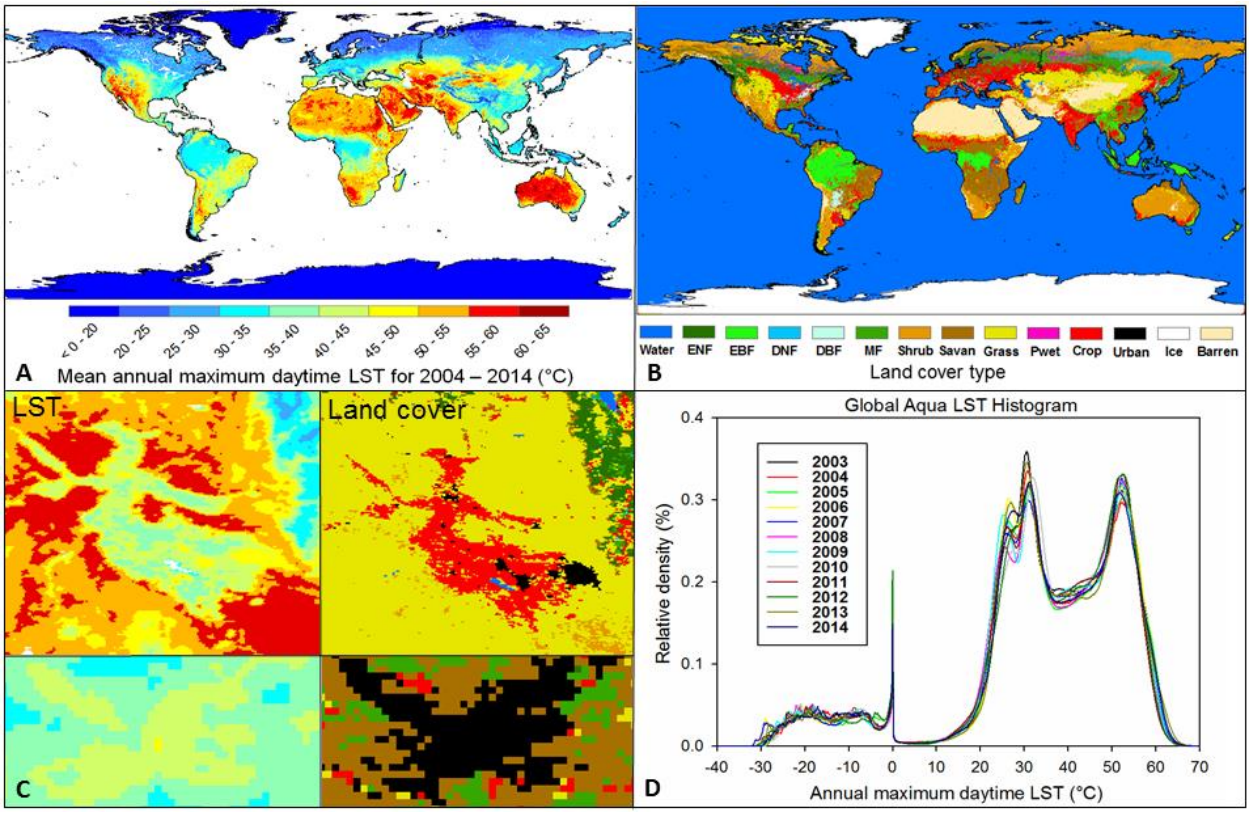

Fig. 2.1. (A) Continuous global map of the mean annual maximum daytime LST (LSTmax) from 2003 to 2014 displays a heterogeneous thermal environment, and close association with the land cover type of the Earth's surface. (B) 2003 MODIS Land Cover dataset (Friedl et al. 2010) with classification system abbreviations defined as Evergreen Needleleaf Forest (ENF), Evergreen Broadleaf Forest (EBF), Deciduous Needleleaf Forest (DNF), Deciduous Broadleaf Forest (DBF), Mixed forests (MF), Shrublands (Shrub), Savannas (Savan), Grassland (Grass), Permanent Wetlands (Pwet), and Croplands (Crop). Note that in this figure, we combined Open and Closed Shrublands into Shrub, and Woody Savannas and Savannas into Savan. (C) The high spatial resolution (1-km^2) LST data detects temperature effect of irrigation in a semi-arid desert in Idaho, USA and urbanization in South Carolina, USA. LST and land cover classifications are the same as in 1A and 1B. (D) The global maximum thermal signature of the Earth's land surface from 2003 to 2014 reveals low interannual variability and a multimodal distribution. Area under annual density curves sum to 1.

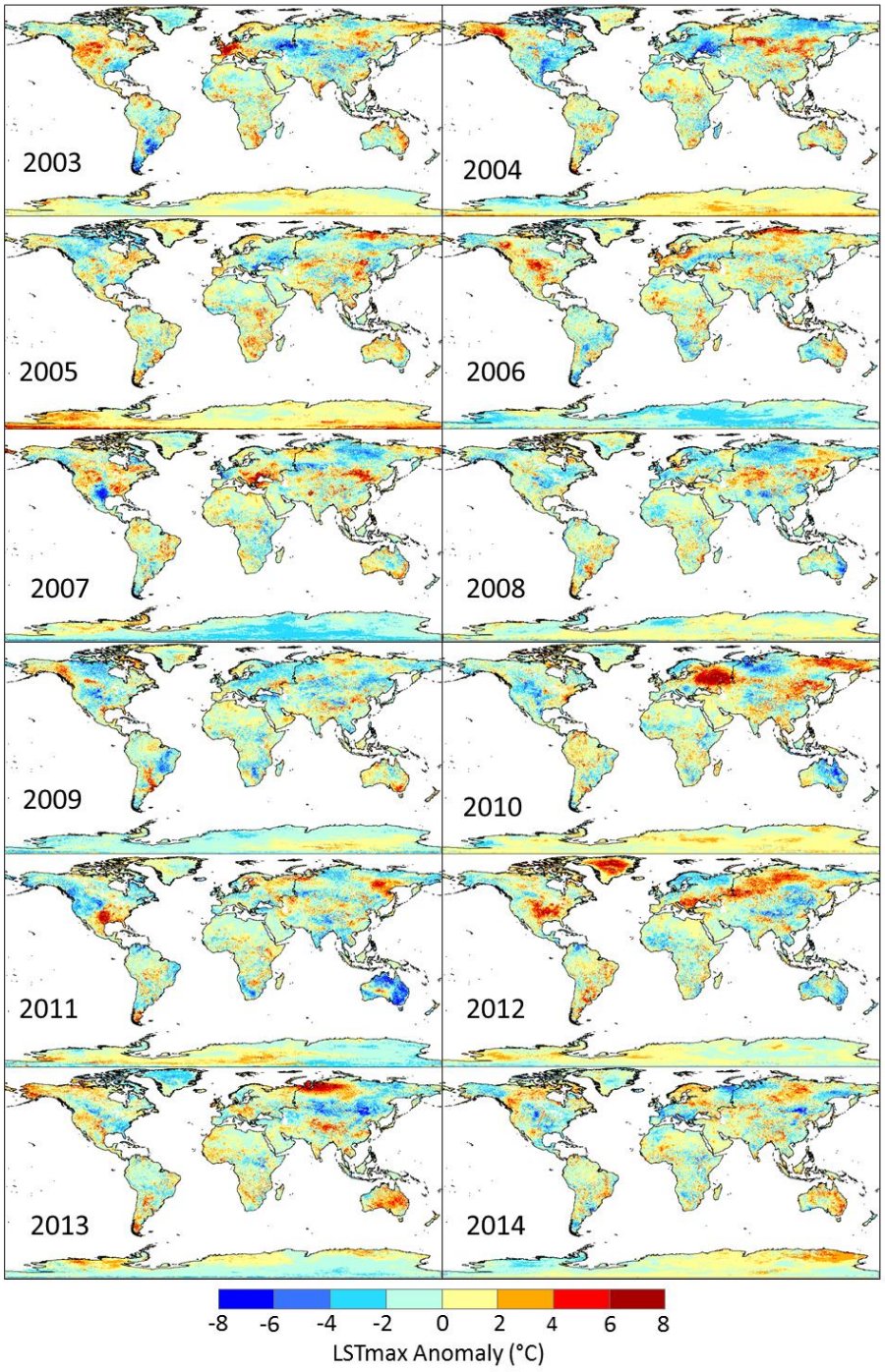

Fig. 2.2. LSTmax annual anomaly maps from 2003 to 2014 mapped in two degree Celsius intervals capture the spatial extent of major droughts and heat waves in detail, providing a powerful visual comparative evaluation for heat waves globally.

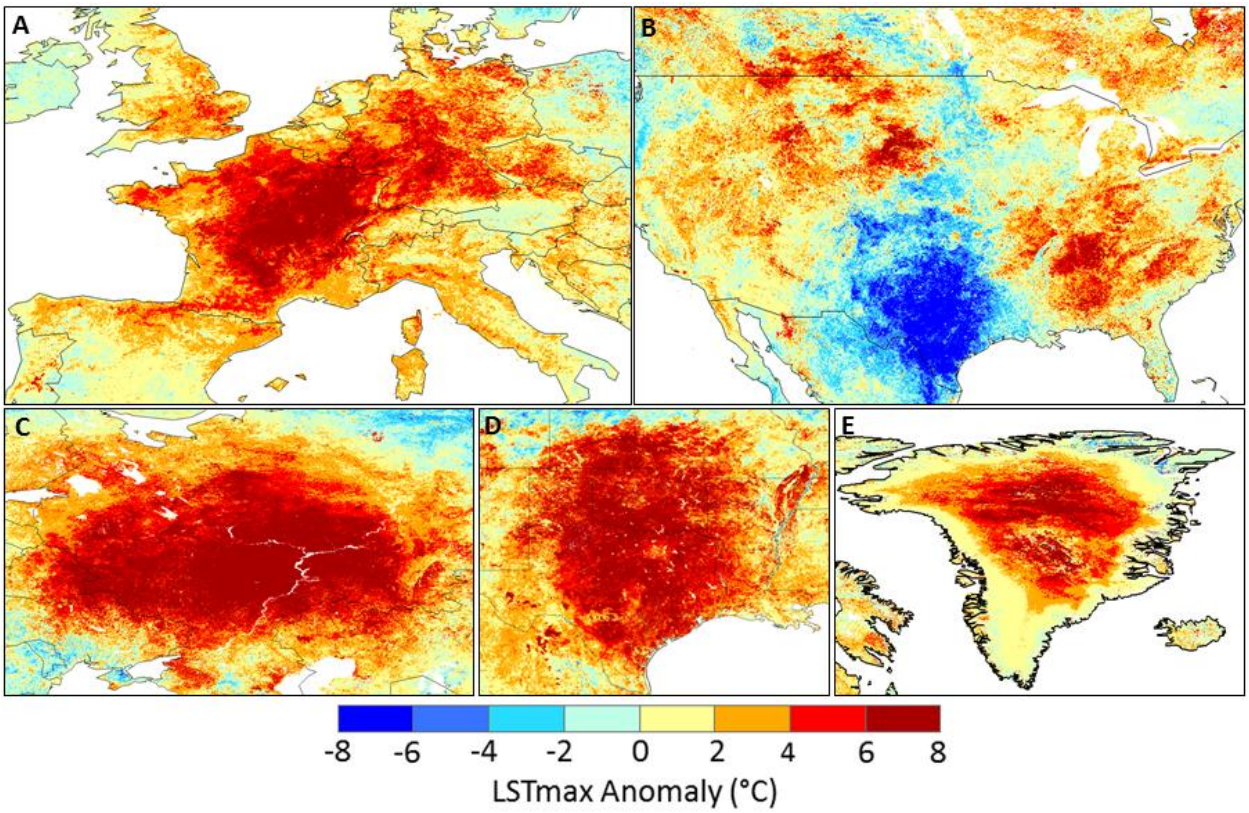

Fig. 2.3. Heat waves and LSTmax anomalies for (A) 2003 European heat wave, (B) 2007 North American heat waves (and cold anomaly in Texas and Oklahoma), (C) 2010 Siberian heat wave, (D) 2011 Texas and Oklahoma heat wave, and (E) 2012 Greenland heat wave.

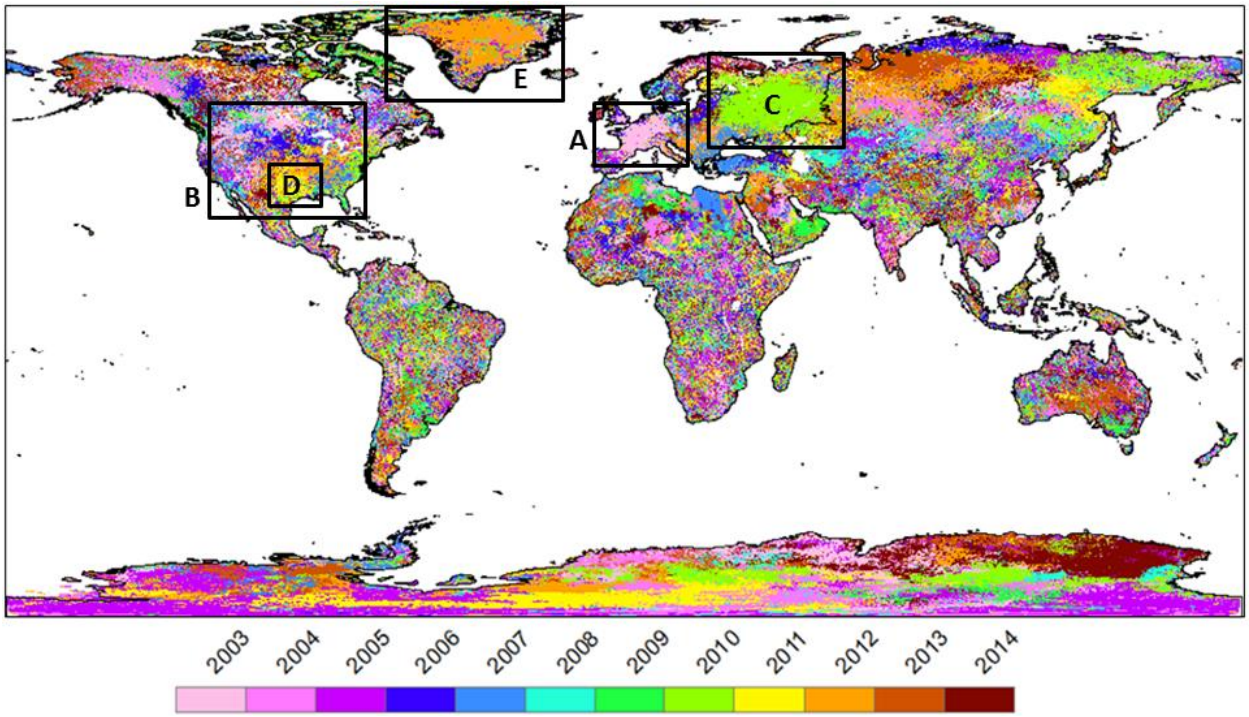

Fig. 2.4. The year during which the highest LSTmax occurred from 2003 to 2014 at every 1-km^2 pixel across the global land surface shows the temporal footprint of numerous large-scale heat waves. Boxes correspond to location of heat waves shown in Figure 2.3.

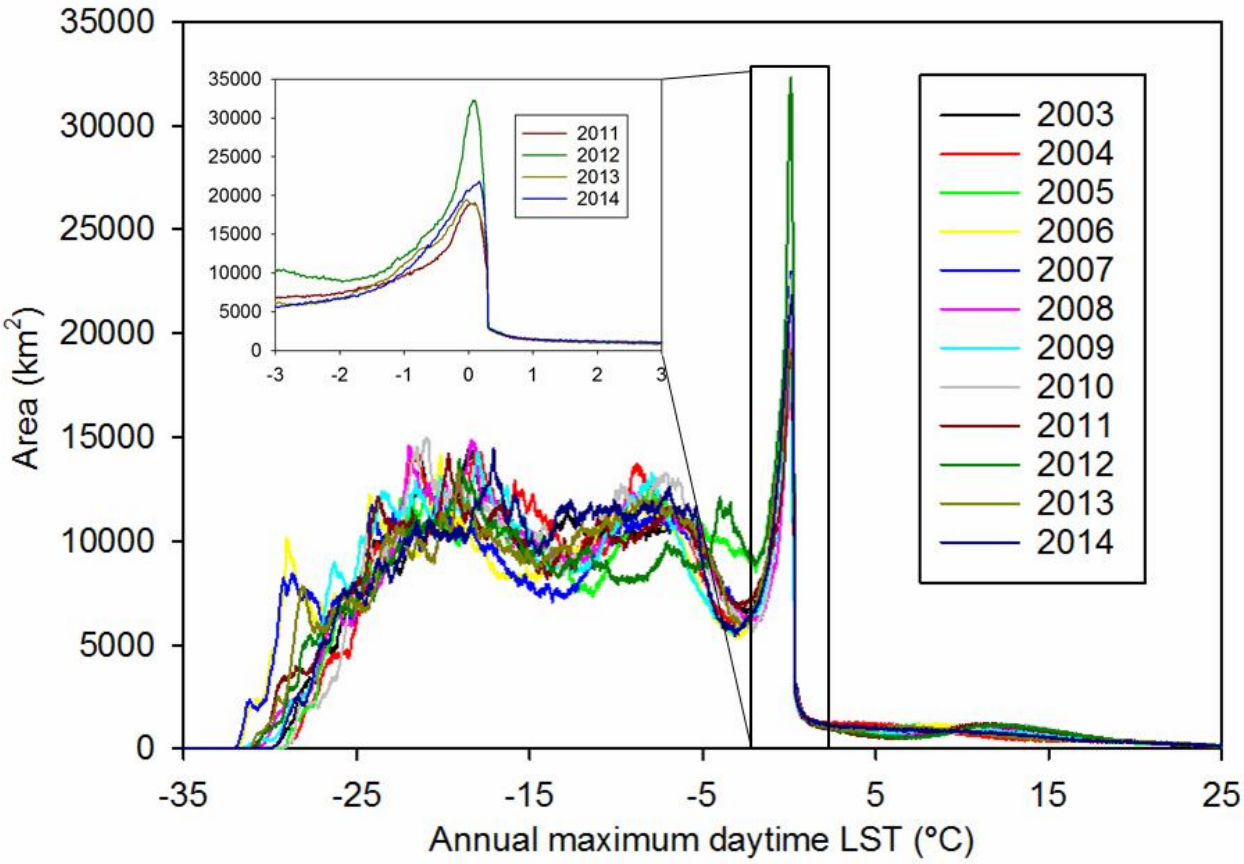

Fig. 2.5. The LSTmax histogram for all pixels labeled as Ice/Snow by MODIS Land Cover (2003) illustrates the unique and critical role of ice and snow-covered lands in regulating the expression of the Earth's upper temperature limit, and reveals a strong kurtosis at the melting point with large interannual variability (inset graph).

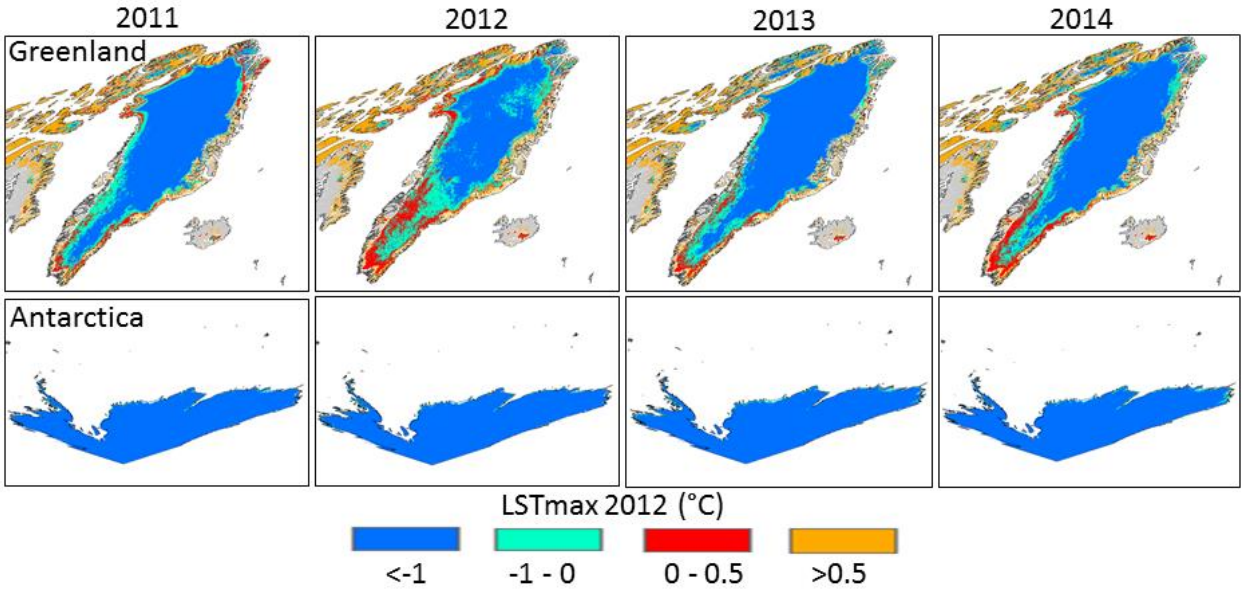

Fig. 2.6. Spatial location of Ice/Snow pixels with temperatures below (<−1°C), within (−1° - 0.5°C) and above (>0.5°C) the ice melt temperature range for Greenland (top panel) and Antarctica (bottom panel). Note that the ice surface temperature of −1°C is used as a melt detection threshold (Nghiem et al. 2012).

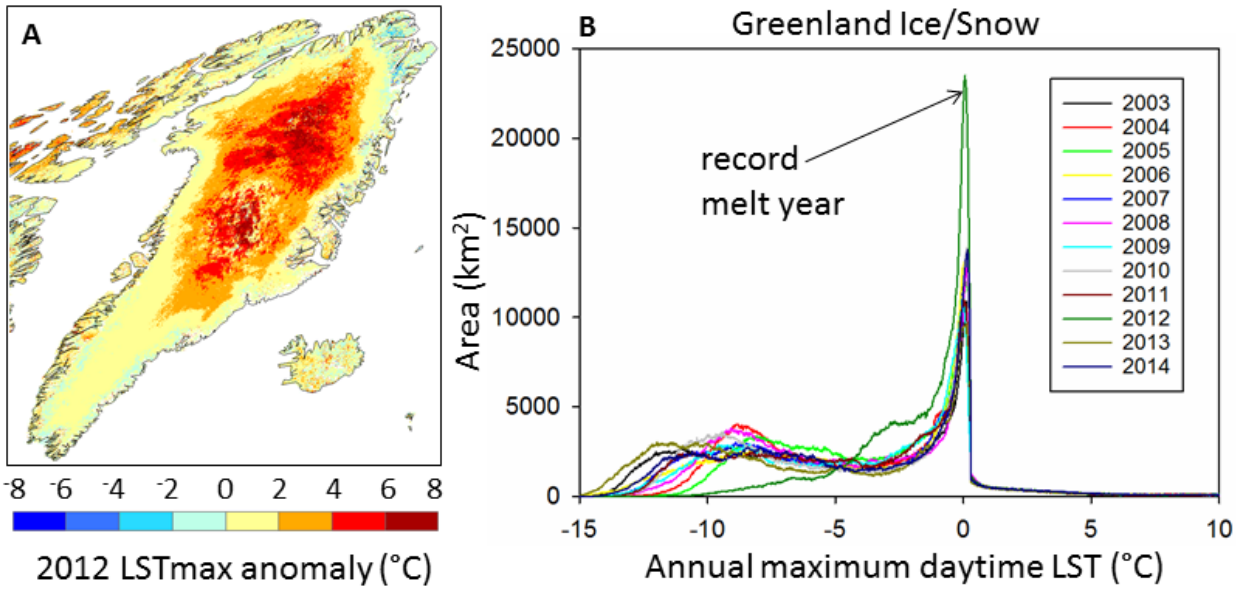

Fig. 2.7. (A) Spatial patterns of 2012 LSTmax positive anomalies extend across Greenland and are most intense in the northern interior of the ice sheet, which includes cold polar areas at high altitudes. (B) The entire distribution for Greenland shifted toward higher temperatures in 2012, with a substantial increase in the melting point kurtosis.

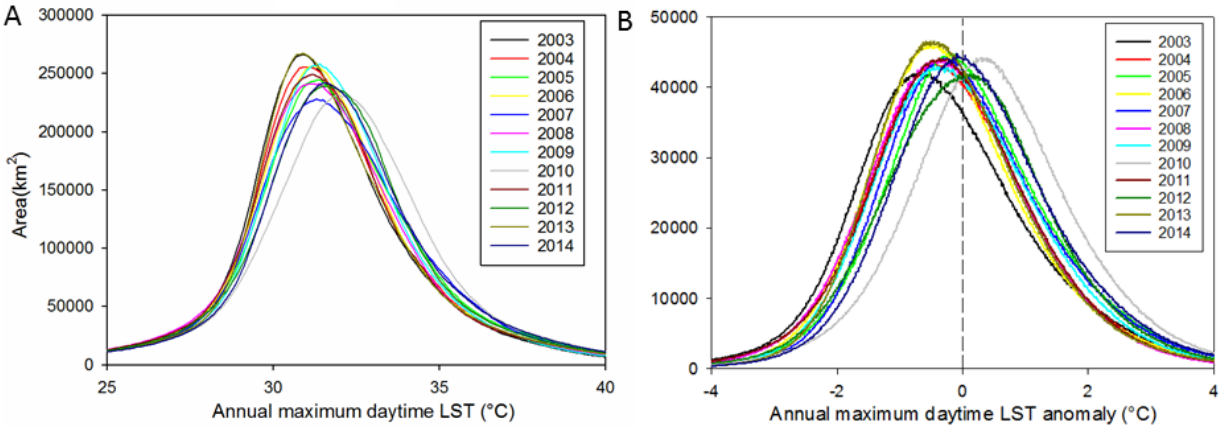

Fig. 2.8. (A) The LSTmax histograms and (B) anomaly distributions for all pixels labeled as EBF by MODIS Land Cover (2003) shifted toward higher temperatures and positive anomaly in 2010 during a short-term severe drought.

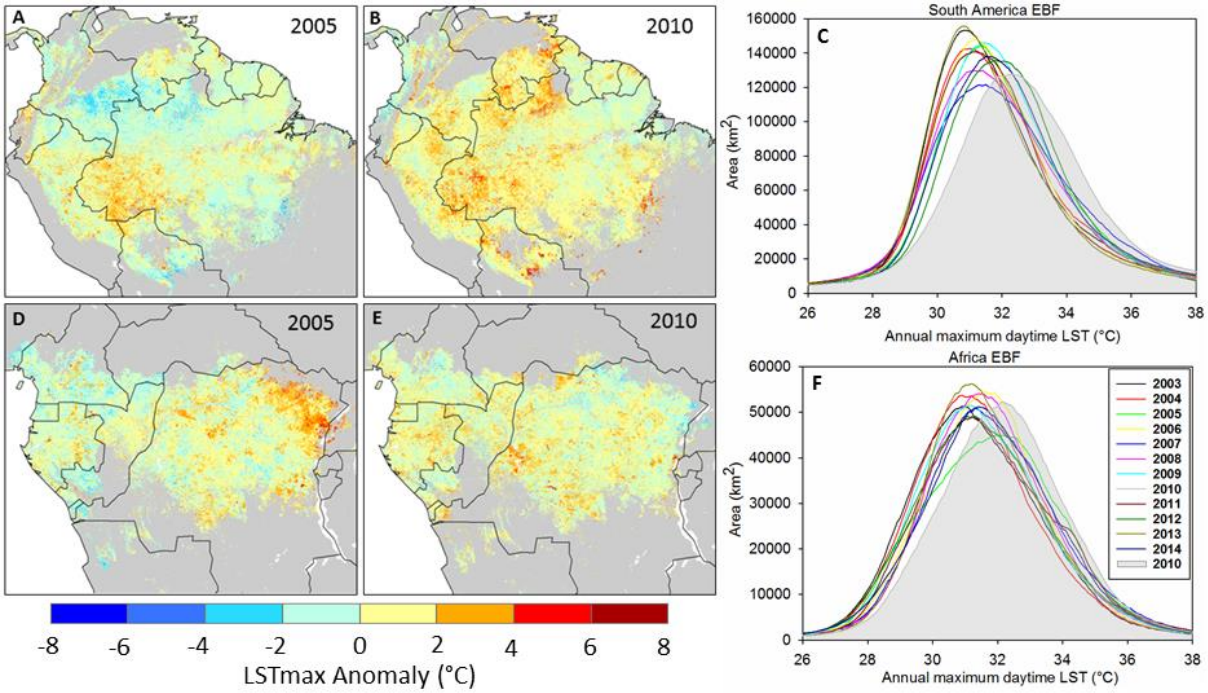

Fig. 2.9. Spatial patterns of LSTmax anomalies in the EBF during the droughts of 2005 (A and D) and 2010 (B and E) for the Amazon (top panel) and Congo (bottom panel) rainforests. The LSTmax histograms for all EBF pixels in South America (C) and Africa (F).

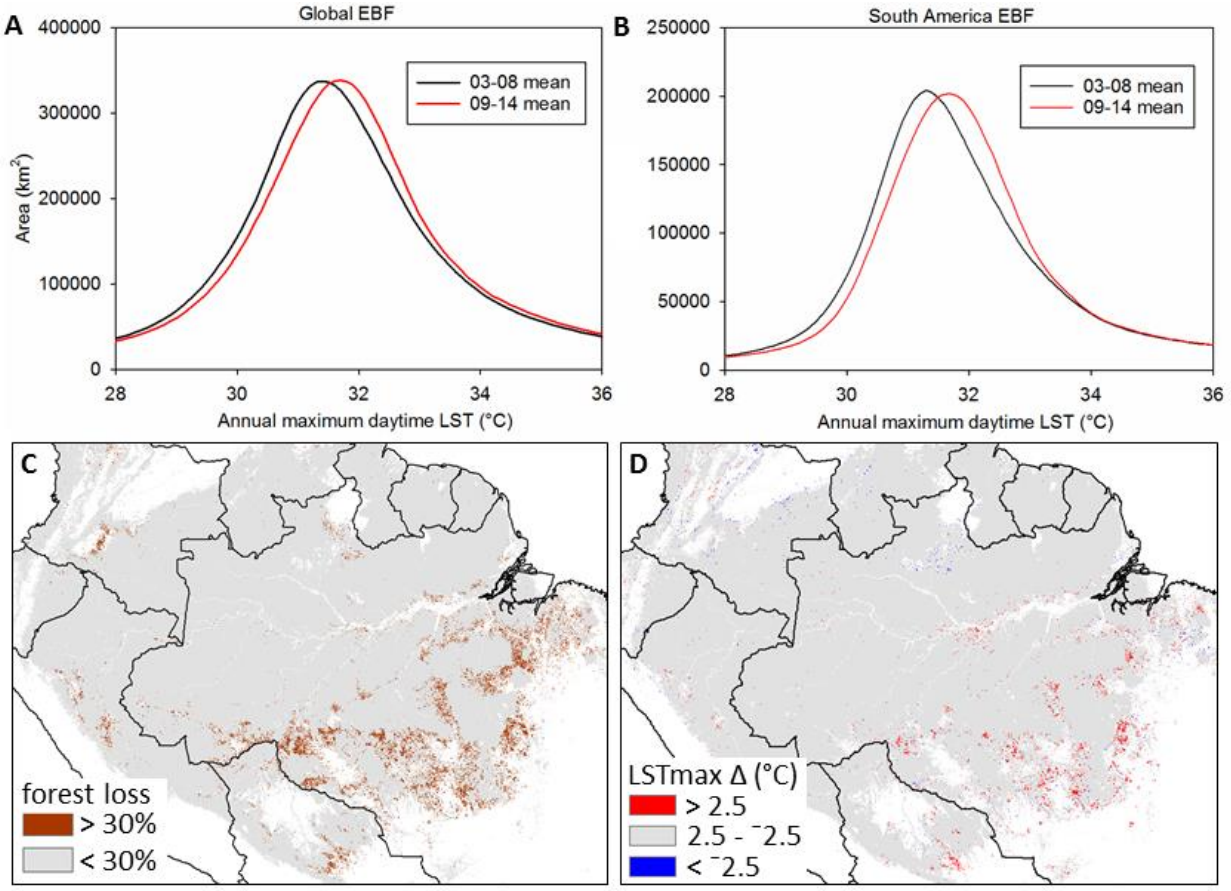

Fig. 2.10. Histograms reveal shifts toward higher mean LSTmax between the first half (2003-2008) and the second half (2009-2014) of the study period for all EBF globally (A) and for South America (B). Spatial patterns of pixels with greater than 30% cumulative forest loss in the Amazon EBF from 2002 to 2012 (C) also experienced significant mean temperature increases (> 2.5°C) between the first (2003-2008) and the second half (2009-2014) of the study period (D).

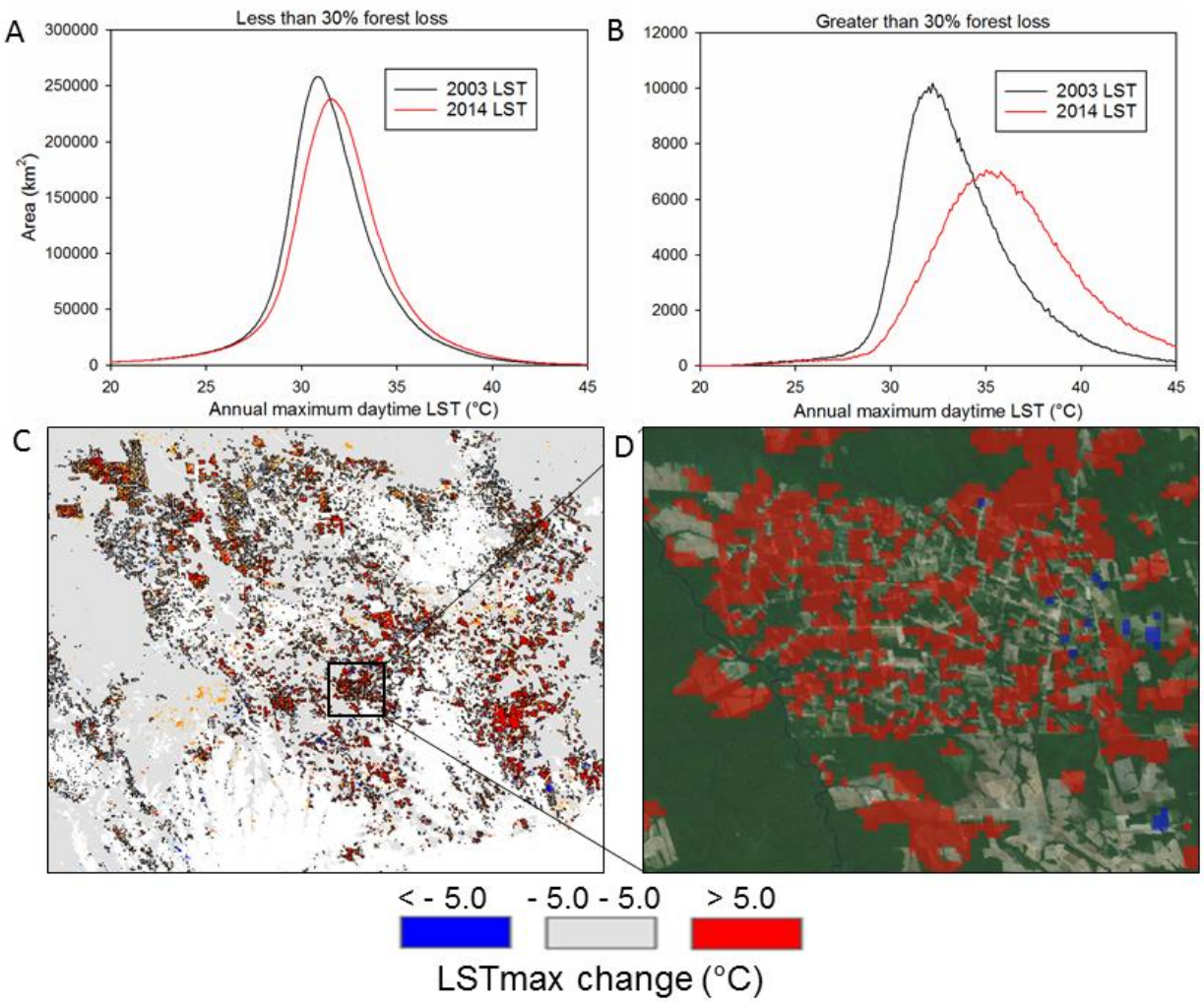

Fig. 2.11. (A and B) The difference between the 2003 and 2014 LSTmax histograms for all EBF globally illustrate the large shift toward warmer temperatures associated with greater than 30% forest cover loss. (C) Major temperature increases are closely associated with deforested areas in the Amazon (black crosshatch) and (D) visible signs of forest loss in Google Earth.

Table 2.1. Documented cases of drought and/or heat waves detected from 2003 to 2014.

Location	**Year**	**References/URL**
Europe	2003	Rebetez et al. (2008); Stott et al. (2004)
Western USA	2003	Bumbaco and Mote (2010)
Alaska	2004	Wendler et al. (2011)
Southern Asia	2005	http://earthobservatory.nasa.gov/IOTD/view.php?id=5603
East Africa	2005	Hastenrath et al. (2007)
Amazon	2005	Marengo et al. (2008)
North America	2006	http://www.noaanews.noaa.gov/stories2006/s2759.htm
Europe	2006	Fouillet et al. 2008; Rebetez et al. (2008)
Australia	2006	http://www.bom.gov.au/climate/current/month/aus/archive/200611.summary.shtml
North America	2007	Fuhrmann et al. (2011)
Southern Europe	2007	Coumou and Rahmstorf (2012); Founda and Giannakopoulos (2009)
Southeast Australia	2009	Coumou and Rahmstorf (2012); Karoly 2009; http://www.bom.gov.au/climate/current/statements/scs17d.pdf
La Plata basin, South America	2009	Chen et al. (2010); http://www.ipsnews.net/2009/01/agriculture-argentina-worst-drought-in-100-years/
Russia; eastern Europe	2010	Barriopedro et al. (2011); Grumm (2011)
Quebec, Ontario	2010	Bustinza et al. (2013)
Brazil	2010	Marengo et al. (2011)
Congo rainforest	2010	Zhou et al. (2014)
Texas and	2011	Hoerling et al. (2013); Hansen et al. (2012); Coumou and

Oklahoma, USA		Rahmstorf (2012); Long et al. (2013)
USA	2012	Cattiaux and Yiou (2013); Karl et al. (2012); Wang et al. (2014)
Greenland	2012	Nghiem et al. (2012); Neff et al. (2014)
Russia	2012	https://www.oxfam.org/sites/www.oxfam.org/files/cs-russia-drought-adaptation-270913-en.pdf
Eurasia	2012	Schubert et al. (2014)
Australia	2013	Lewis and Caroly (2013); http://www.bom.gov.au/climate/current/annual/aus/2013/
Ireland; United Kingdom	2013	Elliot et al. (2014); http://www.metoffice.gov.uk/news/releases/archive/2013/warm-july-stats
Alaska, USA	2013	http://cms.met.psu.edu/sref/severe/2013/18Jun2013.pdf
Eastern China	2013	http://news.xinhuanet.com/english/indepth/2013-08/13/c_132627590.htm
Argentina	2013	http://www.bbc.com/news/world-latin-america-25564633
Northern Europe	2014	Baker-Austin et al. (2016); http://en.ilmatieteenlaitos.fi/press-release/42503751
Australia	2014	http://www.bom.gov.au/climate/current/statements/scs48.pdf
British Columbia, Canada; northwestern USA	2014	http://www.cbc.ca/news/canada/british-columbia/b-c-heat-wave-3-hottest-spots-and-20-records-broken-sunday-1.2705834; http://earthobservatory.nasa.gov/IOTD/view.php?id=84042

Table 2.2. Percent global land surface with positive anomalies greater than 2°C and 4°C.

	Positive anomalies total global land area	
Year	>2°C (%)	>4°C (%)
2003	15.1	3.8
2004	13.3	3.6
2005	15.5	3.5
2006	13.9	3.5
2007	15.1	3.9
2008	10.6	2.2
2009	10.4	2.3
2010	16.0	4.9
2011	11.5	2.9
2012	16.3	5.0
2013	15.8	4.2
2014	14.9	3.0

Chapter 3: A forest vulnerability index based on drought and high temperatures

David Mildrexler[1], Zhiqiang Yang[1], Warren B. Cohen[2], David M. Bell[2]

[1] Oregon State University, College of Forestry, Corvallis, OR USA

[2] USDA Forest Service, Pacific Northwest Research Station, Corvallis, OR USA

Remote Sensing of Environment
Elsevier – Customer Service Department
6277 Sea Harbor Drive
Orlando, FL 32887-4800 USA
Issue 173 (2016), pages 314–325

Abstract

Increasing forest stress and tree mortality have been directly linked to combinations of drought and high temperatures. The climatic changes expected during the next decades – large increases in mean temperature, increased heat waves, and significant long-term regional drying in the western USA – will likely increase chronic forest stress and mortality. The aim of this research is to develop and apply a new forest vulnerability index (FVI) associated with drought and high temperatures across the Pacific Northwest region (PNW; Oregon and Washington) of the USA during the MODIS Aqua era (since 2003). Our technique incorporates the alterations to canopy water and energy exchange processes caused by drought and high temperatures with spatially continuous MODIS land surface temperature (LST) and evapotranspiration (ET), and with Parameter-elevation Relationships on Independent Slopes Model (PRISM) precipitation (P) data. With P and ET, we calculate a monthly water balance variable for each individual pixel normalized by forest type group (FTG), and then difference the water balance with the corresponding normalized monthly mean LST to calculate a monthly forest stress index (FSI). We then extract the pixel-specific (800-m resolution) statistically significant temporal trends of the FSI from 2003 to 2012 by month (April to October). The FVI is the slope of the monthly FSI across years, such that there is a FVI for each month. Statistically significant positive slopes indicate interannual increases in stress leading to expected forest vulnerability (positive FVI) for a given month. Positive FVI values were concentrated in the months of August and September, with peak vulnerability occurring at different times for different FTGs. Overall, increased vulnerability rates were highest in drier FTGs such as Ponderosa Pine, Juniper, and Lodgepole Pine. Western Larch and Fir/Spruce/Mountain Hemlock groups occupy moister sites but also had relatively high proportion of positive FVI values. The Douglas-fir group had the second largest total area of increased vulnerability due to its large areal extent in the study area. Based on an analysis using imagery viewed in Google Earth, we confirm that areas with increased vulnerability are associated with greater amounts of stress and mortality. The FVI is a new way to conceptualize and monitor forest

vulnerability based on first-order principles and has the potential to be generalized to other geographical areas.

Keywords: Forest vulnerability index; Stress, Climate change; Drought; Aqua MODIS Land surface temperature; Evapotranspiration; Water deficit

Introduction

Terrestrial vegetation plays a critical role in water and energy cycles, with transpiration representing about 80 to 90 percent of terrestrial evapotranspiration (ET) and absorbing a tremendous amount of solar energy (Jasechko et al., 2013; Trenberth et al., 2010). Since climate and the distribution of vegetation are so tightly linked (Mather & Yoshioka, 1968; Stephenson, 1990), plants are vulnerable to changes in precipitation, temperature, and related variables when those exceed species-specific physiological stress thresholds (IPCC, 2013; Allen et al., 2010; McDowell & Allen, 2015; Teskey et al., 2015). There is considerable uncertainty in how trees will cope with the rapid changes occurring in the climate system, including increasing global mean temperatures and a changing hydrologic cycle (IPCC, 2013; McDowell et al., 2008; Hartmann et al., 2015). The potential for broad-scale climate-induced forest die-off is of particular concern because of large carbon storage in forests, and their key role in providing a variety of other valuable ecosystem services (Breshears et al., 2005; Kurz et al., 2008; Smith et al., 2014; Millar & Stephenson, 2015; McDowell & Allen, 2015). Urgently needed are remote sensing-based large-area forest stress and mortality detection and attribution techniques that can provide *a priori* assessments of forest status and trends, as in metrics that can be used to infer a measure of possible future harm (Smith et al., 2014; Allen et al., 2015). Vulnerability metrics should have clear mechanistic links with remotely sensed metrics of vegetation that are sensitive to the changes in climate (Smith et al., 2014).

Globally, forests are showing signs of stress, such as reduced growth and leaf area decline, and increasing tree mortality that can be directly linked to combinations of drought and/or high temperatures (Allen et al., 2010; Anderegg et al., 2013; Breshears et al., 2005; Griffin & Anchukaitis, 2014; Martinez-Vilalta et al., 2011; Pravalie et al., 2014; Allen et al., 2015; Vicente-Serrano et al., 2014; Steinkamp & Hickler, 2015). In western North America, climate change has been implicated in rapidly increasing background mortality rates during recent decades, with widespread die-offs affecting tree species across regions, environmental gradients, age and structure classes, and

disturbance regimes (van Mantgem et al., 2009; Vogelmann et al., 2009; Williams et al., 2013; Breshears et al., 2005). Broad-scale drivers of tree mortality known with high confidence, such as droughts that are hotter and more widespread due to continued warming, imply a future greater level of forest vulnerability, independent of the specifics of mortality mechanism (Allen et al., 2015). Higher rates of climate-induced tree mortality can cause major shifts in ecosystem structure and function (Breshears et al., 2005; Allen & Breshears, 1998) that have varied and long-term consequences on ecological communities (Anderegg et al., 2013; McDowell et al., 2008). Changes in forest structure and composition have important implications for availability and distribution of plant and animal habitat, especially in ecosystems dominated by one or a few foundational tree species (Ellison et al., 2005). Mortality events change the albedo and the latent and sensible heat fluxes, with feedbacks on regional climate (Bonan et al., 2008; Chapin et al., 2008; Anderson et al., 2011). Even when mortality is not realized, severe drought has long lasting effects on forests (Anderegg et al., 2015). A growing body of evidence in the literature indicates that there are physical signs of stress and decline that indicate an increased risk of tree mortality. The physical expression of forest stress associated with vulnerability may manifest initially as poor crown condition and/or a decline in leaf area (Dobbertin et al., 2001; Solberg et al., 2004) followed by a reduction in growth (Pedersen, 1998; Suarez et al., 2004; Delucia et al., 2000), and then by the potential increase in susceptibility to insects and fire (Hicke et al., 2012; Westerling et al., 2005). The exceptionally severe 2003 European drought produced widespread stress symptoms in many trees (premature leaf fall, yellowing, shedding) and resulted in a large number of weakened individuals (low radial growth and small amounts of stored carbohydrates) followed by increased mortality rates in 2004 and 2005 in areas where weather conditions remained unfavorable (Bréda et al., 2006). An index that relates climatic drivers of vulnerability directly to physiological stress factors would provide valuable information on forests that are predisposed to increased vulnerability.

Recent observational and experimental studies have highlighted the potential for warmer temperatures to compound the effects of severe drought events and exacerbate

regional forest stress and die-off (Adams et al., 2009; Breshears et al., 2005; Williams et al., 2013; van Mantgem et al., 2009; Griffin & Anchukaitis, 2014). The increased energy load from warmer temperatures during severe drought events acts to heat and stress trees (Stephenson 1990; Breshears et al., 2005; Adams et al., 2009). For example, the precipitation deficits of the 2012-2014 California drought are anonymously low, but not unprecedented. Yet record high temperatures could have exacerbated the drought by approximately 36%, resulting in the most severe drought conditions in over a century of instrumental observations (Griffin & Anchukaitis, 2014). In the southwestern US (SWUS) increasing warm-season vapor pressure deficit (largely controlled by the maximum daily temperature) was found to be the primary driver of an ongoing forest drought-stress event that is more severe than any event since the late 1500s megadrought (Williams et al., 2013). The strong correspondence between temperature-driven forest drought-stress and tree mortality, combined with the relatively high confidence in the projections of continued warming in the SWUS, portends future intensified forest drought stress and increased forest decline (Williams et al., 2013). In a study that estimated vulnerability of 15 tree species in the western USA and Canada to significantly warmed climate conditions, 30% of the species recorded ranges were deemed vulnerable based on the majority of years being unsuitable for the species (Coops & Waring, 2011). Projections for the western USA indicate that far greater chronic forest stress and mortality risk should be expected in coming decades due to the large increases in mean temperature and significant long-term regional drying, as well as the frequency and severity of extreme droughts and heat waves (Allen et al., 2015; Cook et al., 2014; IPCC, 2013; Jentsch et al., 2007; Moritz et al., 2012). Urgently needed is a remote sensing-based forest vulnerability index (FVI) that explicitly tracks where and when forests are becoming increasingly vulnerable to drought and increased temperature stress, to assess potential climate change impacts on vegetation and associated feedbacks to the climate system (Allen et al., 2015; McDowell et al., 2008; Smith et al., 2014).

The majority of vulnerability assessments derived from space-borne data are conducted *a posteriori*, such that the disturbances (e.g., drought, wildfire, hurricane) had

to occur prior to research being conducted (Smith et al., 2014). Global drought monitoring approaches such as the widely applied Vegetation Temperature Condition Index and the more recently developed Global Terrestrial Drought Severity Index have proven effective at providing information on the extent and severity of drought events (Kogan, 1997; Mu et al., 2013). However, these metrics do not track longer term (multiple years to decades) forest stress trends, and lack the ability to deliver *a priori* information regarding where vegetation is likely becoming increasingly vulnerable to drought and increased temperature stress. An FVI at spatial and temporal scales relevant to land management that could be regularly updated would provide managers with knowledge of where and when forests are under multi-year stress so that proactive remedial actions could be better prioritized to have the greatest effect (Smith et al., 2014; Millar &Stephenson, 2015). Our objectives are to: 1) Develop an FVI that detects where and during which month of the growing season (April through October) forests are likely becoming increasingly vulnerable to climate-induced physiological stress associated with drought and high temperatures, and maps vulnerability across the Pacific Northwest region (PNW; Oregon and Washington) of the USA. 2) Understand the behavior of the FVI relative to its driving factors.

Land Surface Temperature and the Biophysical Link to Plant Canopy Stress

Climatological data can be developed for two kinds of surface temperatures: near-surface air temperature (T_{air}) and land surface temperature (LST) (Jin & Dickinson, 2010). T_{air} is measured 1.5 meters above the ground level at official weather stations with sensors protected from radiation and adequately ventilated (Karl et al., 2006). Many standard drought monitoring indices, such as the Palmer drought severity index (PDSI), rely on T_{air} from the weather station network. The inequitable distribution of weather stations over the global land surface and the lack of information in areas with sparse or no stations limit the drought monitoring capability and the spatial resolution of the output products based on T_{air} data (Kogan, 1997; Mu et al., 2007; Daly et al., 2008; Mu et al., 2013). Although correlated with T_{air}, LST differs from T_{air} in its physical meaning,

magnitude, and measurement techniques (Jin & Dickinson, 2010). LST can be estimated from measurements of thermal radiance coming from the land surface, retrieved from satellite, and mapped globally. LST from the Moderate Resolution Imaging Spectroradiometer (MODIS) measures the canopy foliage temperature in vegetated areas, a unique and useful ecological parameter because critical temperature dependent physiological processes and associated energy fluxes occur in the vegetated canopy. A global analysis of the relationship between remotely sensed annual maximum LST from the Aqua MODIS sensor and the corresponding site-based maximum air temperature for every World Meteorological Organization station on Earth showed that LST is more tightly coupled to the radiative and thermodynamic characteristics of the Earth's surface (Mildrexler et al., 2011b). LST is more sensitive to changes in vegetation density compared to T_{air} and captures additional information on the biophysical controls on surface temperature, such as surface roughness and transpirational cooling (Mildrexler et al., 2011b). We use LST rather than T_{air} to emphasize the direct thermal response of rising leaf temperatures and plant moisture stress associated with drought and increasing temperatures in the FVI.

The FVI and Its Conceptual Foundation

We developed a conceptual model to demonstrate the multi-year interactions of LST and water balance (WB) to developing forest stress and increasing vulnerability (Fig. 3.1). WB, calculated as precipitation minus ET (P-ET) and commonly used to represent regional water balance (Swenson & Wahr 2006; Mu et al., 2009; Zhang et al., 2009), is the net flux of water between the atmosphere and the biosphere. At the monthly timestep, P-ET provides a measure of the water surplus or deficit for the analyzed month. We refer to a positive WB (precipitation exceeds evaporative demand) as a *water surplus*, and a negative WB (evaporative demand exceeds precipitation) as a *water deficit*. During a water deficit, soil drying is occurring, and there is less water available for plants to transpire into the atmosphere. Changes in transpiration (latent heat flux) are directly coupled to leaf temperature such that an increase in canopy foliage temperature at

otherwise similar environmental conditions indicates reduced transpiration (Jones et al., 1999; Scherrer et al., 2011). Thus LST and WB generally have an inverse relationship whereby LST increases and peaks around mid-summer, commensurate with an increasing water deficit in the study area (Fig. 3.1). The pixel-specific monthly differences between normalized LST and WB result in a forest stress index (FSI) computed at monthly intervals over the growing season. In spring during low water stress conditions, forests dissipate incoming shortwave solar radiation efficiently through partitioning to the latent heat flux (LE) associated with transpiration, and thereby maintain canopy temperatures close to that of the surrounding air temperatures (Nemani et al., 1997; Mildrexler et al., 2011a). The FSI value associated with a water surplus and low thermal stress is low. In summer, increasing thermal and/or water stress has the effect of lowering midday transpiration and the associated LE (Manzoni et al., 2013). The increased partitioning of solar energy to the sensible heat flux results in a thermal response of rising leaf temperatures (Scherrer et al., 2011) and higher FSI values. The FSI peaks in July and August due to high temperatures and water deficits. During a multi-year drought event, thermal and water stress intensify across years resulting in interannual increases in the FSI values. Increasing FSI values for a given month across years translate into areas of increasing vulnerability detected by the FVI.

We demonstrated the conceptual model at the previously established Oregon Transect Ecosystem Research project sites, which cover much of the broad climate and biomass gradient found in the north-temperate zone (Peterson & Waring, 1994), particularly in the west (sites indicated by black stars on Fig. 3.3). Monthly LST and WB data (described in Data and Methods section) from a three by three 800-m grid centered on the six sites (Peterson & Waring, 1994) were plotted against each other as in the conceptualized model behavior to evaluate the LST and WB relationship (Fig. 3.2). The relationship supports the behavior of LST and WB conceptualized in the FVI model (Fig. 3.1) over the large temperature-moisture gradient and major vegetation zones sampled along the transect (Fig. 3.2). For example, at all six sites LST peaked around mid-summer commensurate with the largest water deficit reflecting the hot dry summers that

characterize the PNW region (Fig. 3.2). The magnitude of these fluctuations varied from the coastal forests (site 1) with relatively low summer LST and large annual WB fluctuations, to juniper forest in the high desert (site 6) with high summer LST and only minor fluctuations in WB due to the lack of rainfall. Higher mid-summer LST values were evident in the drier forest types located within the rainshadow of the Cascades Mountain Range (sites 5 and 6), and in the High Cascades due to high elevation (site 4). Mid-summer LST values were also relatively high and WB fluctuations dampened at site 2 owing to the rainshadow effect of the Coastal Mountain Range. The LST and WB (P-ET) terms used to develop the FVI closely track the dynamics of the climatic factors that limit vegetation growth in the PNW (temperature and water) (Churkina & Running, 1998; Nemani et al., 2003).

Data and Methods

Study area

The PNW region of the USA (Oregon and Washington) covers a broad range of forest types and associated (level 3) ecoregions (Fig. 3.3; Omernik, 1987). This study focuses on forests, and relies on a Forest Type Groups (FTG) map of the United States dataset developed by Ruefenacht et al. (2008). The maritime influence is strong in the Coast Range, West Cascades, Puget Lowland, and North Cascades, and thus these ecoregions contain moist FTGs such as Hemlock/Sitka Spruce, Douglas-fir, Fir/Spruce/Mountain Hemlock, and Alder/Maple (Fig. 3.3). The Eastern Cascades, Northern Rockies, and Blue Mountains ecoregions are in the rain shadow of the Cascades Mountains and thus harbor drier FTGs including Ponderosa Pine, Western Larch, Juniper, and drier Douglas-fir (Fig. 3.3). Fir/Spruce/Mountain Hemlock and Lodgepole Pine are present at higher elevations in eastside ecoregions. The forests of the Klamath Mountains are primarily classified as within the Douglas-fir FTG, but Ponderosa Pine, White Pine, and Western Oak is present. While the precipitation and temperature regimes and associated forest types vary substantially across the study area, the region shares a common climatic feature of little precipitation in summer months. This low summer

precipitation pattern results in typical dry conditions conducive to droughts (Bumbaco & Mote, 2010).

Datasets used to calculate the FVI

We utilize three datasets to map forest vulnerability due to drought and high temperatures across the study area; MODIS LST, MODIS ET, and Parameter-elevation Relationships on Independent Slopes Model (PRISM) Precipitation. These datasets provide systematic and continuous spatial information needed to develop repeatable, quantitative long-term measures of forest vulnerability for large areas.

Aqua MODIS land surface temperature (LST)

Two MODIS instruments, Terra and Aqua, monitor the Earth's LST as derived from the thermal-infrared (TIR) radiation emitted by the land surface (Wan & Li, 1997). The first MODIS instrument on the Terra platform was launched on December 18, 1999 and the second MODIS instrument on the Aqua platform was launched on May 4, 2002. The strengths of the MODIS instruments include continuous spatial coverage, high geolocation accuracy, high radiometric resolution, and accurate calibration in the visible, near-infrared and TIR bands (Wan et al., 2004a). MODIS LST data provides 1-km surface temperature measurements from clear-sky pixels retrieved from brightness temperatures in bands 31 and 32 with the generalized split-window algorithm (Wan & Dozier, 1996). LST from the Aqua MODIS sensor was chosen for this study because of Aqua's afternoon overpass time of approximately 1:30 pm, close to the maximum temperature of the land surface. Measurements close to the high temperature peak of diurnal fluctuation better reflect the thermal response of rising leaf temperatures due to decreased LE as stomata close, and soil litter surfaces dry, accentuating differences in LST among vegetation cover types (Mildrexler et al., 2011a). As a result, it is more suitable for some regional and global change studies and is particularly well-suited for investigations of drought-induced thermal stress (Wan et al., 2004a; Wan et al., 2004b). The high-quality satellite-derived LST datasets from MODIS are currently used for a

variety of applications including large-scale ecosystem disturbance detection (Mildrexler et al., 2009; Coops et al., 2009), drought monitoring (Wan et al., 2004b), land cover monitoring (Julien & Sobrino, 2008), agro-meteorology studies (Anderson et al., 2007), biodiversity studies (Albright et al., 2011), biophysical studies (Li et al., 2015), and have been proposed as an integrative global change metric (Mildrexler et al., 2011b). We derived monthly mean LST from the 1-km 8-day Aqua MODIS LST (MYD11A2) data for further analysis.

MODIS evapotranspiration (ET)

The MODIS ET (MOD16A2) data provides 1-km terrestrial modeled total evapotranspiration estimates at monthly intervals in mm/month for calculations of water and energy balance (Mu et al., 2011). The ET algorithm uses a Penman-Monteith approach driven by MODIS land cover, albedo, leaf area index (LAI) and Enhanced Vegetation Index, and daily surface meteorological inputs (Mu et al., 2011). Terrestrial ET includes evaporation from wet and moist soil, from rainwater intercepted by the canopy before it reaches the ground, and the transpiration through stomata on plant leaves and stems. MODIS ET was used to quantify the effects of land-use change associated with sugar-cane expansion on climate in the Brazilian Cerrado (Loarie et al., 2011), and the effects of afforestation on climate at high latitudes (Montenegro et al., 2009). The biophysical effects of global forest cover changes were examined using MODIS ET and other remote sensing datasets (Li et al., 2015). The MODIS ET is a key input in the Global Drought Severity Index (Mu et al., 2013) and has been used to assess spatial and seasonal patterns in ET across the pan-Arctic domain (Mu et al., 2009).

PRISM precipitation (P)

The PRISM data provides 800-m resolution total monthly precipitation (rain plus melted snow) in mm/month (Daly et al., 2008). The dataset is a spatial interpolation between observational surface stations. PRISM calculates a climate–elevation regression for each digital elevation model (DEM) grid cell, and stations entering the regression are

assigned weights based primarily on the physiographic similarity of the station to the grid cell (Daly et al., 2008). The PRISM method accounts for the major physiographic factors influencing climate patterns at scales of 1 km and greater and are the most accurate representation of the spatial climate patterns in the western USA (Daly et al., 2008). The PRISM datasets have been widely used in climatic and ecosystem response studies (http://www.prism.oregonstate.edu/documents/).

Input datasets and uncertainties

The MODIS LST products have been validated within 1 K at multiple sites in relatively wide ranges of surface and atmospheric conditions (Wan et al., 2004a; Wan, 2008). Refinements to the Version 5 LST product have minimized the main sources of uncertainty caused by cloud contamination and in accurately estimating the surface emissivity, and significantly improved the accuracy and stability of the MODIS LST products (Wan, 2008). For uniform land surfaces with known spectral emissivity characteristics, the uncertainty in LST retrieved by the generalized split-window algorithm could be equal to or smaller than 0.5 K (Wan & Dozier, 1989; Li & Becker, 1993). Since emissivity is well-known for dense evergreen canopies, our focus on the evergreen dominated forests of the PNW helps minimize uncertainty in the LST product (Wan & Li, 1997).

Uncertainty in the MODIS ET data primarily arise from input data sources and algorithm limitations (Mu et al., 2011). The MODIS product inputs and daily surface meteorological inputs can introduce biases to ET estimates that are difficult to detect (Mu et al., 2011). Algorithm limitations are in part due to the large number of physical factors involved in soil surface evaporation and plant transpiration processes. The MODIS ET product used in this study is based on an improved ET algorithm. An examination of the new ET product at 46 AmeriFlux eddy covariance flux towers showed that the improved algorithm estimates capture the magnitudes of the ET measurements better than the old ones, reducing the tower-specific mean absolute error of the daily ET from 0.39 mm

day−1 with the old algorithm to 0.33 mm day−1 (Mu et al., 2011). For an in-depth discussion of MOD16 ET see Mu et al., (2011).

Estimating uncertainty associated with the PRISM data is difficult because the true climate field is unknown, except at a relatively small number of observed points, which are themselves subject to measurement and siting uncertainties (i.e. relocations, changes in instrumentation and/or exposure, effects of land-use change, and changing observing practices; Pielke et al., 2007), and are incorporated into the PRISM dataset itself (Daly et al., 2008). However, a comparison of PRISM with a dynamically downscaled weather model (Weather Research and Forecasting model (WRF)) of winter precipitation over complex terrain revealed that the two datasets provide a very similar overall map of precipitation, with only localized differences, demonstrating a level of model simulation skill that has heretofore been lacking (Gutmann et al., 2012). Comparison with WorldClim and Daymet datasets demonstrated the benefits of using a relatively dense station dataset, and the physiographically sensitive PRISM interpolations process resulted in substantially improved climate grids over those of WorldClim and Daymet (Daly et al., 2008). Greatest improvements were in the mountainous and coastal areas of the western USA.

Forest vulnerability index (FVI)

The FVI is based on the FSI (Fig. 3.1) calculated at the pixel level for each month, from April through October, from the first full year of Aqua LST data (2003) through 2012. This seasonal period captures the primary physiologically active months for plants during which thermal and water stress tend to occur in our study region, and includes the onset and alleviation of these seasonal stress cycles. The ET and monthly mean LST were resampled using bilinear interpolation from 1-km to 800-m to match the precipitation resolution. The FTG data were resampled to 800-m using a majority rule and used as mask to isolate forests in the LST and WB datasets. To contrast LST and WB, as per our conceptual model, it was necessary to normalize those datasets, which was done at the FTG level. The normalized LST and WB were calculated as:

$$Z_i = \frac{y_i - \bar{y}}{\mathrm{SD}_y} \qquad (1)$$

where y_i is either the LST or WB for pixel *i* for a given month in a given year, and $\bar{y}$ and SD_y are the average and standard deviation of LST or WB, respectively, across months (April – October) and years (2003 – 2012). The FSI was calculated as

$$FSI = LSTz - WBz \qquad (2)$$

where *FSI* is the forest stress index value computed, and *LSTz* and *WBz* are the normalized LST and WB, respectively.

The FVI describes the interannual trend (2003 – 2012) of the FSI, on a per month basis for each month from April to October, computed at the FTG level. FVI is the slope of the monthly values across years (Fig. 3.1), as calculated using ordinary least square regression. We chose a *p*-value of 0.1 to declare statistically significant positive or negative FVI slopes to evaluate vulnerability for this initial application, but any *p*-value could be chosen. This results in three general potential FVI outcomes for any given pixel on the landscape: a (1) positive or (2) negative statistically significant FVI slope, and (3) statistically insignificant slopes.

Filtering abrupt disturbances

Abrupt, higher intensity disturbances such as wildfires and harvesting can have significant effects on LST and WB, resulting in positive FVI values that are not of interest for this application. To mask these disturbances, the year and magnitude of abrupt disturbances (less than 4 years in duration) were mapped in this study using the Landsat-based detection of Trends in Disturbance and Recovery (LandTrendr) algorithm (Kennedy et al., 2010). We calculated the proportion of disturbed Landsat pixels, weighted by magnitude, within each 800-m pixel from 2000 to 2012. All pixels with weighted disturbance >30% were masked, following Sulla-Menashe et al. (2014). There is no FVI value associated with masked pixels.

Understanding FVI behavior in relation to driving factors

To understand the behavior of the FVI in relation to LSTz and WBz, we computed the slopes of the monthly FSI components, LSTz and WBz, as was done to calculate the FVI from the monthly FSI values. To determine the upper and lower thresholds for mapping the LSTz and WBz consistently across months, positive and negative slopes were separated for each month. For pixels having statistically significant FVI values (both positive and negative), the corresponding LSTz and WBz slopes were extracted and ranked separately for the positive (ascending) and negative (descending) slopes. Once ranked, the values that correspond to the 95^{th} percentile from the zero point were found for each set of positive and negative slopes for each month. The maximum (positive slopes) and minimum (negative slopes) of the 95^{th} percentile values were then applied to map the scale range for each month.

Linking the FVI to observable stress and mortality

Connecting the FVI to the physical expression of vulnerability, such as reduction in leaf area, growth decline, and mortality is a critical step that needs to be explored in detail. For this initial application, we choose to look for direct visual evidence of canopy die-off and mortality in association with positive FVI areas in Google Earth. A random sample of 132 points was established across Oregon and Washington in forest areas not impacted by abrupt disturbances. At each point, the corresponding 800-m FVI pixel boundary was extracted and imported into Google Earth for visual interpretation. Then, using the time series of high resolution Google Earth images over the study period, presence of stress and mortality (dead and dying trees) was recorded at each plot based on visual interpretation. Pixels that contained widespread canopy die-off and/or mortality, indicated by the presence of dead or dying trees spread across the pixel area, or that contained large patches of mortality, indicated by groups of adjacent dead or dying trees, were recorded as stressed. All other pixels were recorded as background mortality. Correspondingly, each pixels slope (FVI value) and *p-value* were extracted. Since the *p-*

value declares a FVI value statistically significant, we plotted the proportion of observations labeled as stressed against *p-value*.

Results

FVI maps

From April to October, we see interesting trends in the FVI from 2003 to 2012 (Fig. 3.4, top panel). As per our conceptual model, positive FVI values (*p-value* < 0.1) denote increased vulnerability. Negative values, although not explicitly considered in our conceptual model, do have potentially important implications (see Discussion section). Close examination reveals that positive FVI values do not appear until the month of July, and are few and scattered in the southern Blue Mountains and southern East Cascades ecoregions. In August large patches of increased vulnerability emerge in the Blue Mountains, East Cascades, West Cascades, and Klamath Mountains. Positive FVI values can be found in every ecoregion in the study area during August. Additionally, August is a major transition period for the trajectory of the FVI values and thus had the most mixed patterns of positive and negative FVI values of any month (Fig. 3.4). Area experiencing increased vulnerability peaked in September and is most prevalent in the relatively dry Northern Rockies, East Cascades and Blue Mountains ecoregions, but is also widespread in the Oregon portion of the Coast Range and West Cascades. The Blue Mountains are notable for their concentration of area with increased vulnerability in the southeast and northeast portions of the ecoregion in September. Interestingly, the large patches with positive FVI in August do not persist through September. In October there were no positive FVI values.

The area covered by negative FVI increased from April through June. In April and May negative FVI values were limited to portions of the Coast Range, Puget Lowland, Cascades, and Northern Rockies. Then in June and July negative FVI was widespread across all forested ecoregions (Fig. 3.4). Only a small area was covered by negative FVI values during August, and these were essentially absent in September. In

October areas of negative FVI again increased in all ecoregions except the Puget Lowland.

The large area of positive FVI values detected in central Oregon during August (Fig. 3.4) is associated with Juniper forests (Table 1). The proportion of the Juniper FTG with increased vulnerability was nearly threefold higher in August than in September (Table 1). California Mixed Conifer had the second highest proportion of area affected by increased vulnerability in August (12.3%), and a lesser amount in September, although not nearly as dramatic a decrease as for Juniper. Western Oak also had a greater proportion of positive FVI values in August than in September. However, for most FTGs the area of increased vulnerability peaked in September. For example, in the Ponderosa Pine FTG, the area of increased vulnerability went from 5% in August to 32.9% in September. Western Larch went from a very low positive FVI proportion in August, to the second highest in September (25.8%). Both of these FTGs are primarily located in the East Cascades, Blue Mountains, Northern Rockies, North Cascades, and are locally abundant in some areas of the Klamath Mountains ecoregions (Fig. 3.3). In the Douglas-fir FTG, the most important in terms of total areal coverage, the area of vulnerability increased substantially from August (1.1%) to September (7.6%). Hemlock/Sitka Spruce and Alder/Maple were least affected by increased vulnerability in August and September (less than 2%, Table 1), and these FTGs are concentrated within the moist Coast Range and Puget Lowland ecoregions. Lodgepole Pine and Fir/Spruce/Mountain Hemlock showed large increases in area affected by increased vulnerability from August to September. These FTGs tend to occupy higher elevations characterized by extreme annual climatic variations (Coops & Waring, 2011).

Behavior of the FVI

The slopes of LSTz (middle panel) and WBz (lower panel) for each month where positive and negative FVI values were detected illustrate the interactions that drive the FVI (top panel) (Fig. 3.4). Areas experiencing negative FVI from April through October are highly consistent with areas experiencing decreasing interannual monthly

temperatures (LSTz slopes). From April through July, area showing decreased temperatures in association with negative FVI increased from largely the North Cascades, Northern Rockies, and West Cascades to the whole study region. In August, as temperature trends turn from decreasing to increasing, the first major areas of positive FVI values appear with increasing temperature trends in the western Blue Mountains and the southern East Cascades. In September, as positive FVI values surface fully, LSTz slopes are positive.

Trends in water balance (WBz slopes) follow generally similar trends in relation to FVI as trends in temperature, with some notable exceptions in June and July. In June, in the northwest part of the study area, especially the northern Coast Range and the northern part of the North Cascades, trends in water deficit were positive, even while trends in the remaining study area were largely in the opposite direction. Interestingly, locations where there has been a decreasing trend in WBz slopes are locations where there has also been a trend towards decreasing LSTz slopes, the combined effect of which has been towards negative FVI values, consistent across the study area more broadly. In July, we see decreasing WBz slopes across large areas of the east-southeast region of the study area, but little to no effect on the FVI turning positive, suggesting a need for tight coupling between trends in LST and WB to turn the FVI positive. August is interesting because while the areal extent with negative WBz slopes decreased across the east-southeast region, some locations where the Juniper type group experienced a positive FVI (Table 1) were affected more by negative trends in water balance than trends in temperature, a relative anomaly in this regard. In September, where we saw the most dramatic increases in FVI values, there was a tight coupling between trends in both driving variables.

FVI vs. stress and mortality observations

The comparison between the FVI and stress and mortality observed in Google Earth revealed that as *p-value* associated with FVI decreased, the proportion of stressed plots increased, confirming that positive FVI areas with very low *p-values* (high

statistical significance) are associated with greater amounts of stress and mortality (Fig. 3.5). Below a *p-value* of 0.05 (dashed line) the proportion of stressed plots rapidly increased in association with these lower and more significant *p-values* (Fig. 3.5). Stressed plots were also present at higher *p-values*, although at lower proportions, possibly highlighting the limitations in directly linking an 800-m integrated pixel with visual observations of mortality in Google Earth.

Discussion

A growing number of studies have linked forest stress and mortality to drought and increased temperature stress (van Mantgem et al., 2009; Breshears et al., 2009; Williams et al., 2013; Coops & Waring, 2011; Allen et al., 2010; Anderegg et al., 2013; Griffin & Anchukaitis 2014; Martinez-Vilalta et al., 2012; Pravalie et al., 2014) highlighting the urgent need for metrics that can show where these changes are occurring (Smith et al., 2014; Allen et al., 2015). In response we developed and described in detail a new index, the FVI, for large-scale assessment of forest vulnerability to drought and high temperatures and applied it across the PNW region of the USA from 2003 to 2012. The FVI is based on a measure of instantaneous stress levels over the growing season, the FSI (Fig. 3.1). The conception of forest vulnerability as statistically significant trends in the FSI for each month across years is a potentially important new way to monitor forest vulnerability. The FVI characterizes interannual trends in the FSI, highlighting months where forest areas are experiencing longer-term increasing temperatures and water deficits, which does not coincide with the month of peak stress annually in our study region. The highest FSI values were detected during July (data not shown), but the FVI for July was largely decreasing, while the peak months for the FVI were in August and September (Fig. 3.4). It should be noted that negative trends in the WBz (WBz slopes) do not automatically translate to monthly WBz values that are negative. Even though there is a declining trend for a given month in the WBz values (a negative WBz slope), the values themselves can still be positive. This could be an important factor in why, even though there were negative WBz trends for large areas in June and July, slopes in temperature remained negative resulting in a negative FVI. Further study of the joint relationships of

opposing temperature and water balance slopes, by FTG, is important, and could reveal some interesting physiological and/or biophysical setting that predisposes a given forest type to increasing vulnerability.

The FVI growing season monthly assessment across the PNW reveals a possible trajectory toward more extreme conditions indicated by negative FVI values in the spring, followed by a rapid transition to widespread positive FVI values that peak in August and September (Fig. 3.4), depending on forest type (Table 1). Positive FVI values tend to be associated with drier forest types and ecoregions. The proportion of a given FTG with positive FVI values generally increased from August to September, although there were a few notable exceptions that peaked in August (Juniper, California Mixed Conifer, and Western Oak). This indicates that peak vulnerability occurs at different times of the growing season for different FTGs, and there may be different sensitivities to the types relative to the others with respect to the driving variables. The normalization of LST and WB by FTG was critical for elucidating these FTG-specific responses.

It is important to note that the monthly interval used in this study may not be ideal for capturing when peak FVI values occur. For example, it is possible that the second half of August and the first half of September are key periods, and that the arbitrarily defined monthly boundaries used here diminish some of the FVI signal. Furthermore, the timing of peak vulnerability will likely change outside of the study area because LST and WB relations will vary with local conditions. However, the conceptual approach, developed and tested here should be relevant as an indicator of increasing forest vulnerability to climate change more globally. Future work should explore how to fine-tune the analysis to better elucidate peak FVI periods and the dynamics of landscape transition periods where FVI values are shifting from negative to positive, such as observed here during July and August. Moreover, although negative FVI values were not explicitly considered in the conceptual development of the FVI, their emergence towards increasing areal importance leading up to August and September suggests that the PNW region is experiencing more extreme climate conditions from cooler and moister conditions in the fall, spring, and early summer months to warmer and drier conditions in the mid- to late-

summer months. The implication of this on the vegetation could be dramatic in the long term.

Peak vulnerability occurred during September for the majority of FTGs in this study (Table 1). In accordance with these findings field work in southwestern Oregon has shown that peak moisture stress usually occurs in September near the peak of drought (Waring, 1969). Close examination of the September FVI reveals important ecological patterns (Fig. 3.4). Large forested areas with positive FVI values were detected along semi-arid ecotones in the Northern Rockies, Blue Mountains, and Eastern Cascades ecoregions. Ecotonal shifts in vegetation distribution due to climate change are expected to be most rapid in semi-arid ecotones (Allen & Breshears, 1998). The drier FTGs that occupy the ecotonal boundaries also have the most positive FVI values, especially Ponderosa Pine in September and Juniper in August, but also Fir/Spruce/Mountain Hemlock in September (Table 1). Even in the relatively wet Puget Lowland, area of positive FVI was detected within the rain shadow of the Olympic Mountains. In agreement with previous research, our results indicate that increased vulnerability tends to be associated with drier conditions (Steinkamp & Hickler, 2015; Allen et al., 2010). But, even further, we have detected positive FVI values concentrated in the southern portions of the relatively moist Oregon Coast Range and West Cascades ecoregions. A latitudinally-induced hydrological gradient extends from relatively wet northwest Washington, to drier southwest Oregon. Within relatively moist ecoregions we found a potential increase in vulnerability associated with drier environments. Lending confidence to this finding is the fact that the FVI is computed specific to each FTG, accentuating differences along within class moisture gradients. Juniper and Western Oak type groups both peaked in August, and then showed relatively large decreases in their proportion with positive FVI values in September. The Juniper group occupies areas that receive very little annual precipitation and experience extreme summer drought (Fig. 3.2), whereas Western Oak occupy a broader range of climates in our study area, including lower elevations in the interior valleys characterized by hot, dry summer conditions. By September, these areas may be so dry that further increases in LST and

water deficit do not occur. However, a drying trend in August, when some moisture is still available, may have resulted in the negative WBz slopes and mildly increased temperature trends driving the positive FVI (Fig. 3.4).

As seen in the PNW region, the FVI and its input variables are valuable for understanding how temperature and water balance patterns change and interact over the course of the growing season. Prior to the summer drought cycle, an interesting interaction occurs when the WBz slopes begin turning negative (July) earlier than the LSTz slopes (August) (Fig. 3.4). The negative LSTz slopes in July indicate that forests have access to groundwater enabling transpirational cooling of the canopy, an important factor in determining the negative FVI in July (Fig. 3.4). This suggests that future changes in the hydrologic cycle that affect the spring water balance could have important implications for water availability heading into the summer drought cycle in the PNW. These interacting changes include reductions in snowpack (Mote et al., 2005), changes in the rain-snow transition zone (Klos et al., 2014), and changes in spring precipitation (Mote et al., 2010). Changes that cause a shift toward negative WB trends earlier in the growing season will likely result in a commensurate earlier increase in LST trends, driving earlier positive FVI values. Some models project increases in spring precipitation in the PNW ranging from 3% to 8% (Mote et al., 2010). Increasing spring rains could help to maintain positive water balance trends later into the growing season by replenishing soil moisture and buffering forests heading into the impending summer drought cycle (Bumbaco & Mote, 2010). These future WB and LST trends could have important effects on forest vulnerability in the PNW in the coming decades.

The interpretation of FVI significance in relation to *p-value* is critical. With only ten years of data for this initial application, we chose a *p-value* of 0.1 to maintain a relatively conservative threshold, but also to increase the expression of potentially ecologically important vulnerability patterns, beyond the more conventional 0.05 threshold. As we lengthen the data record, it is likely that some trends may reverse themselves over different time scales. We will need to consider the appropriate time scale to examine the trends in the FSI that drive the FVI. A temporal segmentation approach of

the FSI (e.g., the LandTrendr algorithm, Kennedy et al., 2010) may help capture distinct trajectories that relate to FVI changes. Incorporating temporal segmentation into the analysis will also help minimize the effects of initial conditions which have leverage in context of regression on trend estimates. A drought event occurred in 2003, the first year of our study (Bumbaco & Mote, 2010). This resulted in relatively high FSI values in August and September. However, the landscape still has momentum in the positive FVI direction in many different ecoregions driven by warming (positive LSTz slopes) and drying trends (negative WBz slopes) once the full decade is considered (2003 – 2012) (Fig. 3.4). This indicates that the longer term increases in the FSI trend were not diminished by what can be considered conservative initial conditions. The August and September *p-value* maps show a large shift in the distribution of values across the landscape during those two months (Fig. 3.6). Adjusting the *p-value* would have a larger effect on the FVI in September than August due to the different distributions. However, for both months incremental *p-value* adjustments relative to the 0.1 threshold changes the expression of FVI values mostly along the borders of positive FVI areas. Decreasing the *p-value* threshold to 0.05 would result in fewer positive FVI values during September, but the geographic pattern would remain similar with most positive values detected in the Northern Rockies, Blue Mountains, East Cascades, West Cascades, and Oregon Coast Range. Of related importance are the effects of abrupt disturbances on the FVI. The threshold used to filter abrupt disturbance can be changed to examine the effects of more conservative vs. more inclusive thresholds on forest vulnerability patterns. Lowering the threshold below the weighted 30% proportion used in this study would result in increased confidence of removing areas affected by relatively small disturbances, but may also increase errors of commission. Thresholds could also be determined for specific areas. For example, a lower threshold may be desirable in areas dominated by harvest, whereas a higher threshold may be better suited for areas primarily affected by large-scale natural disturbances. The ability to adjust the *p-value* and threshold used to filter abrupt disturbances give the FVI an interactive component that scientists or forest managers (or other users of FVI maps) can adjust for their own assessment needs.

The areas that the FVI identified as increasingly vulnerable to the effects of climate change are either likely to exhibit visible health and vigor effects in the immediate future or are already exhibiting those effects (Fig. 3.5). Vulnerability often differs by species and with changing environmental conditions. In our study area sensitivity to drought varies along an elevational gradient. Dry forests at relatively low elevations have high tolerance for drought, whereas high elevation forests have low tolerance for drought, and mid-elevation forests have medium tolerance (Haugo et al., 2010). Climate change has increased the exposure of high and mid-elevation forests to drought and high temperatures and, consequently, increased mortality in these systems (Westerling et al., 2005). Therefore in our study area we expect that mortality rates should be more sensitive to increased positive FVI values in high elevation FTGs that exhibit limited drought tolerance (Fir/Spruce/Mountain Hemlock and Lodgepole Pine in Table 1). Conversely, drought tolerant species like ponderosa pine have adaptations to drought such as sparse canopies, deep rooting systems, and changes in biomass allocation, that balance reduced productivity in the short term with drought stress avoidance over the long term (Delucia et al., 2000; Williams et al., 2001). Therefore, increased stress associated with positive FVI may not as readily manifest as elevated mortality in drier portions of our study area (Haugo et al., 2010). Preliminary examination between the FVI and mortality measurements from the Forest Inventory and Analysis (FIA) plots across Oregon and Washington confirms this expectation (data not shown) and indicates a possible greater sensitivity of mortality to a high proportion of positive FVI in high (Fir/Spruce/Mountain Hemlock and Lodgepole Pine FTGs) and mid-elevation forests (Western Larch and Douglas-fir FTGs), relative to low elevation forests (Ponderosa Pine, Juniper, Tanoak/Laurel, and Western Oak). Calculating the FVI at the FTG level is essential for varying the interpretation of the FVI in relation to the different FTG tolerances for drought and high temperatures.

This paper has focused on the conceptual development and application of the FVI in response to the profound ecological and societal implications of global forest vulnerability to hotter drought (Overpeck, 2013; Joyce et al., 2014; Allen et al., 2015).

The FVI is based on first principles relating canopy water and energy fluxes to changes in climate. We have shown that the FVI areas with low *p-values* (< 0.05) are associated with greater amounts of mortality (Fig. 3.5). We now need to demonstrate the value of the FVI in relation to a more robust vulnerability signal (i.e. changes in canopy condition, leaf area, and growth rates). As increasingly hot and dry conditions cause reductions in leaf area (Dobbertin et al., 2001; Solberg et al., 2004), these changes will be commensurate with a reduction in ET and an increase in LST, thus changing the FVI. It is important to understand the sensitivity of the FVI to leaf area change, and to separate interannual variability in the plant communities LAI from steady reductions of leaf area over years (Delucia et al., 2000). Examining the LST and WB variables in isolation will help to elucidate the relationship between changes in leaf area, and the effects on the FVI. Hotter and drier conditions may also cause stomatal closure earlier in the growing season, invoking an earlier increase in LST, with possible feedbacks on vulnerability later in the growing season. These and other complex questions that integrate the timing of changing ecological responses reaffirm the need for products such as the FVI as inputs to empirical models (Allen et al., 2015). Moreover, it is necessary to link the FVI with ground-based measurements that record the visual health effects of the forest, structural and compositional states, and growth measurements to examine the relationship between the FVI, and changes in canopy condition and forest growth. The 800-m resolution of our region-wide vulnerability assessment presents a scale mismatch for directly linking the FVI to changes in forest canopy condition and/or growth rates associated with forest stress. To address this scale mismatch we are developing a framework that integrates the FVI with Landsat data, FIA data, and individual-tree models in an effort to link all the relevant scales that influence forest vulnerability. Landsat time series (LTS) data is promising due to its 30-m resolution and distinct spectral trajectories. Long, slow declines in the spectral trajectory of LTS data imply a slow and subtle process for forest change unfolding over many years (Kennedy et al., 2010). However, before meaningful comparisons can be made with the FVI, it is essential to characterize the relationship between the LTS spectral signature and declining canopy condition, just as was done for

the LTS spectral trajectories associated with insect activity of varying duration and severity (Meigs et al., 2011).

Conclusions

We developed a FVI that identifies when and where forests have been experiencing increasingly high surface temperatures and greater growing season water deficits. Our method takes a direct approach to monitoring concurrent changes in canopy water and energy exchange processes that have clear mechanistic links to the effects of drought and high temperatures on vegetation (Fig. 3.1). By directly linking LST to WB for each month (April through October) across years (2003 through 2012), we have characterized how the monthly LST and WB trajectories change in relation to one another over the growing season to express the FVI. This has revealed that positive FVI slopes can result from multiple LST and WB slope combinations, such as occurred during August and September in the PNW (Fig. 3.4).

Ten years of observations from MODIS data are insufficient to establish long-term patterns or thresholds after which die-off might occur (Hilker et al., 2014). However, our results show a clear trend toward warmer and drier conditions in August and September across a variety of ecoregions and FTGs. If this trend continues, it portends increased forest stress and die-off in the PNW. With longer periods of observations we will be able to temporally segment these trends into periods of increasing and decreasing climate-induced stress, so that the FVI will serve as a monitoring tool for where and when different forest areas are vulnerable, and perhaps amenable to management intervention.

The FVI conceptual foundation is robust across one of the largest hydrological gradients in North America (Fig. 3.2) indicating that the metrics may be transferable to different ecosystems and larger areas, especially those characterized by a summer seasonal drought cycle. However, we emphasize that the WB and LST relations, and thus the joint influence on the FVI, will vary with local conditions. Examining the WB and LST relations in different areas, such as we did across the PNW (Fig. 3.2), is a good

starting point for conceptualizing the joint behavior of LST and WB in relation to the FVI.

Acknowledgments

This work was supported by the USDA Forest Service, Region 6 Climate Change Program, and the Graduate School and the Department of Forest Ecosystems and Society at Oregon State University. We thank Maosheng Zhao for providing the MODIS datasets and Robert Kennedy for use of the LandTrendr data.

Figures and Tables

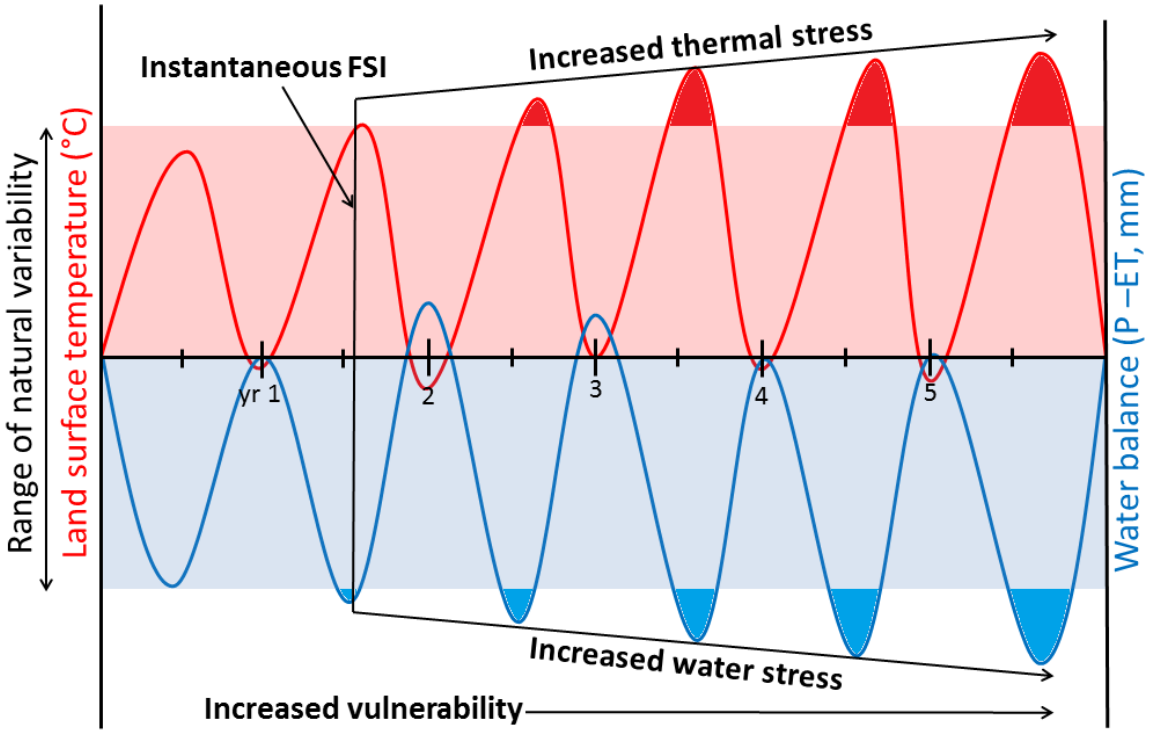

Figure 3.1. Conceptual model for the FVI, showing annual fluctuations in LST and WB for a hypothetical land area (or pixel) through time. As the water deficit increases during drought (increased water stress), LST also increases beyond the range of natural variability (increased thermal stress).The FSI is an instantaneous measure of the difference between normalized LST and WB variables. The FVI translates the increasing FSI values across time into increasing vulnerability.

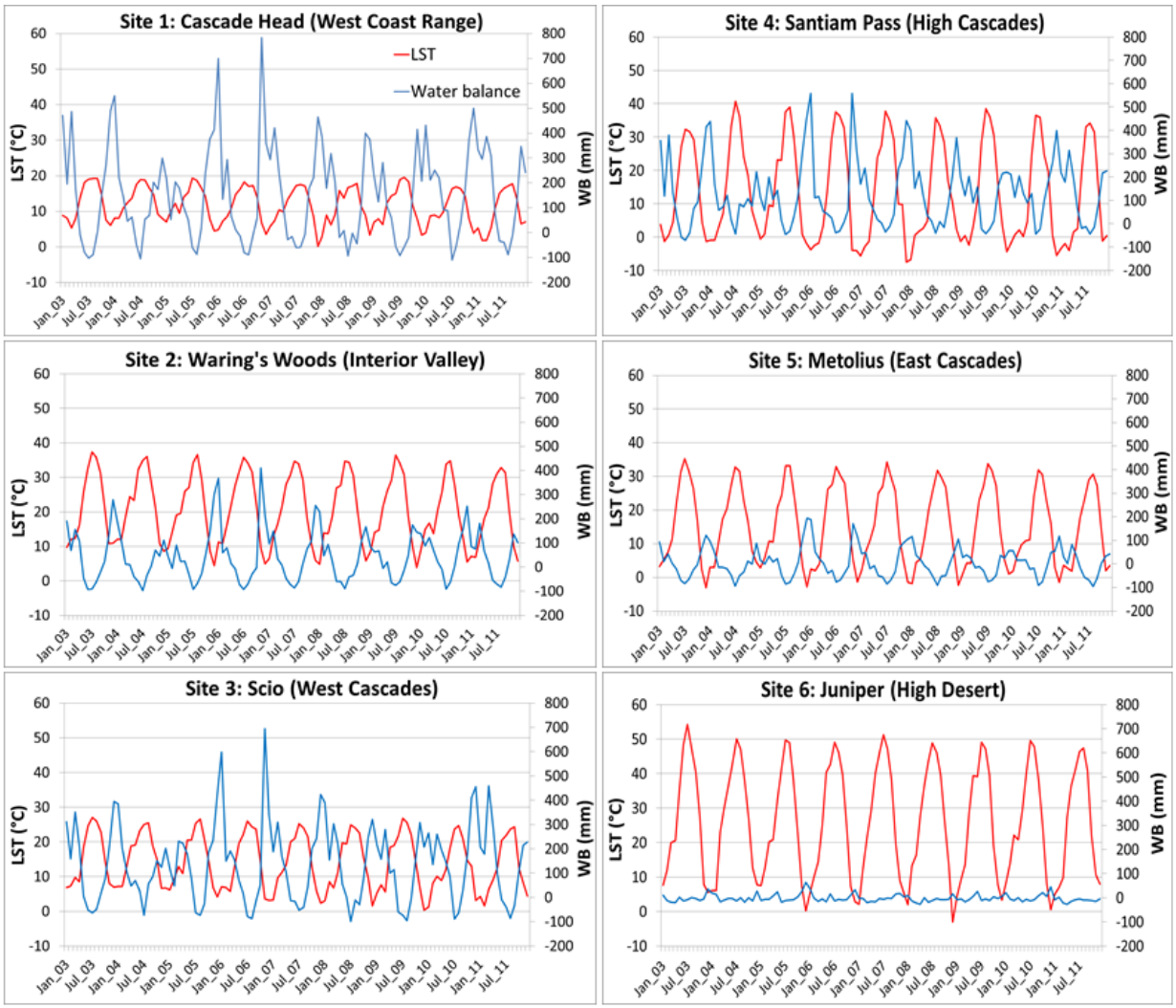

Figure 3.2. LST and WB datasets across the Oregon Transect support the FVI conceptual model (Fig. 3.1) and reflect the different climatic regimes and major vegetation zones sampled along this large temperature-moisture gradient. Major vegetation zones: Site 1: Sitka Spruce; Site 2: Douglas-fir; Site 3: Douglas-fir; Site 4: Subalpine; Site 5: Ponderosa Pine; Site 6: Juniper.

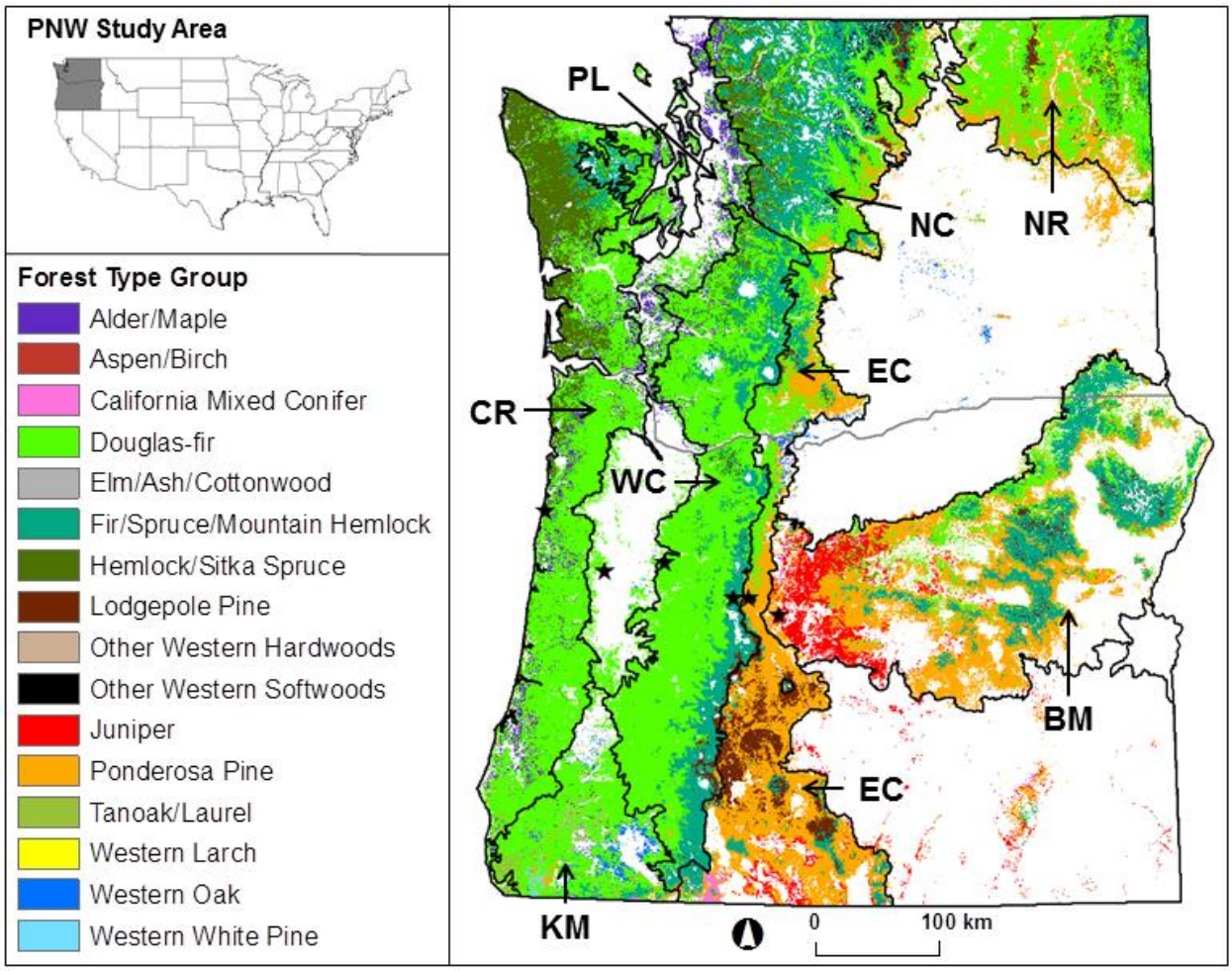

Figure 3.3. Study area (PNW; the States of Washington and Oregon, USA) showing the locations of each FTG and Level 3 Ecoregion boundaries (black lines) from Omernik (1987). Spatial distribution of FTGs reflect the dominant west-to-east moisture gradient resulting in drier FTGs (Ponderosa Pine, Juniper) in the east part of the study area. Ecoregion abbreviations: CR: Coast Range; WC: West Cascades; EC: East Cascades; NC: North Cascades; NR: Northern Rockies; BM: Blue Mountains; KM: Klamath Mountains; PL: Puget Lowland. Black stars indicate location of Oregon Transect sites evaluated in Figure 3.2.

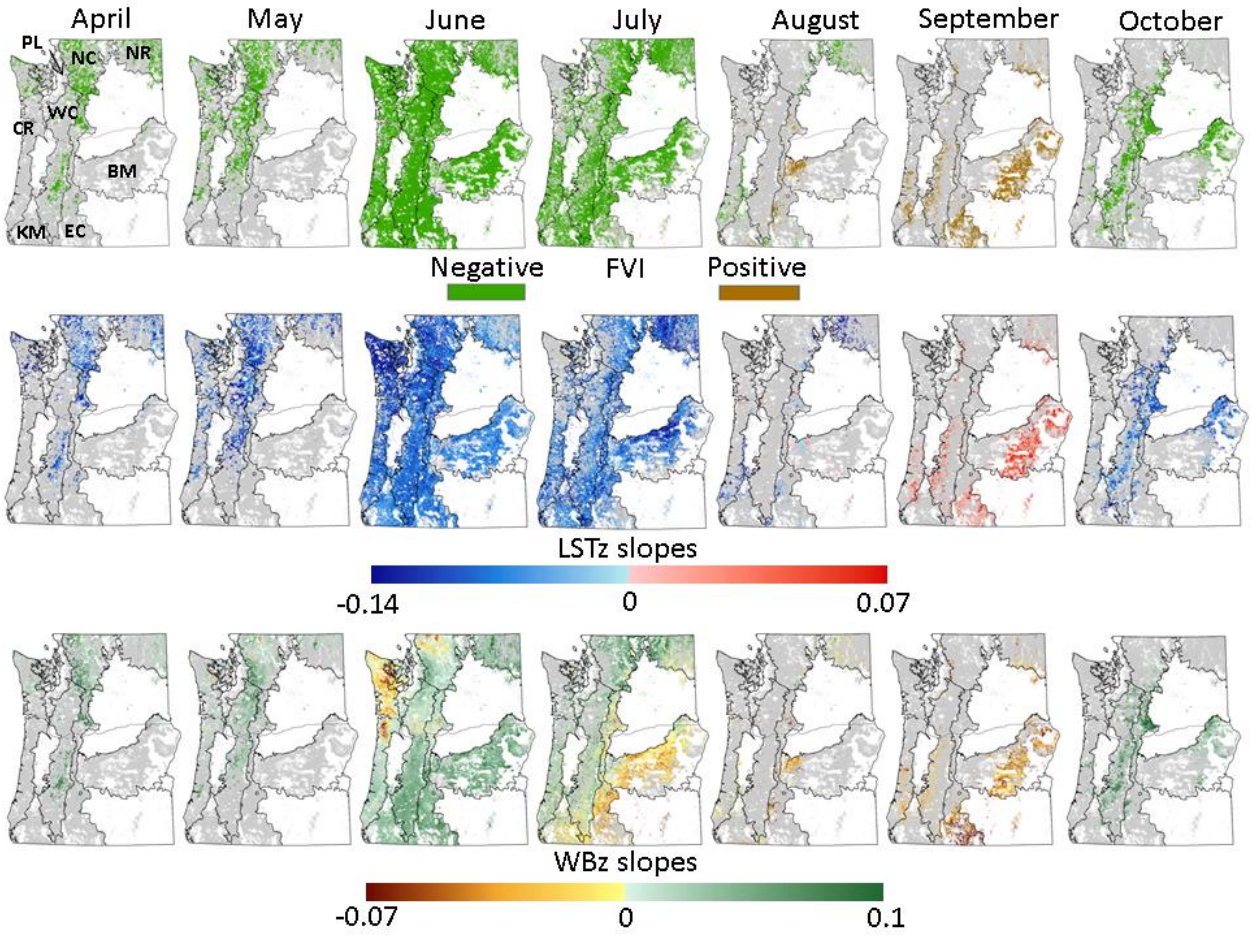

Figure 3.4. FVI results for the forests of Oregon and Washington from 2003 to 2012, masked by significance (top panel; p-value < 0.1). For simplification, all positive and negative values were collapsed into single classes. The slopes of LSTz (middle panel) and WBz (lower panel) for each month where positive or negative FVI values were detected illustrate the interactions that drive the FVI. The scale range corresponds to the global maximum (positive slopes) and global minimum (negative slopes) of the 95th percentile values from the zero point for each month.

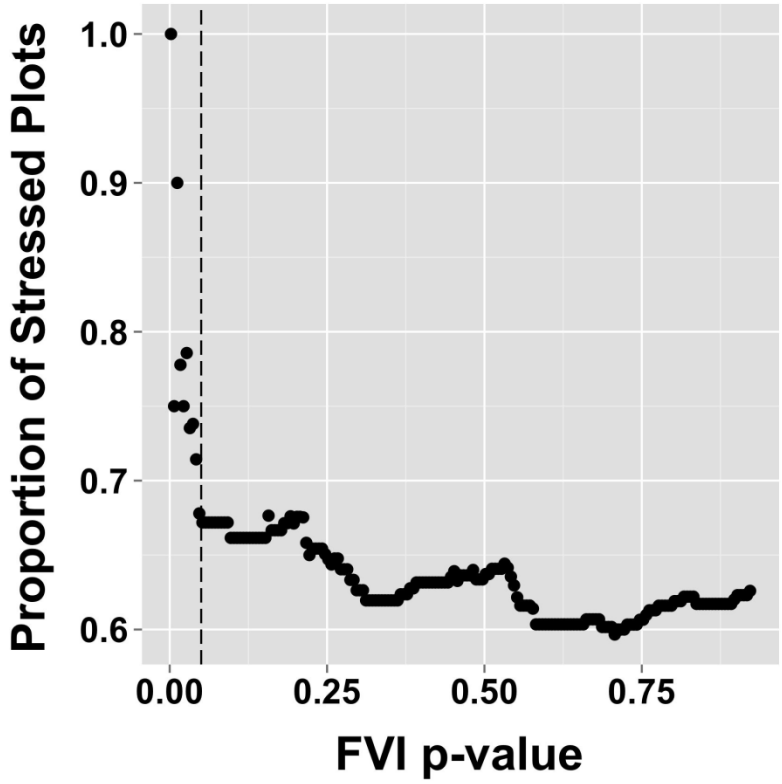

Figure 3.5. The proportion of stressed plots, as observed in Google Earth, relative to changes in FVI statistical significance (p-value).

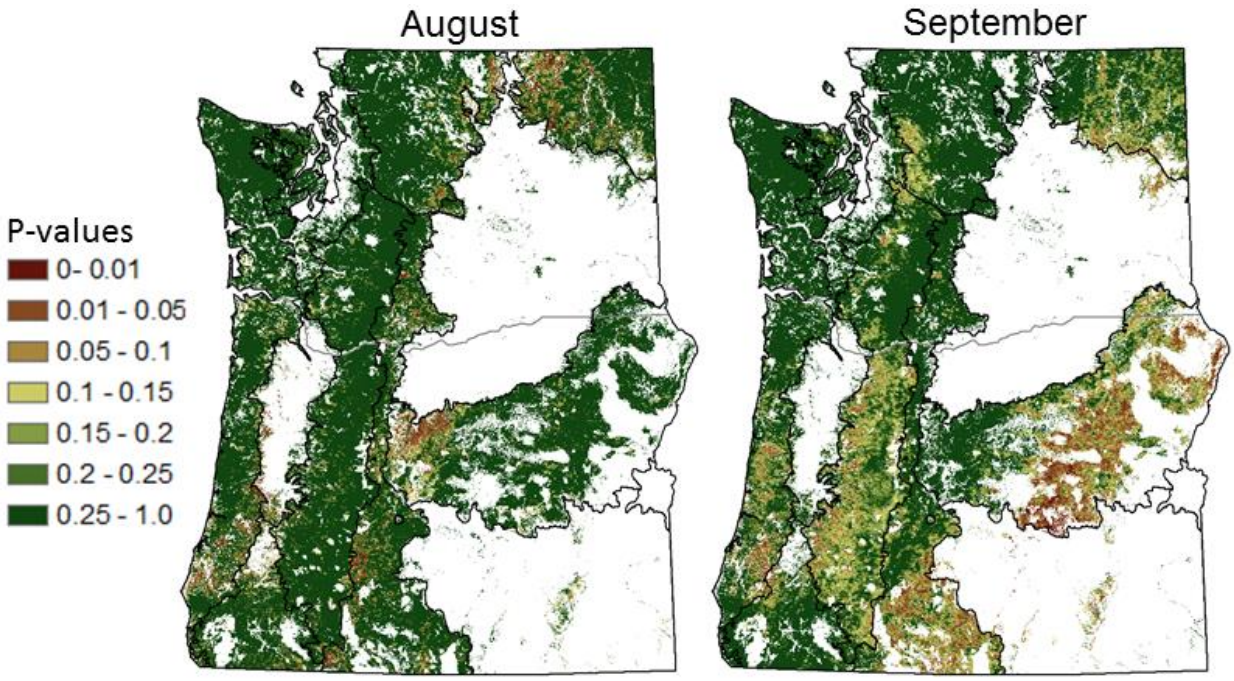

Figure 3.6. P-values associated with FVI for August and September, 2003 to 2012.

Table 3.1. The total area of each FTG, the area not impacted by abrupt disturbances and the proportion/area with positive FVI values relative to the area not impacted by abrupt disturbances during August and September (p-values < 0.1).

		Area not abruptly	Positive FVI area			
	Total area	disturbed	August		September	
Forest Type Group	(km^2)	(km^2)	(%)	(km^2)	(%)	(km^2)
Juniper	7127	7060	29.0	2047	10.4	733
Douglas-fir	104988	98993	1.1	1093	7.6	7544
Ponderosa Pine	41551	39827	5.0	1998	32.9	13084
Western White Pine	205	10.24	0.0	0	0.0	0
Fir/Spruce/Mountain Hemlock	36797	35163	0.9	324	14.6	5151
Lodgepole Pine	6917	6389	4.8	308	21.0	1340
Hemlock/Sitka Spruce	14344	13242	0.8	100	1.5	200
Western Larch	518	507	0.9	4	25.8	131
Other Western Softwoods	807	697	0.8	6	3.8	26
CA Mixed Conifer	673	657	12.3	81	10.0	66
Elm/Ash/Cottonwood	265	255	3.5	9	3.3	8
Aspen/Birch	63	63	2.0	1	7.1	4
Alder/Maple	7361	7119	0.2	14	1.4	99
Western Oak	1559	1430	4.7	68	0.7	10
Tanoak/Laurel	838	740	0.1	1	0.8	6
Other Western Hardwoods	671	659	1.9	13	1.8	12
Combined total	224684	212811		6066		28413

Chapter 4: Exploring the relationship between short-term climate trends and the Swiss needle cast epidemic in Oregon's public and private coastal forestlands

David J. Mildrexler[1], David C. Shaw[1], Warren B. Cohen[2]

[1] Oregon State University, College of Forestry, Corvallis, OR USA

[2] USDA Forest Service, Pacific Northwest Research Station, Corvallis, OR USA

Abstract

Swiss needle cast (SNC) is a fungal disease of Douglas-fir (*Pseudotsuga menziesii*) that is having important consequences on tree growth in the Pacific Northwest (PNW) region of the USA. Once considered innocuous in PNW forests, SNC symptom expression has increased rapidly in extent and intensity in recent decades. Previous research has linked the disease epidemiology of SNC to climate, and observations indicate a link with forestry practices of the 20th century as well. In this study, we investigate the relationship between trends in canopy energy and water flux parameters detected during the spring and early summer months (May – August) along the Pacific Coast of Oregon from 2003 to 2012, and the distribution of SNC symptoms in 2012. Canopy energy and water exchange parameters were calculated with MODIS Land Surface Temperature (LST), and evapotranspiration (ET) data, and with Parameter-elevation Relationships on Independent Slopes Model (PRISM) precipitation data. To evaluate the effects of forestry practices, we stratified the study into private and public lands. Proximity to coast had the strongest explanatory power of the presence/absence of SNC symptoms, explaining 9.3% of the variance on private land and 6.7% on public land. Of the canopy energy and water flux data evaluated, trends in LST had the greatest explanatory power, and the combination of an early growing season (May) and mid-summer (August) month were the most powerful combination. The trends of the May and August LST together explained 7% of the deviance in SNC symptom distribution on private land, and 2% on public land. When combined with proximity to coast, May and August LST explained 14% of the deviance in SNC symptom expression on private land and 8.7% on public land. This study indicates that LST contains important information on leaf wetness, possibly capturing both early season and late season dynamics important to SNC epidemiology. We find evidence that recent short-term directional climate changes may have contributed to the recent increases in SNC symptoms in Douglas-fir forests, and that this influence was stronger on private lands.

Background

Climate is one of the key environmental factors controlling forest pathogens and can play an important role in containing forest pathogens at low levels when climatic conditions are unfavorable (Ayres and Lombardero 2000; Coakley et al. 1999). However, climate change is now altering the energy and water fluxes across virtually all forest ecosystems on Earth with commensurate effects on the coevolved relationship between tree species and their associated pathogen (Allen et al. 2010; Logan et al. 2003). These seasonal changes in temperature and/or precipitation regimes have the potential to shift conditions in favor of pathogens, resulting in widespread epidemics (Logan et al. 2003; Brasier 1996; Williams et al. 2000). Tree species that benefitted from historical climate conditions which held forest pathogens in check may be at the greatest risk (Coakley et al. 1999; Woods et al. 2005). The effects of current and projected climatic changes on tree-pathogen interactions are a considerable source of uncertainty, with important potential ecological, biogeochemical, and socioeconomic consequences (Ayres and Lombardero 2000; Maguire et al. 2002; Kurz et al. 2008).

Most of the concern regarding the vulnerability of forests to future climate change has focused on the effects of warmer and drier conditions (Williams et al. 2013; Allen et al. 2015; McDowell and Allen 2015; Mildrexler et al. 2016; van Mantgem et al. 2009) and how these conditions have affected fungal pathogens (Brasier 1996; Lonsdale and Gibbs 1996). Climatic changes in the opposite trajectory (i.e. toward wetter conditions) might even be favorable to increased growth performance in some settings. However, climatic shifts toward wetter conditions can cause rapid fungal responses and favor pathogens with effects on host trees that far outweigh any benefits to growth (Hawkes et al. 2011). For example, a recent increase in summer precipitation appears to be responsible for the dramatic changes in Dothistroma needle blight in British Columbia (Woods et al. 2005). A foliar disease in temperate forests, Dothistroma historically had only minor impacts on native tree

species, and is now causing extensive mortality in lodgepole pines. Foliar fungi diseases are thought to be more responsive to climate change than most other forest disease organisms, as their ability to sporulate and infect is strongly tied to changes in temperature and precipitation (Peterson 1973; Gadgil 1977; Hoff 1985).

In the Pacific Northwest (PNW) region of the USA, an investigation of forest vulnerability to recent directional climate trends (2003 to 2012) found that the region's forests have experienced more extreme climate conditions from cooler and moister conditions in the fall, spring, and early summer months to warmer and drier conditions in the mid- to late-summer months (Mildrexler et al. 2016). While our Forest Vulnerability Index (FVI) was conceptualized around the effects of hotter and drier conditions on forests, the emergence of cooler and moister conditions dominated the trends for spring and early summer months. During this same period, the region's Douglas-fir forests experienced a large and rapid increase in area of forest exhibiting symptoms of Swiss needle cast (SNC), a foliar fungus endemic to the region (Ritokova et al. 2016). In this study, we investigate the relationship between climatic trends detected during the spring and early summer months (May – August) along the Pacific Coast of Oregon from 2003 to 2012, and the distribution of forests with visible symptoms of SNC in 2012. Our objectives were to: 1) Calculate the relationship between LST and water balance (WB) trends and pixel-level presence/absence of SNC symptoms. 2) Compare the relationship between private and public forest lands to make inferences about the effects of forestry practices on forest vulnerability to SNC intensification.

Swiss needle cast in the Pacific Northwest

SNC is a foliar disease specific to Douglas-fir (*Pseudotsuga menziesii*) and is caused by the ascomycete fungus, *Phaeocryptopus gaeumannii*. Although the forest pathogen that causes SNC is native to western North America, the disease was first noticed in Switzerland and Germany where Douglas-fir was planted in the early 20th

century (Hansen et al. 2000; Rosso and Hansen 2003). It was subsequently found in Oregon, but was thought to be innocuous in western North American forests prior to 1950 due to the absence of physical symptoms (Boyce 1940; Manter et al. 2005). The effects of SNC on Douglas-fir include chlorosis, premature needle loss and decreased needle retention, and reduction in tree height and diameter (Hansen et al. 2000; Lee et al. 2013). The primary mechanism for this reduction in forest productivity is the physical obstruction of stomata by the fruiting-bodies (Manter et al. 2000). Stomatal occlusion prevents both CO_2 uptake and transpiration needed for photosynthesis (Manter et al. 2000). Needle abscission typically occurs after 50% or more of the stomata are occluded by fruiting bodies (Hansen et al. 2000). A SNC growth impact monitoring plot network in the northwest Oregon Coast Range found that between 1996 and 2015 volume growth was reduced 23 - 50% by SNC (Maguire et al. 2002; Ritokova et al. 2016). Douglas-fir is a tremendously important commercial timber producing species in the region making these reductions in tree growth a major concern in commercial forestry operations (Maguire et al. 2002).

In the 1970's and 1980's epidemic outbreaks of SNC symptoms emerged in Christmas tree plantations in Oregon, and later were noticed in forest plantations along the Pacific Coast (Hadfield and Douglas 1982; Michaels and Chastagner 1984; Shaw et al. 2011). As a result, the first annual aerial survey was initiated in 1996 to determine the area of visible symptoms. These surveys have continued through to the present, revealing that forested area with visible symptoms increased from 53,050 hectares in 1996 to 156,630 hectares in 2002 (Ritokova et al. 2016). The area with symptoms was reduced from 2003 to 2005 during which two droughts affected the Pacific Northwest (Bumbaco and Mote 2005). After this period, symptom expression has steadily increased through 2015, peaking at 238,705 hectares (Ritokova et al. 2016). Evidence suggests that SNC is affected by climate, alone or in combination with forestry practices of the 20th century (Rosso and Hansen 2003; Manter et al. 2005; Stone et al. 2008b; Lee et al. 2013). The temporal period of the FVI (2003 to

2012) overlaps with a period of steady increase in SNC symptoms in Oregon, providing a good natural experiment to evaluate if short-term directional climate changes have been favorable to SNC.

Oregon's Coast Range study area

The most significant area of intensification of SNC symptoms has occurred within the Douglas-fir forests of Oregon's Coast Range, a region well-known for its dense conifer forests and productive growing conditions. The Coast Range ecoregion extends the length of Oregon's coastline and is bounded on the west by the Pacific Ocean (Fig. 4.1). The terrain ranges from sea level to 1249 m in elevation, and overall the climate is maritime, with mild wet winters and cool dry summers (Ohmann and Gregory 2002). However, the rugged coastal mountain range and resulting rainshadow results in geographic climate variations with extremely wet conditions and associated forest types in the west (*Picea sitchensis –Tsuga heterophylla*), and drier conditions and associated forest types in the east (*Pseudotsuga menziesii*) (Peterson and Waring 1994). The fungus is common throughout the range of the host, but it causes disease symptoms in forests and plantations of the coastal rainforest zone on the western slopes of the Oregon Coast Range, especially at low elevations within the coastal fog belt where needle wetness is maintained by coastal fog and drizzle (Lee et al. 2013; Shaw et al. 2011).

Historic variations in species composition and forest structure in Oregon's coastal forest ecosystems were primarily associated with climate, natural disturbances (i.e. wildfire, windthrow), and local environmental conditions (Ohmann and Spies 1998; Wimberly and Spies 2001). Simulations of historical variability in Oregon's Coast Range forests show that old-growth forests occupied 25% to 75% of the total area at the province scale with wildfire acting as the predominant driver of fluctuations (Wimberly et al. 2000). In the modern Coast Range landscape, ownership has dramatically altered disturbance regimes and forest structure (Wimberly et al. 2000).

Industrial logging of private lands, especially from the 1960's to the 1990's, converted many of the old-growth mixed-conifer forests to young even-aged Douglas-fir monoculture plantations (Cohen et al. 2002). These forest industry lands typically occur in large intensively managed blocks, and the disturbance regime is dominated by regularly timed timber harvests at 30- to 60-year rotations (Cohen et al. 2002; Wimberly et al. 2000). In contrast, forests in public ownership contain a mix of old and young forest as a result of staggering small harvests in space (Cohen et al. 2002). Old-growth was estimated to cover about 5% of the Oregon Coast province in the year 2000 (Wimberly et al. 2000), and nearly all old-growth forest that remains is located on the public forest land base (i.e. State and Federal forestland).

Evidence of climatic and forest structural linkages

The first observations of SNC in North America provided a contrasting picture to that of Europe. Whereas abundant fruiting bodies were present on infected trees in Europe, visible symptoms were scarce in western North America, leading to speculations about how different seasonal patterns of local climate between the PNW and interior Europe were affecting the disease spread. Boyce (1940) pointed to the warm, humid summers with episodic rain typical of continental Europe as being more conducive to fungal growth, in contrast to the comparatively arid summer climate of the PNW. Subsequent research confirmed these climatic influences and found factors that affect spring leaf wetness, such as fog frequency and precipitation patterns as possible factors affecting disease severity (Hood et al. 1982; Hansen et al. 2000; Rosso and Hansen 2003; Manter et al. 2005; Stone et al. 2008a; Maguire et al. 2011; Zhao et al. 2011). More specifically, SNC disease severity has been linked with favorable weather conditions for pathogen development which includes spring leaf wetness during the spore dispersal period (May, June, July, and possibly August) (Manter et al. 2005; Stone et al. 2008b). Summer conditions have also been found to be important factors in epidemiology of SNC (Rosso and Hansen 2003; Zhao et al. 2011). In a study

predicting SNC disease distribution and severity, Rosso and Hansen (2003) found that July maximum temperature tends to correspond to lower disease values, which they attributed to the inhibiting effect of high summer temperatures and dry conditions on fungal development.

To our knowledge this is the first study to evaluate the link between SNC affected forest and satellite-derived land surface temperature (LST). LST measures the emission of thermal radiance from the surface of the forest canopy, emphasizing the direct thermal response of the forest canopy to changing water and energy fluxes (Li et al. 2013; Scherrer et al. 2011). Thus, LST differs from air temperature in that it measures the actual canopy temperature where surface evaporation and transpiration affect partitioning to sensible and latent heat fluxes (Mildrexler et al. 2011a; Kim et al. 2016). Since springtime leaf wetness and summer dryness are important factors in SNC disease epidemiology, we hypothesize that LST may provide valuable information on leaf temperature as related to changes in leaf moisture condition.

Forest management practices, particularly on private lands, are also thought to be an important factor in the ecology and epidemiology of *P. gaeumannii*. The homogenous forest structural and compositional conditions of Douglas-fir plantations appear to promote spore dispersal and infection, whereas old-growth forests are relatively resistant to the disease (Hansen et al. 2000; Maguire et al. 2002; Shaw et al. 2011; Ritokova et al. 2016). Thus the SNC epidemic is positively correlated with the increase in Douglas-fir plantations, and the conversion of mixed-conifer forests to young monocultures of Douglas-fir (Hansen et al. 2000; Ritokova et al. 2016). The first observations of SNC disease in Switzerland and Germany in 1925 were in Douglas-fir plantations (Boyce 1940; Lee et al. 2013), pre-dating the large-scale conversion of western North America's old-growth forests to plantations. This forest structural factor of SNC disease epidemiology may have contributed to the difference between early observations in European and PNW forests.

Given this forest structural component of SNC disease epidemiology, it is possible that seasonal changes in temperature and/or precipitation regimes may relate more strongly to the distribution of SNC symptoms on structurally homogenous Douglas-fir plantations that dominate private land compared to public land. Thus, we analyze private forestlands separate from the more structurally diverse public lands to test for differences. We hypothesize that relationships between the estimated variables and pixel-level presence/absence of SNC will be higher for private lands than for public lands.

Recent regional LST and water balance trends

Mildrexler et al. (2016) quantified monthly trends in canopy energy and water exchanges across the forests of Oregon and Washington during the growing season from 2003 to 2012 (Fig. 4.2) with spatially continuous MODIS LST and evapotranspiration (ET), and with Parameter-elevation Relationships on Independent Slopes Model (PRISM) precipitation data. Water balance (WB) calculated as precipitation (PRISM, 800-m^2) minus ET (MODIS, resampled to 800-m^2) and commonly used to represent regional water balance (Swenson & Wahr 2006; Zhang et al., 2009), is the net flux of water between the atmosphere and the biosphere. MODIS data were resampled to 800-m^2 to match the resolution of the precipitation data. The slope of every specific 800-m^2 pixel for each month across time (e.g., the slope of a regression fit to every April from 2003 to 2012 for a given pixel) illustrates complex spatial patterns across the large hydrological gradients of the PNW (Fig. 4.2).

We found a trend toward wetter conditions (characterized by positive slopes for WB) for the study area in May and June (Fig. 4.2). Localized exceptions include the northern Coast Range which experienced an intense patch of increasing water deficit in June, and localized patches in the southern Coast Range that experienced a drying trend of varying intensity across months. The emergence of negative WB slopes during July in the Coast Range indicates the beginning of a switch toward drier

conditions, but most of the forested area retains positive WB slopes through July. In August, the switch is complete, and most of the Coast Range forests show a drying trend (negative WB slopes). This drying trend is important for SNC because a higher vapor pressure deficit (VPD) and lower water potential within the foliage negatively affect fungal development and increase needle retention (Zhao et al. 2011; Lee et al. 2013).

Related to the trends in WB, the slopes of the LST data were predominantly negative for the study area from May to July indicating a trend toward cooler conditions (Fig. 4.2). Even in July and August, as WB turned negative, LST continued to decrease, possibly due to plenty of water available for transpirational cooling and a lag time for LST to respond to changes in available soil moisture (Mildrexler et al. 2016). The first significant trends toward warmer temperatures in the Coast Range appear in August, especially in the northern Coast Range, but most LST trends remain negative, although of a lesser magnitude (indicated by light blue color). These biophysical datasets indicate that WB and LST trends in May, June, and July are consistent with increased leaf wetness, a key factor in SNC disease epidemiology.

Forest vulnerability index and Swiss needle cast

Using the LST and WB data shown in Figure 4.2, we formulated a pixel-specific forest stress index (FSI) that contrasts LST and WB, such that the FSI is low when LST is low and WB is high, and the FSI high when LST is high and WB is low (Mildrexler et al. 2016). This is done for each month across the years of the MODIS time series. We then calculated the pixel-level month-specific FVI as the inter-annual slope of the FSI for each month. The FVI is then filtered by *p-value* to identify where on the landscape significant FVI slopes exist. Positive FVI values indicate hotter and drier conditions, whereas negative FVI values indicate cooler and/or wetter conditions. For a more detailed description of the FVI algorithm and the input datasets and their uncertainties, see Mildrexler et al. (2016).

Negative FVI dominated the Oregon Coast Range during spring and early summer, indicating conditions favorable to SNC (Fig. 4.3). June and July showed the strongest trends toward negative FVI. August captures the transition from positive to negative slopes across the landscape, and highlights the complex spatiotemporal patterns of the regions combined energy and water balance changes (i.e. positive FVI can be seen in the northern Coast Range, and negative in the southern portion). The right panel displays the spatial extent of the SNC symptomatic Douglas-fir forest in the Coast Range of Oregon detected in the 2012 aerial survey (Fig. 4.3). The importance of proximity to coast, a key factor in SNC distribution and severity, is clearly visible (Rosso and Hanson 2003). To focus our analysis on the area of symptomatic forest, we computed a proximity to coast layer based on the 800-m^2 raster data and limited the analysis to the area of visible SNC symptoms in 2012.

Aerial detection data and logistic regressions

We evaluated the relationship between each monthly factor (LST, WB, and FVI) and SNC presence/absence individually, and in multi-factor combinations for private and public lands (Table 4.1). Prior to data extraction, the ODF aerial detection data was converted to raster data and only MODIS pixels with greater than 50% of their area affected by SNC symptoms were used in the analysis. Pixels with less than 50% were discarded. Monthly scatterplots (Appendix: Figs. A-4.1 thru A-4.4) and correlations (Appendix: Tables A-4.1 thru A-4.4) for all factors were evaluated to check for collinearity. Factors with correlations above 0.7 were not tested together in regressions. We then performed logistic regressions using Statsgraphics software to examine the relationship between the FVI, LST, and WB variables and pixel-level presence/absence of SNC symptoms. Private/ public land classifications were based on the forest ownership data (Fig 4.1).

Overall we found that LST trends had greater power than WB trends in explaining SNC symptom distribution (Table 4.1). Combining monthly LST in multi-

factor regressions increased the explanatory power of LST, whereas this effect was minimal for WB. We generally found that a higher percentage of the deviance in SNC symptom expression was explained on private land than on public land (all values over 5% are in bold). Proximity to coast was the single most powerful explanatory factor, accounting for almost 10% of the deviance for private land and 6.7% for public land.

At the individual month level, the slope of the monthly LST values from 2003 to 2012 explained little of the deviance in SNC symptom distribution on private or public land, although May LSTz trends on private lands were an exception, explaining nearly 4% of the deviance (Table 4.1). The combination of LST slopes for May, June and August explained 7.0% of the SNC symptom occurrence on private land, and 3% on public land. Since the slopes of the July and August LST values were highly correlated (r = 9.0), these months were not tested together due to collinearity (Appendix: Table 4.1). Despite the high correlation between July and August LST slopes, the inclusion of August LST values rather than July increased the deviance explained from 5.2% to 7.0%. Moreover, the removal of June LST slopes had no effect on the total deviance explained, indicating that an early and late season month captures most of the deviance in SNC symptom expression that could be explained by LST trends on private land. Monthly water balance values individually explained little of the deviance on private and public lands (Table 4.1). Multi-factor regressions among months increased this to around 3.0% (July and August WB values did not show high correlation). FVI values also explained little of the deviance on their own, the highest being for May on private land (3.5%). Together, FVI growing season values explained 5.6% of the deviance on private land, and 3.3% on public lands.

We tested multi-factor regressions with LST and WB for May and August and found that the addition of WB added little (7.3%) to the deviance explained by LST alone (7.0%). When combined with proximity to coast, May and August LST explained 14% of the deviance in SNC symptom expression on private land and 8.7%

on public land, and the addition of WB did not increase explanatory power (Table 4.1).

SNC distribution: Importance of LST trends and private forestlands

The goal of this exploratory study was to evaluate the relationship between short-term directional climate changes detected across the PNW region from 2003 to 2012 and the recent SNC epidemic. Since forest management has increased host abundance and possibly vulnerability to SNC at the landscape scale, we compared public and private forests separately to evaluate differences. Proximity to coast had the greatest explanatory power because SNC distribution is strongly coupled with the low elevation coastal-forest fog belt (Rosso and Hansen 2003). Given the complexity of SNC disease epidemiology and the number of factors involved, two interesting findings emerge from this study. First, of the canopy energy and water flux data evaluated, trends in LST were most effective in explaining the distribution of SNC symptoms, and the combination of an early growing season (May) and mid-summer (August) month had the most explanatory power. Second, we found that a greater percentage of deviance in SNC symptom expression was explained on private land than on public land.

Our finding that short-term directional trends in LST have the strongest relationship with SNC distribution (notwithstanding proximity to coast), highlights that LST contains implicit information about changing canopy water and energy fluxes that are relatable to complex ecological processes such as forest pathogen interactions. LST temporal variations contain information about the partitioning of solar radiation among the land surface energy balance components (sensible (SH) and latent heat (LE)) (Bateni and Entekhabi 2012). Controls on the fluxes, such as from moisture limitation over the growing season, impose a strong limitation on the partitioning among the sensible and latent heat fluxes and affect the evolution of LST (Bateni and Entekhabi 2012). In spring, canopy wetness in the Oregon Coast Range is high due to

rainfall, mist, and fog. With plenty of water available to evaporate and transpire from the forest canopy, and a low VPD, canopy surface temperature remains relatively cool. In August, dry conditions coupled with increased direct solar radiation dry the forest canopy, and higher VPD can reduce transpiration, increasing the canopy surface temperature. The importance of temperature found in our study is consistent with previous work that showed that *P. gaeumannii* is sensitive to relatively small temperature differences, and that spatial variability in SNC disease severity has been influenced by regional climate trends (Stone et al. 2008a). Moreover, the importance of early growing season (May) and mid-summer (August) temperature trends agrees with previous research that found a positive relationship between SNC and spring leaf wetness, and a negative relationship between SNC impact and summer temperature (Rosso and Hansen 2003; Zhao et al. 2011; Lee et al. 2013). *P. gaeumannii* spore dispersal and infection begins in May, shortly after bud break of Douglas-fir, making May a critical month in the life cycle of *P. gaeumannii.* August captures a period when the fungus is susceptible to desiccation as conditions warm and dry (Shaw et al. 2011; Lee et al. 2013). Thus, May and August together capture temperature changes associated with canopy wetness and dryness during critical periods in the development stages of the pathogen (Rosso and Hansen 2003).

Given the importance of leaf wetness in SNC disease epidemiology, it is somewhat surprising that the WB trends showed such a poor relationship with SNC presence/absence. This may be due in part to the uncertainties associated with the PRISM precipitation and the MODIS ET datasets. For example, the MODIS ET algorithm uses VPD alone to estimate water stress (i.e. no soil moisture data) which results in an underestimation of water stress, an overestimation of ET, and difficulty in capturing seasonality in some regions (Mu et al. 2007). Examining the LST and WB variables in isolation was key to elucidating the different relationships between these variables and the distribution of SNC symptoms.

The higher level of deviance in SNC symptom expression explained on public land vs. private land raises questions about how the different structural characteristics associated with these land ownerships may affect SNC disease epidemiology. Interestingly, while the magnitude of deviance explained differs between land ownership patterns, the relative changes among factors show a similar pattern, suggesting a consistent difference (Table 4.1). One possible explanation for the difference in deviance explained is that the factors may have less explanatory power on public lands due to their increased heterogeneity. For example, public lands contain a mix of forest successional stages, and natural disturbance regimes maintain a stronger presence on public lands compared with private lands. Mixed-conifer forests are typical of public lands, as are a variety of stand ages. Public lands are managed for a variety of objectives, and these objectives shift in importance across management area designations, resulting in another layer of complexity. Taken together, these factors contribute to a relatively heterogeneous forest landscape. By comparison, industrial private forestlands are generally managed for the sole purpose of timber production. Natural disturbances are replaced by cycles of harvesting and reforestation that result in even-aged, single-species plantations. These young forests have a more homogenous structure than young forests that establish following natural disturbances (Hansen et al. 1991). Further insights about the potential effects of forest structure can be gleaned from research of SNC in Christmas tree plantations, where epidemic like conditions were first observed in the PNW. Practices in Christmas tree plantations, such as shearing and fertilizing, are designed to develop trees with dense foliage (Hadfield and Douglas 1982). Because infection occurs on newly emerging needles, more dense foliage provides more opportunity for infection (Hadfield and Douglas 1982). Also the close spacing of trees in Christmas tree plantations restricts air circulation, keeping foliage wet, favoring infection (Hadfield and Douglas 1982). While not as dense as Christmas tree farms, tree plantations are managed much like a crop, and are known to have a much greater stand density than forests that regenerate

naturally. Plantations often have overlapping forest canopies, resulting in self-pruning of the limbs in the lower canopy. These canopy characteristics reduce windspeed and increase shading, factors that help to maintain moister conditions that favor SNC infection. Moreover, uniform age classes result in low canopy heterogeneity, a key factor that drives turbulent heat and moisture exchange with the atmosphere. Lastly, overlaying SNC symptoms on a map of forest ownership provides compelling evidence that SNC is affecting these two land bases differently. The patterns of SNC symptoms reveal close spatial association with private lands along the whole Oregon coast, and show a sharp reduction on public lands (Fig. 4.4). Symptoms on public lands tend to be small isolated patches, whereas on private lands symptoms have a much larger patch size, contain more high severity symptoms, and are nearly contiguous across large swaths of private lands (Fig. 4.4).

Limitations and future research

While this study does find evidence that short-term directional climate changes may have contributed to the recent SNC epidemic, and that this influence was stronger on private lands, we present these results with caution. Our study compared monthly climate trends computed over a 10-year period to a snap shot of SNC symptoms at the end of this period. A 10-year period is too short to evaluate longer-term climate cycles that may be important for SNC dynamics (Lee et al. 2013). Second, the majority of the deviance in SNC symptoms was not explained by our factors. Clearly other factors are important, raising questions about how significant the climate influence is. Having said this, very subtle shifts in climate can alter host-pathogen interactions such that major changes result (Hansen et al. 2000). At the very least, our study indicates that seasonal LST trends contain important information on leaf wetness, possibly capturing both early season and late season dynamics important to SNC disease epidemiology, and that the effects of forestry practices on vulnerability to SNC warrant further study.

Future research should explore the relationship between annual changes in the monthly climate data and SNC symptom distribution over a longer time period. This would provide more detailed information on how interannual climate variability relates to changes in symptom expression. Meteorological data could be used to calculate the relationship between the timing and duration of rainfall events, changes in LST, and SNC symptoms. This approach may be useful for identify moisture and temperature thresholds that best match up with the expression of SNC symptoms.

Figures and Tables

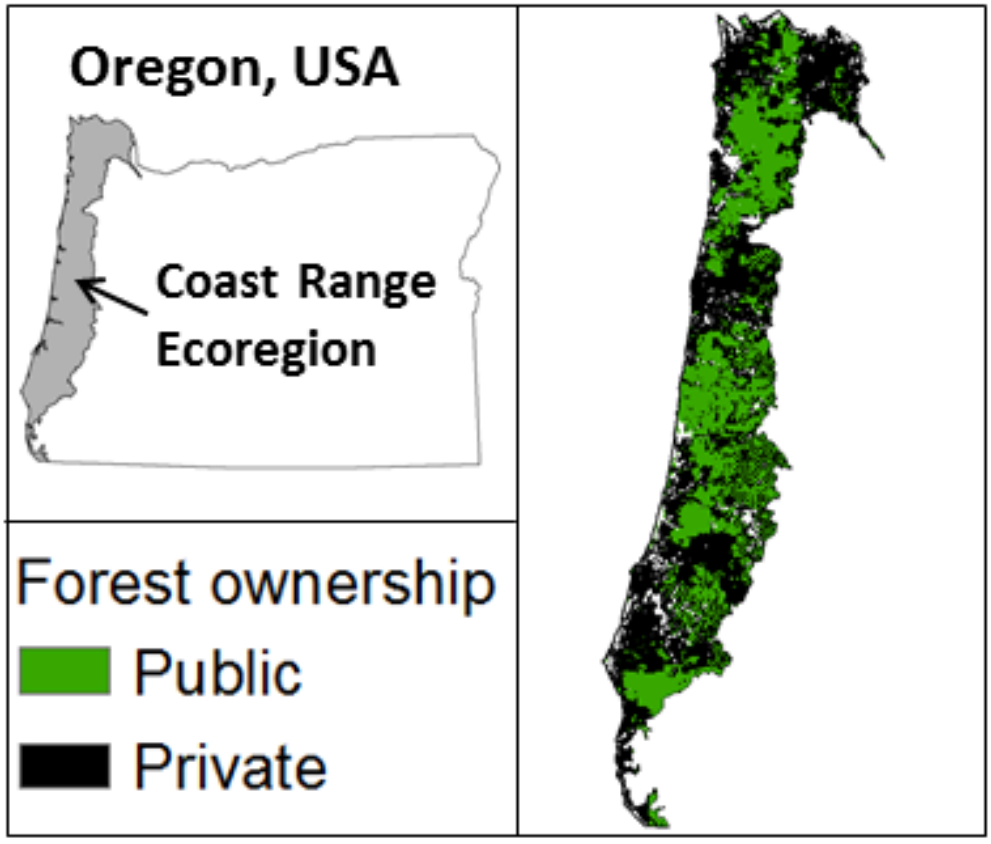

Figure 4.1. Map of Oregon, USA showing the Coast Range ecoregion. Forest land ownership patterns from U.S. Geological Survey, Gap Analysis Program, May 2016. Public land includes State and Federal lands (Bureau of Land Management, United Service Forest Service).

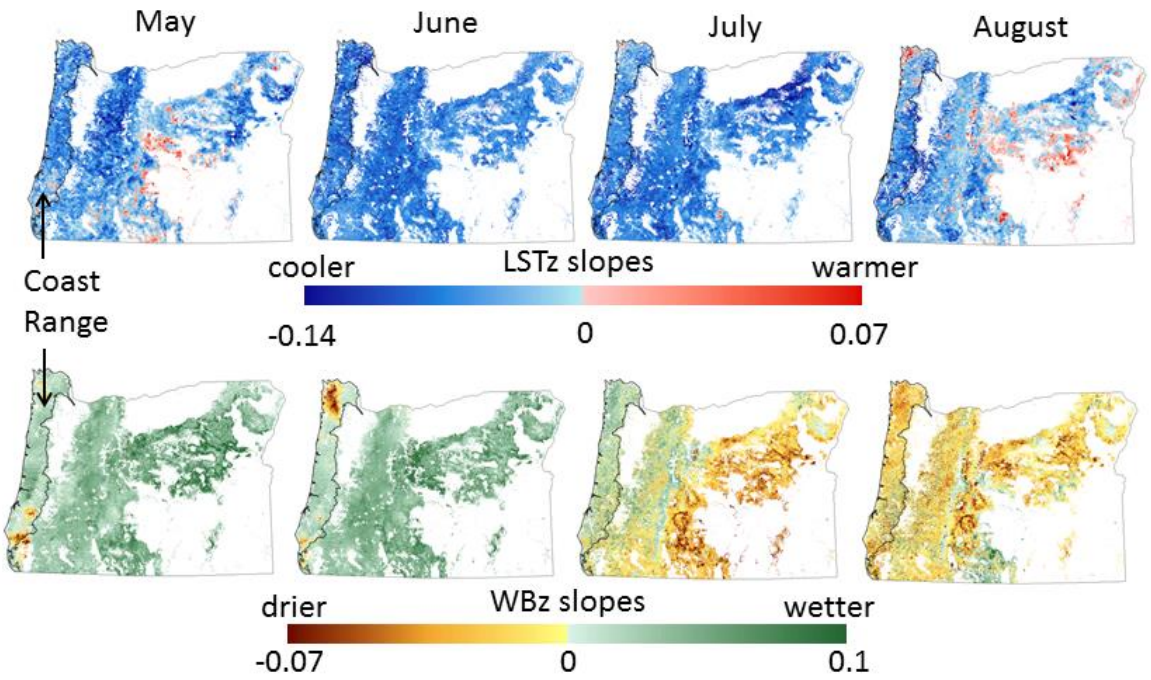

Figure 4.2. Changes in land surface temperature (LST) and water balance (WB) from 2003 to 2012 across the forests of Oregon (adapted from Mildrexler et al. 2016).

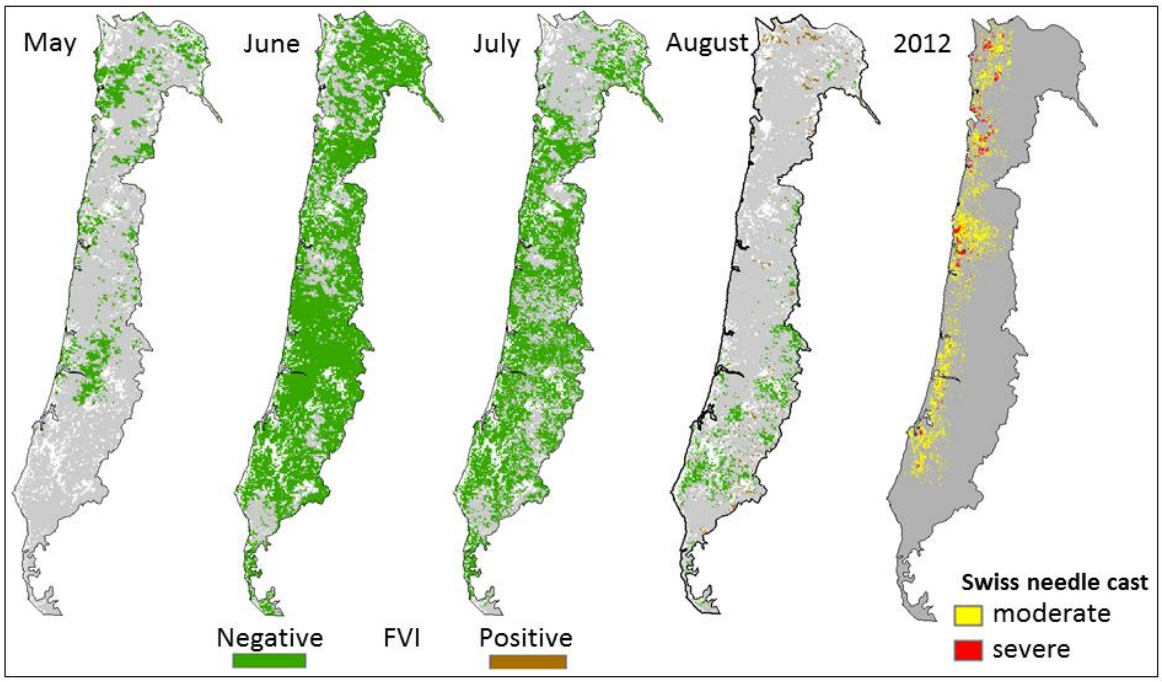

Figure 4.3. Forest vulnerability index for May through August masked by significance (p-value < 0.1). From 2003 to 2012, decreased temperatures and increased water balance resulted in negative FVI values (although note emergence of positive FVI values in August), conditions favorable to SNC. Spatial pattern of Swiss needle cast symptoms in the Coast Range of Oregon detected by the 2012 Oregon Department of Forestry (ODF) aerial survey (far right panel).

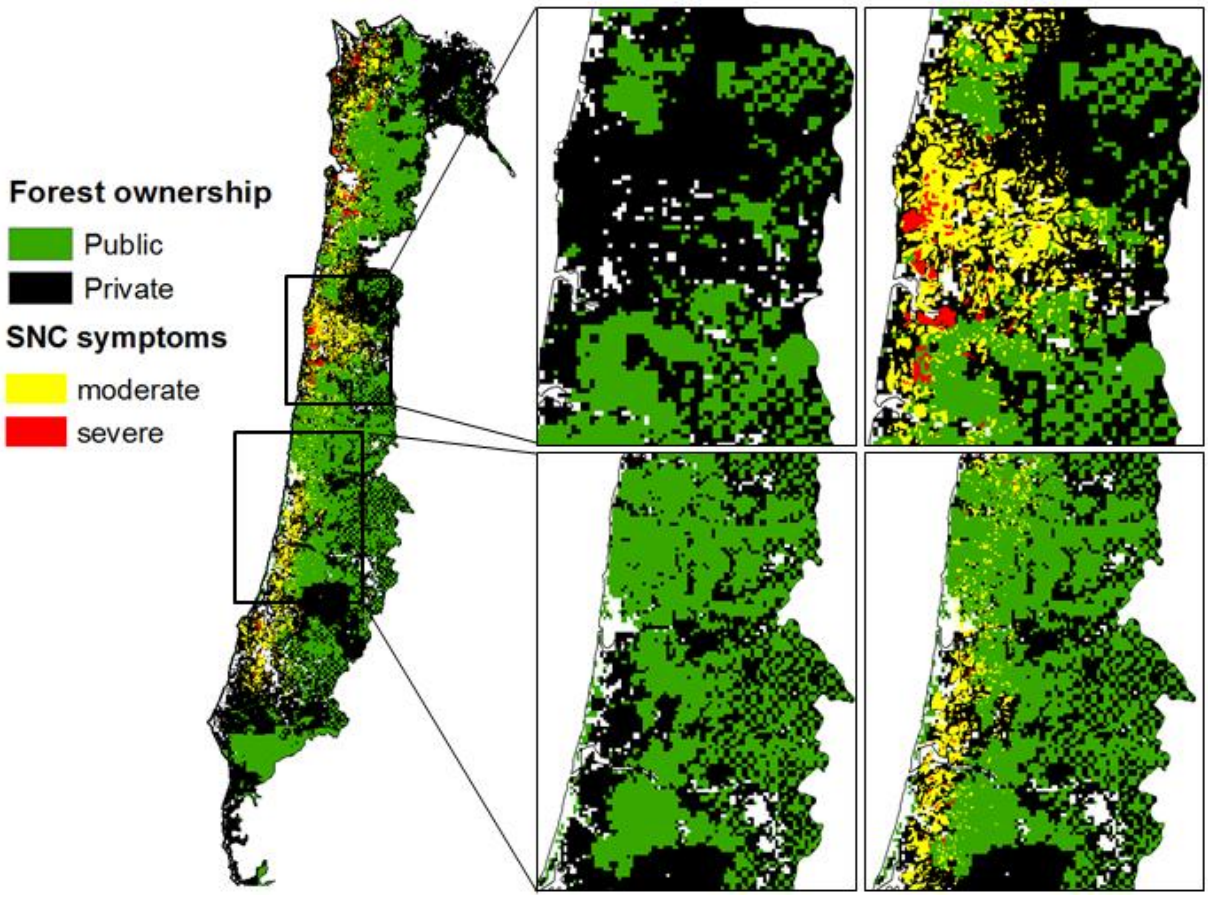

Figure 4.4. Swiss needle cast symptoms overlain on a forest ownership map reveals a strong spatial association between SNC symptoms and private lands.

Table 4.1. Percent deviance of SNC presence/absence data explained by the various factors individually and in combinations.

	Private land Deviance explained	Public land Deviance explained
Factors	(%)	(%)
Geographic		
Proximity to coast	**9.34**	**6.7**
Land Surface Temperature		
May LSTz	3.91	1.0
June LSTz	0.37	0.73
July LSTz	0.01	0.08
August LSTz	0.45	0.74
May, June, July LSTz	**5.2**	1.63
May, June, August LSTz	**7.0**	3.1
May, August LSTz	**7.0**	2.5
Water Balance		
May WBz	1.40	0.0
June WBz	0.04	0.31
July WBz	0.43	1.54
August WBz	.06	0.03
May, June, July, August WBz	2.9	3.0
Forest Vulnerability Index		
May FVI	3.5	0.55
June FVI	0.5	0.35
July FVI	0.0	0.16
August FVI	0.4	0.64
May, June, July, August FVI	**5.6**	3.3
LST and WB		
WBz and LSTz (May, August)	**7.3**	**5.4**
LST, WB and geographic		
May, August LSTz, proximity to coast	**14.0**	**8.7**
May, August (LSTz and WBz), proximity to coast	**14.0**	**8.7**

Chapter 5: Conclusion

Research summary and synthesis

The Earth's ecosystems are experiencing change that is unprecedented in human history (Rockström et al. 2009). Given the vital interactions and feedbacks between the Earth's land surface and climate, these changes threaten to initiate potentially irreversible changes in the Earth system (Hansen et al. 2015; IPCC 2013; Rockström et al. 2009). Therefore it is important to develop new ways to measure global changes and their consequences on climate that are relevant and communicable to society and decision-makers (Janetos et al. 2012; USGCP 2014). Land surface temperature (LST) measurements link surface conditions and climate to provide critical information on important biospheric changes occurring in the Earth system at local through global scales (Mannstein 1987; Li et al. 2013; Wan et al. 2004). This dissertation uses satellite-derived LST data from the Aqua MODIS sensor to develop new, novel methodologies that address key topics in Earth science research – global heat waves, a melting cryosphere, vegetation disturbance, the effects of droughts and rising temperatures on forests, and how seasonal shifts in water and energy might affect host pathogen interactions.

In the first study of this dissertation (Chapter 2), we apply a new global change indicator based on an annual measure of the Earth's maximum land surface temperature (LSTmax). Using the high-resolution 1-km^2 Aqua LST data, we have for the first time characterized a fundamental aspect of Earth's surface-climate system, the LSTmax distribution. The multi-modality in distributions is reflective of ecosphere patterns, and the low interannual variability reflects the robustness of LSTmax against the many intra- and interannual variations and fluctuations in LST (Fig. 2.1D). We hypothesized that shifts in LSTmax distributions might hence serve as a proxy for more deeply rooted shifts in Earth system properties that could indicate drifts of ecosystems and biomes toward thresholds of profound change. Our findings show that

entire biomes are experiencing shifts in their LSTmax distributions driven by extreme climatic events and large-scale land surface changes. LSTmax anomalies provide detailed spatial information on droughts and heat waves that can be used to better understand the ecosystem changes associated with extreme high-temperature events, which are projected to continue increasing in the future (Hansen et al. 2012). This research offers a substantial advancement in turning the unique LSTmax measurement into a useful, spatially comprehensive global temperature monitor.

The role of rising temperatures in driving increased drought stress is evident in recent studies of tree vulnerability, mortality, and net primary production (Allen et al. 2015; McDowell and Allen 2015; Mildrexler et al. 2016; van Mantgem et al. 2009; Williams et al. 2013). Rising temperatures coupled with decreasing precipitation are a potent combination, especially in semi-arid ecosystems (Adams et al. 2009). One of the most promising approaches to gain information about the water status of trees is thermal imaging of leaves or forest canopy foliage as a proxy for the energy balance, and thus for concurrent transpiration and carbon cycling (Leuzinger et al. 2007; Scherrer et al. 2011; Kim et al. 2016; Mildrexler et al. 2016). By incorporating thermal observations from the Aqua MODIS sensor with MODIS based ET and PRISM precipitation measurements, we developed a new forest vulnerability index (FVI) that captures the variable spatial and temporal energy and water balance (WB) changes that forests are experiencing during the growing season (April through October), and translated this information into maps of forest vulnerability across the Pacific Northwest (PNW) region (Oregon and Washington) of the USA (Chapter 3). These maps reveal complex temporal and spatial patterns and interactions between LST and WB that contribute to the forest vulnerability measurement (Figure 3.4). Our findings indicate that the PNW may be on a trajectory toward more extreme climatic conditions, from moister and cooler in the Spring and Fall, to warmer and drier in Summer. If this trajectory continues, it will have profound implications for the regions vegetation.

In examining the emergence of more extreme climatic conditions detected by the FVI, we realized that the early spring months displayed trends favorable for a native forest pathogen having important effects on the region's Douglas-fir forests, Swiss needle cast (SNC). This led to the final chapter (Chapter 4) in which we explored the relationship between climate trends from 2003 to 2012 and the distribution of SNC symptoms in 2012. Our finding that LST during the early growing season (May) and mid-summer (August) was relatively effective at explaining the deviance in SNC symptom presence/absence data reinforces the importance of thermal data as a measure of surface moisture status, a key factor in SNC disease epidemiology. Our spatially exhaustive remote sensing data allowed us to investigate private vs. public land responses with a simple stratification. Although we did find some evidence to support the idea that short-term directional climate changes may have contributed to the recent SNC epidemic, and that this influence was stronger on private lands, additional research is needed to confirm these findings.

Emergent themes

The LST measurement emerges as a key biophysical dataset for monitoring a variety of critical Earth system changes across a broad range of spatial and temporal scales. This dissertation has merged the entire Earth's annual LSTmax into a single integrated measure to evaluate biome-level surface temperature changes across ice sheets and tropical forests, computed regional-scale LST changes across temperate forests at a monthly time-step, and made pixel-specific comparisons with forest disease symptom polygons at the local scale. The relevance of LST from local to global scales underscores the fundamental role of LST in physical processes of climate (Li et al. 2014), and in biological processes ranging from leaf-level physiology to biome-level distribution (Teskey et al. 2015). Because temperature is constantly changing, it is critical to use temporal compositing approaches of LST that relate closely to one's research question. For example, the LSTmax metric is an extreme

condition robust against the complex influences in monthly or daily temperature values with direct relevance to high-temperature biome thresholds and the expression of extreme events like heat waves. However, since it's an annual measurement, LSTmax could not capture dynamics over the growing season. Thus, our forest vulnerability study used a monthly mean LST computation which was critical for detecting the evolution of thermal stress over the growing season. Moreover, by coupling LST with other complementary biophysical datasets that relate directly to the signal of interest, novel mathematical approaches can be developed that magnify important ecosystem changes (Mildrexler et al. 2009; Mildrexler et al. 2016).

The trajectory toward more extreme climatic conditions also emerged as an important factor in the forests of the PNW (Fig. 3.4). This was a surprise finding given that we set out to detect areas affected by increasing temperatures and drought. However, by creating a mathematical model —the forest vulnerability index — that captures the relationship between water and temperature trends from one month to the next, both hotter and drier, and cooler and wetter trajectories were a possible outcome. The increasing water deficits and rising temperatures found in August and September were immediately preceded by cooler and moister conditions in April-July. Climatic extremes have emerged as a critically important part of climate variability due to their disproportionately large effects on ecosystems and society (Easterling et al. 2000; Jentsch et al. 2007; Smith 2011). The climatic changes expected during the next decades – large increases in mean temperature, increased heat waves, and significant long-term regional drying in the western USA – will likely increase chronic forest stress and mortality (Allen et al. 2015; Cook et al. 2014; IPCC 2013; Jentsch et al. 2007; Moritz et al. 2012). However, less is known about the effects of cooler and wetter spring conditions should this trajectory continue. Will more rainfall in the spring help to offset the effects of increasing temperatures and water deficits in the late summer? Or will more heavy rainfall events increase flooding, only to be followed by more severe heat waves and droughts? While our analysis does not

answer these questions, it does show that divergent climate trends can occur from one season to the next, and that forest vulnerability can arise from both hotter and drier, and cooler and wetter conditions.

A final emergent theme from this research is the importance of species-specific adaptations and sensitivities to climate change. While we found a variety of forest type groups are experiencing hotter and drier conditions, the ecological effects of these changes will vary between types. A recent study of water limitations on growth in the Cascade Mountains of Oregon found that growth of species in relatively dry environments (ponderosa pine, western juniper) tracked climate changes closely, whereas species in moist environments (grand fir) did not track temperature or moisture-related climate variables (Berner and Law 2015). It is possible that shifts toward warmer and drier conditions may cause immediate reductions in the growth of dry forest types, but could improve growth in moist forest types where water is not limiting and rising temperatures reduce constraints on productivity from frost during periods when VPD is low. However, as we have seen in the Oregon Coast Range, subtle shifts in climate can also increase forest vulnerability to pathogens, exemplifying the complex relationships between species and the climatic conditions to which they are adapted. For example, in northern lodgepole pine forests warming conditions that might have otherwise improved growth helped trigger widespread beetle outbreaks (Kurz et al. 2008). Furthermore, change in growth is only one of the potential stress responses. Mortality is another potential response, and in our study area sensitivity to drought varies along an elevational gradient. While dry forests may show a more immediate response to hotter and drier conditions in terms of growth, these forests have evolved mechanisms to cope with hot, dry conditions (Haugo et al., 2010). On the other hand, moist forests did not evolve in areas that experienced seasonal dryness regularly, and may be highly vulnerable to the increasingly severe and rapid onset high temperature droughts expected in the coming decades (Hansen et al. 2012).

Final thoughts

While change is a constant aspect of ecosystems, human-induced climate and land use changes are pushing ecosystems and species toward extreme thresholds of profound change. Projections indicate with high confidence that temperatures will continue to rise in the future, and every ecosystem on Earth will be affected (IPCC 2013). Urgently needed are new ways to monitor and understand these impacts, especially with metrics that are relevant and communicable to society, land managers, and decision-makers. LST is a fundamental aspect of climate and biology, affecting ecosystems from local to global scales. This dissertation demonstrates that satellite-derived LST data from the Aqua MODIS sensor can address key topics in Earth science research. As the period of observation lengthens and longer trend detection is possible, LST will become an increasingly valuable metric of critical changes in the Earth system. Additional efforts are needed to link temperature shifts to physiological thresholds, and to link canopy water and energy changes to ground-based measurements and observations. Continuity in Earth observation measurements of high-quality LST data with continuous spatial coverage is necessary for effectively monitoring our rapidly changing planet.

Bibliography

Adams, H.D., M. Guardiola-Claramonte, G.A. Barron-Gafford, J.C. Villegas, D.D. Breshears, C.B. Zou, P.A. Troch, and T.E. Huxman. 2009. Temperature sensitivity of drought-induced tree mortality portends increased regional die-off under global-change-type drought. *Proceedings of the National Academy of Sciences U.S.A.,* 106, 7063–7066.

Albright, T.P., A.M. Pidgeon, C.D. Rittenhouse, M.K. Clayton, C.H. Flather, P.D. Culbert, and V.C. Radeloff. 2011. Heat waves measured with MODIS land surface temperature data predict changes in avian community structure. *Remote Sensing of Environment,* 115, 245-254, doi:10.1016/j.rse.2010.08.024.

Allen, C. D., D. D. Breshears, and N. G. McDowell. 2015. On underestimation of global vulnerability to tree mortality and forest die-off from hotter drought in the Anthropocene. *Ecosphere,* 6, 129, doi:10.1890/ES15-00203.1.

Allen, C.D. and D.D. Breshears. 1998. Drought-induced shift of a forest-woodland ecotone: rapid landscape response to climate variation. *Proceedings of the National Academy of Sciences U.S.A.,* 95, 14839–14842.

Allen, C.D., and Coauthors. 2010. A global overview of drought and heat-induced tree mortality reveals emerging climate change risks for forests. *Forest Ecology and Management,* 259, 660-684.

Anderegg, W.R.L, J. Kane, and L.D.L. Anderegg. 2013. Consequences of widespread tree mortality triggered by drought and temperature stress. *Nature Climate Change,* 3, 30-36, doi:10.1038/nclimate1635.

Anderegg, W.R.L., and Coauthors. 2015. Pervasive drought legacies in forest ecosystems and their implications for carbon cycle models. *Science,* 349, 528–532, doi:10.1126/science.aab1833.

Anderson, M.C., J.M. Norman, J.R. Mecikalski, J.A. Otkin, and W.P. Kustas. 2007. A climatological study of evapotranspiration and moisture stress across the continental United States based on thermal remote sensing: 2. Surface moisture climatology. *Journal of Geophysical Research,* 112, doi:10.1029/2006JD007507.

Anderson, R.G., and Coauthors. 2011. Biophysical considerations in forestry for climate protection. *Frontiers in Ecology and the Environment,* 9, 174-182, doi:10.1890/090179.

Asner, G.P., P.G. Brodick, C.B. Anderson, N. Vaughn, D.E. Knapp, and R.E. Martin. 2016. Progressive forest canopy water loss during the 2012-2015, *Proceedings of the National Academy of Sciences U.S.A.,* 113, E249-E255, doi:10.1073/pnas.1523397113.

Ayres, M. P., and M. J. Lombardero. 2000. Assessing the consequences of global change for forest disturbance from herbivores and pathogens. *Science of the Total Environment,* 262, 263–286, doi:10.1016/S0048-9697(00)00528-3.

Baker-Austin, C., J.A. Trinanes, S. Salmenlinna, M. Löfdahl, A. Siitonen, N.G.H. Taylor, and J. Martinez-Urtaza. 2016. Heat wave–associated vibriosis, Sweden and Finland, 2014. *Emerging Infectious Diseases,* 22, 1216-1220, doi:10.32032/eid2207.151996.

Barriopedro, D., E.M. Fischer, J. Luterbacher, R.M. Trigo, and R. Garcia-Herrera. 2011. The hot summer of 2011: redrawing the temperature record map of Europe. *Science,* 333, 220-224, doi:10.1126/science.1201224.

Bateni, S.M., and D. Entekhabi. 2012. Relative efficiency of land surface energy balance components. *Water Resources Research,* 48, W04510, doi:10.1029/2011WR011357.

Berner, L. T, and B. E. Law. 2015. Water limitations on forest carbon cycling and conifer traits along a steep climatic gradient in the Cascade Mountains, Oregon. *Biogeosciences*, 12, 6617-6635.

Bonan, G.B. 2008. Forests and Climate Change: Forcings, Feedbacks, and the Climate Benefits of Forests. *Science,* 320, 1444-1449, doi:10.1126/science.1155121.

Bouchama, A. 2004. The 2003 European heat wave. *Intensive Care Medicine,* 30, 1–3, doi:10.1007/s00134-003-2062-y.

Bowman, D.M.J.S., J. K Balch, P. Artaxo, W.J. Bond, J.M. Carlson, and M.A. Cochrane. 2009. Fire in the earth system. *Science,* 324, 481–484, doi:10.1126/science.1163886.

Box, J.E., X. Fettweis, J.C. Stroeve, M. Tedesco, D.K. Hall, and K. Steffen. 2012. Greenland ice sheet albedo feedback: thermodynamics and atmospheric drivers. *The Cryosphere,* 6, 821-839, doi:10.5194/tc-6-821-2012.

Boyce, J. S. 1940. A needle cast of Douglas-fir associated with *Adelopus gaeumannii*. *Phytopathology*, 30, 649–659.

Brasier, C. M. 1996. *Phytophthora cinnamomi* and oak decline in southern Europe: Environmental constraints including climate change. *Annals of Forest Science,* 53, 347–358, doi:10.1051/forest:19960217.

Bréda, N., R. Huc, A. Granier, and E. Dreyer. 2006. Temperate forest trees and stands under severe drought: a review of ecophysiological responses, adaptation processes and long-term consequences. *Annals of Forest Science,* 63, 625-644, doi:10.1051/forest:2006042.

Breshears, D. D., and Coauthors. 2005. Regional vegetation die-off in response to global-change type drought. *Proceedings of the National Academy of Sciences U.S.A.,*102, 15144-15148, doi:10.1073/pnas.0505734102.

Bumbaco, K.A., and P.W. Mote. 2010. Three Recent Flavors of Drought in the Pacific Northwest. *Journal of Applied Meteorology and Climatology,* 49, 2058-2068, doi:10.1175/2010JAMC2423.1.

Bustinza R., G. Lebel, P. Gosselin, D. Belanger, and F. Chebana. 2013. Health impacts of the July 2010 heat wave in Québec, Canada. *BMC Public Health,* 13, 56, doi:10.1186/1471-2458-13-56.

Cai, S., D. Liu, D. Sulla-Menashe, and M.A. Friedl. 2014. Enhancing MODIS land cover product with a spatial-temporal modeling algorithm. *Remote Sensing of Environment,* 147, 243-255, doi:10.1016/j.rse.2014.03.012.

Cattiaux, J., and P. Yiou. 2013. U.S. heat waves of spring and summer 2012 from the flow-analogue perspective [in "Explaining Extreme Events of 2012 from a Climate Perspective"]. *Bulletin of the American Meteorological Society,* 94, S10-S13, doi:10.1175/BAMS-D-13-00085.1.

Chapin III, F. S., J. T. Randerson, A. D. McGuire, J. A. Foley, and C. B. Field. 2008. Changing feedbacks in the climate-biosphere system. *Frontiers in Ecology and the Environment,* 6, 313-320, doi:10.1890/080005.

Chen, J.L., C.R. Wilson, B.D. Tapley, L. Longuevergne, Z.L. Yang, and B.R. Scanlon. 2010. Recent La Plata basin drought conditions observed by satellite gravimetry. *Journal of Geophysical Research,* 115, D22108, doi:10.1029/2010JD014689.

Christidis, N., G.S. Jones, and P.A. Stott. 2015. Dramatically increasing chance of extremely hot summers since the 2003 European heatwave. *Nature Climate Change,* 5, 46–50, doi:10.1038/nclimate2468.

Churkina G., and Running S.W. 1998. Contrasting climatic controls on the estimated productivity of different biomes. *Ecosystems, 1*, 206–215.

Ciais, P., and Coauthors. 2005. Europe-wide reduction in primary productivity caused by the heat and drought in 2003. *Nature*, 437, 529-533, doi:10.1038/nature03972.

Clausen, H.B., N.S. Gundestrup, S.J. Johnsen, R. Bindschadler, and J. Zwally. 1988. Glaciological investigations in the Crete area, central Greenland: A search for a new deep-drilling site. *Annals of Glaciology*, 10, 10–15.

Coakley, S. M., H. Scherm, and S. Chakraborty. 1999. Climate change and plant disease management. *Annual Review of Phytopathology*, 37, 399–426, doi:10.1146/annurev.phyto.37.1.399.

Cohen, W.B., T. A. Spies, R. J. Alig, D. R. Oetter, T. K. Maiersperger, and M. Fiorella. 2002. Characterizing 23 years (1972 – 1995) of stand replacement disturbance in western Oregon forests with Landsat imagery. *Ecosystems*, 5, 122–137, doi: 10.1007/s10021-001-0060-X.

Cook, B.I., J.E. Smerdon, R. Seager, and S. Coats. 2014. Global warming and 21st century drying. *Climate Dynamics*, 43, 2607-2627, doi:10.1007/s00382-014-2075-y.

Coops, N.C., and R.H. Waring. 2011. Estimating the vulnerability of fifteen tree species under changing climate in Northwest North America. *Ecological Modelling, 222*, 2119-2129.

Coops, N.C., M.A. Wulder, and D. Iwanicka. 2009. Large area monitoring with a MODIS-based Disturbance Index (DI) sensitive to annual seasonal variations. *Remote Sensing of Environment, 113*, 1250-1261.

Coumou, D., and S. Rahmstorf. 2012. A decade of weather extremes. *Nature Climate Change*, 2, 491-496, doi:10.1038/nclimate1452.

Cox, P.M., R.A. Betts, M. Collins, P.P. Harris, C. Huntingford, and C.D. Jones. 2004. Amazonian forest dieback under climate-carbon cycle projections for the 21st century. *Theoretical and Applied Climatology*, 78, 137-156, doi:10.1007/s00704-004-0049-4.

Daly, C., M. Halbleib, J.I. Smith, W.P. Gibson, M.K. Doggett, G.H. Taylor, J. Curtis, and P.P. Pasteris. 2008. Physiographically-sensitive mapping of temperature

and precipitation across the conterminous United States. *International Journal of Climatology*, 28, 2031-2064, doi:10.1002/joc.1688.

Delucia E.H., H. Maherali, and E.V. Carey. 2000. Climatic-driven changes in biomass allocation in pines. *Global Change Biology, 6*, 587-593.

Dobbertin M., and P. Brand. 2001. Crown defoliation improves tree mortality models. Forest *Ecology and Management, 141*, 271–284.

Easterling D. R., J. L. Evans, P. Y. Groisman, T. R. Karl, K. E. Kunkel, and P. Ambenje. 2000. Observed variability and trends in extreme climate events: a brief review. *Bulletin of the American Meteorological Society*, 81, 417–42, doi.org/10.1175/1520-0477(2000)081<0417:OVATIE>2.3.CO;2.

Elliot, A.J., and Coauthors. 2014. Using real-time syndromic surveillance to assess the health impacts of the 2013 heatwave in England. *Environmental Research*, 135, 31-36, doi:10.1016/j.envres.2014.08.031.

Ellison, A.M., and Coauthors. 2005. Loss of foundation species: consequences for the structure and dynamics of forested ecosystems. *Frontiers in Ecology and the Environment, 3*, 479-486.

Feldpausch, T.R., and Coauthors. 2016. Amazon forest response to repeated droughts. *Global Biogeochemical Cycles*, 30, 964-982, doi:10.1002/2015GB005133.

Fischer, E.M., and C. Schär. 2010. Consistent geographical patterns of changes in high-impact European heatwaves. *Nature Geoscience*, 3, 398-403, doi:10.1038/ngeo866.

Fouillet, A., and Coauthors. 2008. Has the impact of heat waves on mortality changed in France since the European heat wave of summer 2003? A study of the 2006 heat wave. *International Journal of Epidemiology*, 37, 309-317, doi:10.1093/ije/dym253.

Founda, D., and C. Giannakopoulos. 2009. The exceptionally hot summer of 2007 in Athens, Greece — A typical summer in the future climate? *Global Planetary Change*, 67, 227–236 doi:10.1016/j.gloplacha.2009.03.013.

Friedl, M.A., and Coauthors. 2002. Global land cover mapping from MODIS: algorithms and early results. *Remote Sensing of Environment*, 83, 287-302, doi:10.1016/S0034-4257(02)00078-0.

Friedl, M.A., and F.W. Davis. 1994. Sources of Variation in Radiometric Surface Temperature over a Tallgrass Prairie. *Remote Sensing of Environment*, 48, 1-17, doi:10.1016/0034-4257(94)90109-0.

Friedl, M.A., D. Sulla-Menashe, B. Tan, A. Schneider, N. Ramankutty, A. Sibley, and X.M. Huang. 2010. MODIS Collection 5 global land cover: Algorithm refinements and characterization of new datasets. *Remote Sensing of Environment*, 114, 168-182, doi:10.1016/j.rse.2009.08.016.

Fuhrman, C. M., C. E. Konrad II, M. M. Kovach, and D. J. Perkins. 2011. THE AUGUST 2007 HEAT WAVE IN NORTH CAROLINA: METEOROLOGICAL FACTORS AND LOCAL VARIABILITY, *Physical Geography*, 32, 217-240, doi: 10.2747/0272-3646.32.3.217.

Gadgil, P. D. 1977. Duration of leaf wetness periods and infection of *Pinus radiata* by *Dothistroma pini. New Zealand Journal of Forest Science*, 7, 83–90.

Goward, S. N., and Coauthhors. 2008. Forest Disturbance and North American Carbon Flux, *EOS, Transactions*, *89*, 105-116, doi:10.1029/2008EO110001.

Goward, S.N., G.D. Cruickshanks, and A.S. Hope. 1985. Observed relation between thermal emission and reflected spectral radiance of a complex vegetated landscape. *Remote Sensing of Environment*, 18, 137-146, doi:10.1016/0034-4257(85)90044-6.

Griffin, D., and K.J. Anchukaitis. 2014. How unusual is the 2012–2014 California drought? *Geophysical Research Letters*, *41*, 9017–9023, doi:10.1002/2014GL062433.

Grimm, N.B., and Coauthors. 2013: The impacts of climate change on ecosystem structure and function. *Frontiers in Ecology and the Environment*, 11, 474-482, doi:10.1890/120282.

Grumm, R.H., 2011. The central European and Russian heat event of July-August 2010. *Bulletin of the American Meteorological Society*, 92, 1285-1296, doi:10.1175/2011BAMS3174.1.

Gutmann, E.D., R.M. Rasmussen, C. Liu, K. Ikeda, D.J. Gochis, M.P. Clark, J. Dudhia, and G. Thompson. 2012. A Comparison of Statistical and Dynamical Downscaling of Winter Precipitation over Complex Terrain. *Journal of Climate,* 25, 262–281, doi:10.1175/2011JCLI4109.1.

Hadfield, J., and B. Douglas. 1982. Protection of Douglas-fir Christmas trees from Swiss needle cast in Oregon. *American Christmas Tree Journal*, 26, 31–33.

Hansen, A. H., T. A. Spies, F. J. Swanson, and J. L. Ohmann. 1991. Conserving biodiversity in managed forests. *BioScience*, 41, 382-292.

Hansen, E. M., J. K. Stone, B. R. Capitano, P. Rosso, W. Sutton, L. Winton, A. Kanaskie, and M. G. McWilliams. 2000. Incidence and impact of Swiss needle cast in forest plantations of Douglas-fir in coastal Oregon. *Plant Disease*, 84, 773–778, doi:10.1094/PDIS.2000.84.7.773.

Hansen, J., M. Sato, R. Ruedy, K. Lo, D. W. Lea, and M. Medina-Elizade. 2006. Global Temperature Change, *Proceedings of the National Academy of Sciences U.S.A.*, 103, 14288-14293, doi:10.1073/pnas.0606291103.

Hansen, J., M. Sato, and R. Ruedy. 2012. Perception of climate change. *Proceedings of the National Academy of Sciences U.S.A.*, 109, E2415-E2423, doi:10.1073/pnas.0808533106.

Hansen, M. C., and Coauthors, 2013. High-resolution global maps of 21st-century forest cover change. *Science*, 342, 850-853, doi:10.1126/science.1244693.

Hartmann, H., H.D. Adams, W.R.L. Anderegg, S. Jansen, and M.J.B. Zeppel. 2015. Research frontiers in drought-induced tree mortality: crossing scales and disciplines. *New Phytologist*, 205, 965-969.

Hastenrath, S., D. Polzin, and C. Mutai. 2007. Diagnosing the 2005 drought in equatorial East Africa. *Journal of Climate*, 20, 4628-4637 doi:10.1175/JCLI4238.1.

Haugo, R.D., S.A. Hall, E.M. Gray, P. Gonzalez, and J.D. Bakker. 2010. Influences of climate, fire, grazing, and logging on woody species composition along an elevational gradient in the eastern Cascades, Washington. *Forest Ecology and Management*, 260, 2204–2213.

Hawkes, C. V., S. N. Kivlin, J. D. Rocca, V. Huguet, M. A. Thomsen, and K. B. Suttle. 2011. Fungal community responses to precipitation. *Global Change Biology*, 17, 1637–1645. doi:10.1111/j.1365-2486.2010.02327.x.

He, T., S. Liang, Y. Yu, Q. Liu, D. Wang, F. Gao and Q Liu. 2013. Greenland surface albedo changes in July 1981–2012 from satellite observations. *Environmental Research Letters*, 8, 1-9, doi:10.1088/1748-9326/8/4/044043.

Hicke, J.A., and Coauthors. 2012. Effects of bioticdisturbance on forest carbon cycling in the United States and Canada. *Global Change Biology, 18*, 7-34.

Hilker, T., A. I. Lyapustin, C. J. Tucker, F. G. Hall, R. B. Myneni, Y. Wang, J. Bi, Y. Mendes de Moura, and P. J. Sellers. 2014. Vegetation dynamics and rainfall sensitivity of the Amazon. *Proceedings of the National Academy of Sciences U.S.A.*, 111, 16041-16046, doi:10.1073/pnas.1404870111.

Hoerling, M., and Coauthors, 2013. Anatomy of an Extreme Event. *Journal of Climate*, 26, 2811-2832 doi:10.1175/JCLI-D-12-00270.1.

Hoff, R. J. 1985. Susceptibility of Lodgepole Pine to the Needle Cast Fungus *Lophodermella concolor*. Ogden (UT): US Department of Agriculture Forest Service, Intermountain Experiment Station. Research Note INT-349.

Hood, I. A. 1982. *Phaeocryptopus gaeumannii* on *Pseudotsuga menziesii* in southern British Columbia. *New Zealand Journal of Forestry Science*, 12, 415–424.

IPCC. 2013. *Climate Change 2013: The Physical Science Basis. Contribution of Working Group I to the Fifth Assessment Report of the Intergovernmental Panel on Climate Change*, T. F. Stocker, D. Qin, G.-K. Plattner, M. Tignor, S. K. Allen, J. Boschung, A. Nauels, Y. Xia, V. Bex, P. M. Midgley, Eds. (Cambridge Univ. Press, 2013), 1535 pp.

Janetos, A.C., R.S. Chen, D. Arndt, M.A. Kenney. 2012. *National Climate Assessment Indicators: Background, Development, and Examples*. Columbia University Academic Commons, http://hdl.handle.net/10022/AC:P:21146.

Jasechko, S., Sharp, Z.D., Gibson, J.J., Birks, S.J., Yi, Y., and Fawcett, P.J. 2013. Terrestrial water fluxes dominated by transpiration. *Nature, 496*, 347-351.

Jentsch, A., J. Kreyling, and C. Beierkuhnlein. 2007. A new generation of climate change experiments: events, not trends. *Frontiers in Ecology and the Environment*, 5, 365-374, doi:10.1890/1540-9295(2007)5[365:ANGOCE]2.0.CO;2.

Jentsch, A., J. Kreyling, J. Boettcher-Treschkow, and C. Beierkuhnlein. 2009. Beyond gradual warming: extreme weather events alter flower phenology of European grassland and heath species. *Global Change Biology*, 15, 837–849. doi:10.1111/j.1365-2486.2008.01690.x.

Jin, M. S., and T. J. Mullens. 2012. Land–biosphere–atmosphere interactions over the Tibetan plateau from MODIS observations. *Environmental Research Letters,* 7, 014003, doi: 10.1088/1748-9326/7/1/014003.

Jin, M., and R. E. Dickinson. 2010. Land surface skin temperature climatology: benefitting from the strengths of satellite observations. *Environmental Research Letters*, 5, 1-13, doi:10.1088/1748-9326/5/4/044004.

Jones, H.G. 1999. Use of thermography for quantitative studies of spatial and temporal variation of stomatal conductance over leaf surfaces. *Plant Cell Environment, 22, 9*, 1043–1055.

Joyce, L.A., S.W. Running, D.D. Breshears, V.H. Dale, R.W. Malmsheimer, R.N. Sampson, B. Sohngen, and C.W. Woodall. 2014. Ch. 7: Forests. *Climate Change Impacts in the United States: The Third National Climate Assessment*. In J. M. Melillo, T. C. Richmond, and G. W. Yohe (Eds.), U.S. Global Change Research Program, 175-194, doi:10.7930/J0Z60KZC.

Julien, Y., and J.A. Sobrino. 2008. The Yearly Land Cover Dynamics (YLCD) method: An analysis of global vegetation from NDVI and LST parameters. *Remote Sensing of Environment, 113*, 329-334, doi:10.1016/j.rse.2008.09.016.

Karl, T. R., and Coauthors. 2012. U.S. temperature and drought: Recent anomalies and trends. *Eos, Transactions,* 93, 473-474, doi:10.1029/2012EO470001.

Karl, T. R., C. D. Miller, and W. L. Murray. 2006. Temperature Trends in the Lower Atmosphere: Steps for Understanding and Reconciling Differences. In T. R. Karl, S. J. Hassol, C. D. Miller, and W. L. Murray (Eds.), *A Report by the Climate Change Science Program and the Subcommittee on Global Change Research*, Washington, DC.

Karoly, D. J. 2009. The recent bushfires and extreme heat wave in southeast Australia, *Bulletin of the Australian Meteorological and Oceanographic Society,* 22, 10-13.

Katz, R. W., and B. G. Brown. 1992. Extreme events in a changing climate: Variability is more important than averages. *Climatic Change*, 21, 3, 289–302, doi:10.1007/BF00139728.

Kennedy, R.E., Z.G. Yang, and W.B. Cohen. 2010. Detecting trends in forest disturbance and recovery using yearly Landsat time series: 1. LandTrendr - Temporal segmentation algorithms. *Remote Sensing of Environment, 114*, 2897-2910.

Kenney, M. A., and A. C. Janetos. 2014. *National Climate Indicators System Report*, National Climate Assessment and Development Advisory Committee, http://www.globalchange.gov/sites/globalchange/files/Pilot-Indicator-System-Report_final.pdf.

Kerr, J., and Coauthors. 2015. Climate change impacts on bumblebees converge across continents. *Science*, 349, 177–180, doi:10.1126/science.aaa7031.

Khan, S. A., and Coauthors. 2014. Sustained mass loss of the northeast Greenland ice sheet triggered by regional warming. *Nature Climate Change*, 4, 292-299, doi:10.1038/nclimate2161.

Kim, Y., C. J. Still, C. V. Hanson, H. Kwon, B. T. Greer, and B. E. Law. 2016. Canopy skin temperature variations in relation to climate, soil temperature, and carbon flux at a ponderosa pine forest in central Oregon, *Agricultural and Forest Meteorology*, 226, 161-173.

King, M. D. 1999. *EOS Science Plan: The State of Science in the EOS Program*, 397 pp., NASA, Washington, D.C.

Klos, P.Z., T.E. Link, and J.T. Abatzoglou. 2014. Extent of the rain-snow transitionzone in the western U.S. under historic and projected climate. *Geophysical Research Letters, 41*, 4560-4568, doi:10.1002/ 2014GL060500.

Kogan, F.N. 1997. Global Drought Watch from Space. *Bulletin of the American Meteorological Society*, 78, 621–636, doi:10.1175/1520-0477(1997)078<0621:GDWFS>2.0.CO;2.

Kurz, W. A., G. Stinson, G. J. Rampley, C. C. Dymond, and E. T. Neilson. 2008. Risk of natural disturbances makes future contribution of Canada's forests to the global carbon cycle highly uncertain. *Proceedings of the National Academy of Sciences U.S.A., 105*, 1551-1555.

Lambin, E. F., and D. Ehrlich. 1995. Combining vegetation indices and surface temperature for land-cover mapping at broad spatial scales. *International Journal of Remote Sensing*, 16, 573-579, doi:10.1080/01431169508954423.

Lee, E., P. Beedlow, R. Waschmann, C. Burdick, and D. Shaw. 2013. Tree-ring analysis of the fungal disease Swiss needle cast in Western Oregon coastal forests. *Canadian Journal of Forest Research*, 43(8), 677-690, doi:dx.doi.org/10.1139/cjfr-2013-0062.

Lee, X., and Coauthors. 2011. Observed increase in local cooling effect of deforestation at higher latitudes. *Nature*, 479, 384-387, doi:10.1038/nature10588.

Lenaerts, J.T.M., J.H. van Angelen, M.R. van den Broeke, A.S. Gardner, B. Wouters, and E. van Meijgaard. 2013. Irreversible mass loss of Canadian Arctic Archipelago glaciers. *Geophysical Research Letters*, 40, 870-874, doi:10.1002/grl.50214.

Lewis, S.C., and D.J. Karoly. 2013. Anthropogenic contributions to Australia's record summer temperatures of 2013. *Geophysical Research Letters*, 40, 3705-3709, doi:10.1002/grl.50673.

Lewis, S.L., P.M. Brando, O.L. Phillips, G.M.F. van der Heijden, and D. Nepstad. 2011. The 2010 Amazon drought. *Science*, 331, 554, doi:10.1126/science.1200807.

Li, Y., M. Zhao, S. Motesharrei, Q. Mu, E. Kalnay, and S. Li. 2015. Local cooling and warming effects of forests based on satellite observations. *Nature Communications*, 6, 6603, doi:10.1038/ncomms7603.

Li, Z.L., B.H. Tang, H. Wu, H. Ren, G. Yan, Z. Wan, I.F. Trigo, and J.A. Sobrino. 2013. Satellite-derived land surface temperature: Current status and perspectives. *Remote Sensing of Environment*, 131, 14-37, doi:10.1016/j.rse.2012.12.008.

Li, Z.-L., and J. Becker. 1993. Feasibility of land surface temperature and emissivity determination from AVHRR data. *Remote Sensing of Environment*, 43, 67-85.

Loarie, S.R., Lobell, D.B., Asner, G.P., Mu, Q., and Field, C.B. 2011. Direct impacts on local climate of sugar-cane expansion in Brazil. *Nature Climate Change, 1*, 105-109.

Logan, J. A., J. Régnière, and J. A. Powell. 2003. Assessing the impacts of global warming on forest pest dynamics. *Frontiers in Ecology and the Environment*, 130–137, doi:10.1890/1540-9295(2003)001[0130:ATIOGW]2.0.CO;2.

Long, D., B.R. Scanlon, L. Longuevergne, A.Y. Sun, D.N. Fernando, and H. Save. 2013. GRACE satellites monitor large depletion in water storage in response to the 2011 drought in Texas. *Geophysical Research Letters*, 40, 3395-3401, doi:10.1002/grl.50655.

Lonsdale D., and J. N. Gibbs. 1996. Effects of climate change on fungal diseases of trees. In Frankland J. C., N. Magan, G. M. Gadd, eds. 1996. *Fungi and Environmental Change*. Cambridge (United Kingdom): Cambridge University Press, 1–19, doi:10.1017/CBO9780511753190.002.

Maguire, D. A., A. Kanaskie, W. Voelker, R. Johnson, and G. Johnson. 2002. Growth of young Douglas-fir plantations across a gradient in Swiss needle cast severity. *Western Journal of Applied Forestry*, 17(2), 86-95.

Malhi, Y., J.T. Roberts, R.A. Betts, T.J. Killeen, W.H. Li, and C.A. Nobre. 2008. Climate change, deforestation, and the fate of the Amazon. *Science*, 319, 169-172, doi:10.1126/science.1146961.

Malhi, Y., L.E.O.C. Aragão, D. Galbraith, C. Huntingford, R. Fisher, P. Zelazowski, S. Sitch, C. McSweeney, and P. Meir. 2009. Exploring the likelihood and mechanism of a climate-change-induced dieback of the Amazon rainforest. *Proceedings of the National Academy of Sciences U.S.A.*, 106, 20610-20615, doi:10.1073/pnas.0804619106.

Mannstein, H. 1987. Surface energy budget, surface temperature and thermal intertia, in *Remote Sensing Applications in Meteorology and Climatology*, edited by R. A. Vaughan and D. Reidel, pp. 391-410, A Reidel Publishing Co., Dordrecht, Netherlands.

Manter, D. K., B. J. Bond, K. L. Kavanagh, P. H. Rosso, and G. M. Filip. 2000. Pseudothecia of Swiss needle cast fungus, Phaeocryptopus gaeumannii, physically block stomata of Douglas fir, reducing CO2 assimilation. *New Phytologist*, 148, 481–491, doi:10.1046/j.1469-8137.2000.00779.x.

Manter, D. K., P. W. Reeser, and J. K. Stone. 2005. A climate-based model for predicting geographic variation in Swiss needle cast severity in the Oregon Coast Range. *Phytopathology*, 95, 1256–1265, doi:10.1094/PHYTO-95-1256.

Manzoni, S., G. Vico, A. Porporato, and G. Katul. 2013. Biological constraints on water transport in the soil-plant-atmosphere system. *Advances in Water Resources, 51, 292-304, doi:*10.1016/j.advwatres.2012.03.016.

Marengo, J. A., C. Nobre, J. Tomasella, G. Sampaio, and H. Camargo. 2008. The drought of Amazonia in 2005. *J. Climate*, 21, 495-516, doi:10.1175/2007JCLI1600.1.

Marengo, J.A., J. Tomasella, L.M. Alves, W.R. Soares, and D.A. Rodriguez. 2011. The drought of 2010 in the context of historical droughts in the Amazon

region. *Geophysical Research Letters*, 38, L12703, doi:10.1029/2011GL047436.

Martinez-Vilalta, J., F. Lloret, and D. Breshears. 2011. Drought-induced forest decline: causes, scope and implications. *Biology Letters, 8*, 689-691.

Mather, J.R., and G.A.Yoshioka. 1968. The role of climate in the distribution of vegetation. *Annals of the Association of American Geographers, 58*, 29-41.

McDowell, N.G. and Coauthors, 2015. Global satellite monitoring of climate-induced vegetation disturbances. *Trends in Plant Science*, 20, 114–123, doi:10.1016/j.tplants.2014.10.008.

McDowell, N.G, and C.D. Allen. 2015. Darcy's law predicts widespread forest mortality under climate warming. *Nature Climate Change, 5*, 669-672, doi:10.1038/NCLIMATE2641.

McDowell, N.G., W.T. Pockman, C.D. Allen, D.D. Breshears, N. Cobb, T. Kolb, J. Plaut, J. Sperry, A. West, D.G. Williams, and E.A. Yepez. 2008. Mechanisms of plant survival and mortality during drought: why do some plants survive while others succumb to drought? *New Phytologist*, 178, 719–739.

McKechnie, A.E., P.A. Hockey, and B.O. Wolf. 2012. Feeling the heat: Australian landbirds and climate change. *Emu*, 112, i-vii, doi:10.1071/MUv112n2_ED.

McMillan, M., and Coauthors. 2016. A high-resolution record of Greenland mass balance. *Geophysical Research Letters*, 43, 7002-7010, doi:10.1002/2016GL069666.

Mearns, L. O., R. W. Katz, and S. H. Schneider. 1984. Extreme high temperature events: Changes in their probabilities with changes in mean temperature. *Journal of Climate and Applied Meteorology*, 23, 1601–1613, doi.org/10.1175/1520-0450(1984)023<1601:EHTECI>2.0.CO;2.

Meehl, G. A., and Coauthors. 2000. An Introduction to Trends in Extreme Weather and Climate Events: Observations, Socioeconomic Impacts, Terrestrial Ecological Impacts, and Model Projections. *Bulletin of the American Meteorological Society*, 81, 3, doi.org/10.1175/1520-0477(2000)081<0413:AITTIE>2.3.CO;2.

Meigs, G.W., R.E. Kennedy, and W.B. Cohen. 2011. A Landsat time series approach to characterize bark beetle and defoliator impacts on tree mortality and surface fuels in conifer forests. *Remote Sensing of Environment*, 115, 3707-3718.

Melillo J. M., T. C. Richmond, and G. W. Yohe, (Eds). 2014. Climate Change Impacts in the United States: The Third National Climate Assessment, U.S. Global Change Research Program, 841 pp., doi:10.7930/J0Z31WJ2.

Michaels, E., and G. A. Chastagner. 1984. Distribution, severity and impact of Swiss needle cast in Douglas-fir Christmas trees in western Washington and Oregon. *Plant Disease*, 68, 939–942, doi:10.1094/PD-69-939.

Mildrexler, D.J., M. Zhao, and S.W. Running. 2011a. A global comparison between station air temperatures and MODIS land surface temperatures reveals the cooling role of forests. *Journal of Geophysical Research*, 116, G03025, doi:10.1029/2010JG001486.

Mildrexler, D.J., M. Zhao, and S.W. Running. 2011b. Satellite Finds Highest Land Skin Temperatures on Earth. *Bulletin of the American Meteorological Society*, 92, 855-860, doi:10.1175/2011BAMS3067.1.

Mildrexler, D.J., M. Zhao, and S.W. Running. 2009. Testing a MODIS Global Disturbance Index across North America. *Remote Sensing of Environment*, 113, 2103-2117, doi:10.1016/j.rse.2009.05.016.

Mildrexler, D.J., M. Zhao, F.A. Heinsch, and S.W. Running. 2007. A new satellite-based methodology for continental scale disturbance detection. *Ecological Applications*, 17, 235-250, doi:10.1890/1051-0761(2007)017[0235:ANSMFC]2.0.CO;2.

Mildrexler, D.J., Z. Yang, W.B. Cohen, and D.M. Bell. 2016. A forest vulnerability index based on drought and high temperatures. *Remote Sensing of Environment*, 173, 314-325, doi:10.1016/j.rse.2015.11.024.

Millar, C.I. and N. L. Stephenson. 2015. Temperature forest health in an era of emerging megadisturbance. *Science, 349,* 823-826.

Mitchell, P.J., A.P. O'Grady, K.R. Hayes, and E.A. Pinkard. 2014. Exposure of trees to drought-induced die-off is defined by a common climatic threshold across different vegetation types. *Ecology and Evolution*, 4, 1088-1101, doi:10.1002/ece3.1008.

Montenegro, A., M. Eby, Q. Mu, M. Mulligan, A.J. Weaver, E.C. Wiebe, and M. Zhao. 2009. The net carbon drawdown of small scale afforestation from satellite observations. *Global and Planetary Change, 69,* 195-204.

Moritz, M. A., M.-A. Parisien, E. Batllori, M.A. Krawchuk, J. Van Dorn, D.J. Ganz, and K. Hayhoe. 2012. Climate change and disruptions to global fire activity. *Ecosphere*, 3, 1-22, doi:10.1890/ES11-00345.1.

Mote, P.W. and E.P. Salathé, Jr. 2010. Future climate in the Pacific Northwest. *Climatic Change*, doi:10.1007/ s10584-010-9848-z.

Mote, P.W., A.F. Hamlet, M.P. Clark, and D.P. Lettenmaier. 2005. Declining mountain snowpack in western North America. *Bulletin of the American Meteorological Society,* 86, 39-49.

Mu, Q., Jones, L.A., Kimball, J.S., McDonald, K.C., and S.W. Running. 2009. Satellite assessment of land surface evapotranspiration for the pan-Arctic domain. *Water Resources Research, 45,* W09420, doi:10.1029/2008WR007189.

Mu, Q., M. Zhao, J.S. Kimball, N.G. McDowell, and S.W. Running. 2013. A Remotely Sensed Global Terrestrial Drought Severity Index. *Bulletin of the American Meteorological Society*, 94, 83-98, doi:10.1175/BAMS-D-11-00213.1.

Mu, Q., M. Zhao, and S.W.Running. 2011. Improvements to a MODIS Global Terrestrial Evapotranspiration Algorithm. *Remote Sensing of Environment, 115*, 1781-1800.

Mu, Q., M. Zhao, F.A. Heinsch, M. Liu, H. Tian, and S.W. Running. 2007. Evaluating water stress controls on primary production in biogeochemical and remote sensing based models. *Journal of Geophysical Research, 112*, G01012.

Neff, W., G.P. Compo, F.M. Ralph, and M.D. Shupe. 2014. Continental heat anomalies and the extreme melting of the Greenland ice surface in 2012 and 1889. *Journal of Geophysical Research Atmospheres*, 119, 6520-6536, doi: 10.1002/2014JD021470.

Nemani, R. R., and S. W. Running. 1989. Estimation of Regional Surface Resistance to Evapotranspiration from NDVI and Thermal-IR AVHRR Data. *Journal of Applied Meteorol*ogy, 28, 276-284, doi.org/10.1175/1520-0450(1989)028<0276:EORSRT>2.0.CO;2.

Nemani, R. R., and S. W. Running. 1997. Land cover characterization using multitemporal red, near-IR, and thermal-IR data from NOAA/AVHRR. *Ecological Applications,* 7, 79-90, doi:10.1890/1051-0761(1997)007[0079:LCCUMR]2.0.CO;2.

Nemani, R.R., L.L. Pierce, and S.W. Running. 1993. Developing satellite derived estimates of surface moisture status. *Journal of Applied Meteorol*ogy, 32, 548-557, doi:10.1175/1520-0450(1993)032<0548:DSDEOS>2.0.CO;2.

Nemani, R.R., and S.W. Running, 2003. Climate-driven increases in global terrestrial net primary production from 1982 to 1999. *Science, 300*, 1560−1563.

Nghiem, S.V., and Coauthors. 2012. The extreme melt across the Greenland ice sheet in 2012. *Geophysical Research Letters*, 39, L20502, doi:10.1029/2012GL053611.

Norman, J. M., and F. Becker. 1995. Terminology in thermal infrared remote sensing of nature surfaces. *Agricultural and Forest Meteorology*, 77, 153–66, doi:10.1016/01681923(95)02259-Z.

Ohmann, J. L. and M. J. Gregory. 2002. Predictive mapping of forest composition andstructure with direct gradient analysis and nearest-neighbor imputation in coastal Oregon, U.S.A. *Canadian Journal of Forest Research*, 32, 725–741, doi:10.1139/X02-011.

Ohmann, J. L., and T. A. Spies. 1998. Regional gradient analysis and spatial pattern of woody plant communities of Oregon forests. *Ecological Monographs*, 68, 151 – 182.

Omernik, J.M. 1987. Ecoregions of the conterminous United States. *Annals of the Association of American Geographers, 77*, 118–125.

Overpeck, J.T. 2013. The challenge of hot drought. *Nature, 503*, 350–351.

Oyler, J.W., S.Z. Dobrowski, Z.A. Holden, and S.W. Running. 2016. Remotely sensed land skin temperature as a spatial predictor of air temperature across the conterminous United States. *Journal of Applied Meteorology and Climatology*, 55, 1441-1457, doi:10.1175/JAMC-D-15-0276.1.

Parkinson, C. L. 2003. Aqua: An Earth-observing satellite mission to examine water and other climate variables, *IEEE Transactions on Geoscience and Remote Sensing*, 41, (2), 173–183, DOI: 10.1109/TGRS.2002.808319

Parkinson, C. L. 2013. Summarizing the First Ten Years of NASA's Aqua Mission. *IEEE Journal of Selected Topics in Applied Earth Observations and Remote Sensing*, 6, 1179-1188, doi:10.1109/JSTARS.2013.2239608.

Pedersen, B.S. 1998. The role of stress in the mortality of Midwestern oaks as indicated by growth prior to death. *Ecology, 79*, 79–93.

Penuelas, J., and I. Filella. 2001. Phenology – responses to a warming world. *Science*, 294, 793–795, doi:10.1126/science.1066860.

Perkins, S.E., L.V. Alexander, and J.R. Nairn. 2012. Increasing frequency, intensity and duration of observed global heatwaves and warm spells. *Geophysical Research Letters*, 39, L20714, doi:10.1029/2012GL053361.

Peterson, D.L, and R.H. Waring. 1994. Overview of the Oregon Transect Ecosystem Research Project. *Ecological Applications*, 4, 211–225.

Peterson, G. W. 1973. Infection of Austrian and ponderosa pines by *Dothistroma pini* in Eastern Nebraska. *Phytopathology*, 63, 1060–1063, doi:10.1094/Phyto-63-1060.

Peterson, T. C., D. M. Anderson, S. J. Cohen, M. Cortez-Vázquez, R .J. Murnane, C. Parmesan, D. Phillips, R. S. Pulwarty, J. M. R. Stone. 2008. Why Weather and Climate Extremes Matter in *Weather and Climate Extremes in a Changing Climate. Regions of Focus: North America, Hawaii, Caribbean, and U.S. Pacific Islands*. T.R. Karl, G.A. Meehl, C.D. Miller, S.J. Hassol, A.M. Waple, and W.L. Murray (eds.). A Report by the U.S. Climate Change Science Program and the Subcommittee on Global Change Research, Washington, DC.

Pielke, R.A., Sr., and Coauthors. 2007. Unresolved issues with the assessment of multidecadal global land surface temperature trends. *Journal of Geophysical Research*, 112, D24S08, doi:10.1029/2006JD008229.

Potter, C., P. Tan, M. Steinback, S. Klooster, V. Kumar, R. Myneni, and V. Genovese. 2003. Major Disturbance Events in Terrestrial Ecosystems Detected using Global Satellite Data Sets. *Global Change Biology*, 9, 1005-1021, doi:10.1046/j.1365-2486.2003.00648.x.

Prata, A.J., V. Caselles, C. Coll, J.A. Sobrino, and C. Ottlé. 1995. Thermal remote sensing of land surface temperature from satellites: Current status and future prospects. *Remote Sensing Reviews*, 12, 175-224, doi:10.1080/02757259509532285.

Pravalie, R., I. Sîrodoev, and D. Peptenatu. 2014. Detecting climate change effects on forest ecosystems in Southwestern Romania using Landsat TM NDVI data. *Journal of Geographical Science, 24*, 815–832.

Rebetez, M., O. Dupont, and M. Giroud. 2008. An analysis of the July 2006 heatwave extent in Europe compared to the record year of 2003. *Theoretical and Applied Climatology*, 95, 1–7, doi:10.1007/s00704-007-0370-9.

Rich, P. M., D. D. Breshears, and A. B. White. 2008. Phenology of mixed woody-herbaceous ecosystems following extreme events: net and differential response. *Ecology*, 89, 342–352. doi:10.1890/06-2137.1.

Ritokova, G., D. C. Shaw, G. Filip, A. Kanaskie, J. Browning and D. Norlander. 2016. Swiss Needle Cast in Western Oregon Douglas-Fir Plantations: 20-Year Monitoring Results. *Forests*, 7, 155, doi:10.3390/f7080155.

Rockström, J., and Coauthors. 2009. Planetary boundaries: exploring the safe operating space for humanity. *Ecology and Society*, 14, 32.

Rosso, P. H., and E. M. Hansen. 2003. Predicting Swiss needle cast disease distribution and severity in young Douglas-fir plantations in coastal Oregon. *Phytopathology*, 93, 790–798, doi:10.1094/PHYTO.2003.93.7.790.

Ruefenacht, B., and Coauthors. 2008. Conterminous U.S. and Alaska Forest Type Mapping Using Forest Inventory and Analysis Data. *Photogrammetric Engineering and Remote Sensing, 74 (11)*, 1379-1388.

Running, S. W. 2008. Ecosystem Disturbance, Carbon, and Climate. *Science*, 321, 652-653, doi: 10.1126/science.1159607.

Saatchi, S., S. Asefi-Najafabady, Y. Malhi, L.E.O.C. Aragao, L.O. Anderson, R.B. Myneni, and R. Nemani. 2013. Persistent effects of a severe drought on Amazonian forest canopy. *Proceedings of the National Academy of Sciences U.S.A.*, 110, 565-570, doi:10.1073/pnas.1204651110.

Sandholt, I., K. Rasmussen, and J. Andersen. 2002. A simple interpretation of the surface temperature/vegetation index space for assessment of surface moisture status. *Remote Sensing of Environment*, 79, 213-224, doi:10.1016/S0034-4257(01)00274-7.

Scherrer, D.M., K-F. Bader, and C. Korner. 2011. Drought-sensitivity ranking of deciduous tree species based on thermal imaging of forest canopies. *Agricultural Forest Meteorology, 151*, 1632-1640.

Schubert, S. D., H. Wang, R. D. Koster, M. J. Suarez, and P. Y. Groisman. 2014. Northern Eurasian heat waves and droughts. *Journal of Climate*, 27, 3169-3207, doi:10.1175/JCLI-D-13-00360.1.

Schwalm, C. R., and Coauthors. 2012. Reduction in carbon uptake during turn of the century drought in western North America. *Nature Geoscience*, 5, 551-556, doi:10.1038/ngeo1529.

Seneviratne, S. I., M.G. Donat, B. Mueller, and L.V. Alexander. 2014. No pause in the increase of hot temperature extremes. *Nature Climate Change*, 4, 161-163, doi:10.1038/nclimate2145.

Shaposhnikov, D., and Coauthors. 2014. Mortality related to air pollution with the moscow heat wave and wild fire of 2010. *Epidemiology*, 25, 359-364, doi:10.1097/EDE.0000000000000090.

Shaw, D. C., G. M. Filip, A. Kanaskie, D. A. Maguire, and W. A. Littke. 2011. Managing an epidemic of Swiss needle cast in the Douglas-fir region of Oregon: The role of the Swiss Needle Cast Cooperative. *Journal of Forestry*, 2011, 109, 109–119.

Sinclair, J. G. 1922. Temperatures of the soil and air in a desert. *Mon. Wea. Rev*., 50, 142-144, doi:10.1175/1520-0493(1922)50<142b:TOTSAA>2.0.CO;2.

Smith, A. M. S., and Coauthors. 2014. Remote sensing the vulnerability of vegetation in natural terrestrial ecosystems. *Remote Sensing of Environment, 154*, 322-337.

Smith, M. D. 2011. The ecological role of climate extremes: current understanding and future prospects. *Journal of Ecology*, 99, 651–655, doi:10.1111/j.1365-2745.2011.01833.x

Smith, R. C. G., and B. J. Choudhury. 1990. Analysis of normalized difference and surface temperature observations over southeastern Australia. *International Journal of Remote Sensing*, 12, 2021-2044, doi:10.1080/01431169108955234.

Solberg, S. 2004. Summer drought: a driver for crown condition and mortality of Norway spruce in Norway. *Forest Pathology, 34*, 93–104.

Steffen, W., P.J. Crutzen, and J R. McNeill. 2007. The Anthropocene: are humans now overwhelming the great forces of Nature? *Ambio*, 36, 614-621.

Steinkamp, J. and T. Hickler. 2015. Is drought-induced forest dieback globally increasing? *Journal of Ecology*, 103, 31-42.

Stephenson, N. 1990. Climatic control of vegetation distribution: the role of the water balance. *The American Naturalist*, 135(5), 649-670.

Stone, J. K., L. B. Coop, and D. K. Manter. 2008a. Predicting effects of climate change on Swiss needle cast disease severity in Pacific Northwest forests. *Canadian Journal of Plant Pathology*, 30, 169–176, doi:10.1080/07060661.2008.10540533.

Stone, J. K., B. R. Capitano, and J. L. Kerrigan. 2008b. The histopathology of *Phaeocryptopus gaeumannii* on Douglas-fir needles. *Mycologia*, 100, 431–444. doi:10.3852/07-170R1.

Stott, P.A., D.A. Stone, and M.R. Allen. 2004. Human contribution to the European heatwave of 2003. *Nature*, 432, 610-614, doi: 10.1038/nature03089.

Suarez M.L., L. Ghermandi, and T. Kitzberger. 2004. Factors predisposing episodic drought-induced tree mortality in *Nothofagus*-site, climatic sensitivity and growth trends. *Journal of Ecology*, 92, 954-966.

Sulla-Menashe D., R.E. Kennedy, Z. Yang, J. Braaten, O.N. Krankina, and M.A. Friedl. 2014. Detecting forest disturbance in the Pacific Northwest from MODIS time series using temporal segmentation. *Remote Sensing of Environment*, 151, 114-123.

Sun, Y., X. Zhang, F.W. Zwiers, L. Song, H. Wan, T. Hu, H. Yin, and G. Ren. 2014. Rapid increase in the risk of extreme summer heat in Eastern China. *Nature Climate Change*, 4, 1082-1085, doi:10.1038/nclimate2410.

Sunday, J. M., A. E. Bates, and N. K. Dulvy. 2012. Thermal tolerance and the global redistribution of animals. *Nature Climate Change*, 2, 686–690, doi:10.1038/nclimate1539.

Swenson, S., and J. Wahr. 2006. Estimating Large-scale Precipitation Minus Evapotranspiration from GRACE Satellite Gravity Measurements. *Journal of Hydrometeorology*, 7(2), 252-270, doi:10.1175/JHM478.1.

Tao, J., Y. Zhang, X. Yuan, J. Wang and X. Zhang. 2013. Analysis of forest fires in Northeast China from 2003 to 2011. *International Journal of Remote Sensing*, 34 (22), 8235-8251, doi:10.1080/01431161.2013.837229.

Tedesco, M., X. Fettweis, M.R. van den Broeke, R.S.W. van de Wal, C.J.P.P. Smeets, W.J. van de Berg, M.C. Serreze, and J.E. Box. 2011. The role of albedo and accumulation in the 2010 melting record in Greenland. *Environmental Research Letters*, 6, 014005, doi:10.1088/1748-9326/6/1/014005.

Teskey, R., T. Wertin, I. Bauweraerts, M. Ameye, M. A. Mcguire, and K. Steppe. 2014. Responses of tree species to heat waves and extreme heat events. *Plant, Cell and Environment*, 38, 1699-1712, doi:10.1111/pce.12417.

Toomey, M., D. A. Roberts, C. Still, M. L. Goulden, and J. P. McFadden. 2011. Remotely sensed heat anomalies linked with Amazonian forest biomass declines. *Geophysical Research Letters*, 38, L19704, doi:10.1029/2011GL049041.

Trenberth, K.E., J.T. Fasullo, and J. Kiehl. 2009. Earth's global energy budget. *Bulletin of the American Meteorological Society, 90*, 311–323.

Turner, M. G. 2010. Disturbance and landscape dynamics in a changing world. *Ecology*, 91(10), 2833-2849, doi:10.1890/10-0097.1.

Van De Kerchove, R., S. Lhermitte, S. Veraverbeke, and R. Goossens. 2013. Spatio-temporal variability in remotely sensed land surface temperature, and its relationship with physiographic variables in the Russian Altay Mountains. *International Journal of Applied Earth Observation and Geoinformation*, 20, 4-19, doi:10.1016/j.jag.2011.09.007.

van Mantgem, P.J., and N.L. Stephenson. 2007. Apparent climatically induced increase of tree mortality rates in a temperate forest. *Ecology Letters, 10*, 909–916.

van Mantgem, P.J., and Coauthors. 2009. Widespread increase of tree mortality rates in the western United States. *Science, 323*, 521-524.

Vicente-Serrano, and Coauthors. 2014. Evidence of increasing drought severity caused by temperature rise in Southern Europe. *Environmental Research Letters, 9*, 044001, doi:10.1088/1748-9326/9/4/044001.

Vogelmann, J.E., B. Tolk, and Z. Zhu. 2009. Monitoring forest changes in the southwestern United States using multitemporal Landsat data. *Remote Sensing of Environment, 113*, 1739-1748.

Wan, Z. and Z.L. Li. 1997. A Physics-Based Algorithm for Retrieving Land-Surface Emissivity and Temperature from EOS/MODIS Data. *IEEE Transactions on Geoscience and Remote Sensing, 35*, 980-996.

Wan, Z., and J. Dozier. 1996. A generalized split-window algorithm for retrieving land-surface temperature from space. *IEEE Transactions on Geoscience and Remote Sensing, 34*, 892–905, doi:10.1109/36.508406.

Wan, Z. 2008. New refinements and validation of the MODIS Land-Surface Temperature/Emissivity products. *Remote Sensing of Environment*, 112, 59-74, http://dx.doi.org/10.1016/j.rse.2006.06.026.

Wan, Z., P. Wang, and X. Li. 2004b. Using MODIS land surface temperature and normalized difference vegetation index products for monitoring drought in the Southern Great Plains, USA. *International Journal of Remote Sensing, 25*, 61-72.

Wan, Z., Y. Zhang, Q. Zhang, and Z.-L. Li. 2004a. Quality assessment and validation of the MODIS global land surface temperature. *International Journal of Remote Sensing*, 25, 261-274, doi:10.1080/0143116031000116417.

Wang, H., S. Schubert, R. Koster, Y.-G. Ham, and M. Suarez. 2014. On the role of SST forcing in the 2011 and 2012 extreme U.S. heat and drought: A study in contrasts. *Journal of Hydrometeorology*, 15, 1255-1273, doi:10.1175/JHM-D-13-069.1.

Waring, R.H. 1969. Matching Species to Site. In R.K. Herman (Ed.), *Proceedings of the Symposium on Regeneration of Ponderosa Pine*. September 11-12, Corvallis, Oregon: Oregon State University.

Wendler, G., J. Conner, B. Moore, M. Shulski, and M. Stuefer. 2011. Climatology of Alaskan wildfires with special emphasis on the extreme year of 2004. *Theoretical and Applied Climatology*, 104, 459-472, doi:10.1007/s00704-010-0357-9.

Westerling, A.L., H.G. Hidalgo, D.R. Cayan, and T.W. Swetnam. 2006. Warming and Earlier Spring Increase Western U.S. Forest Wildfire Activity. *Science*, *313*, 940-943.

Williams, A.P., and Coauthors. 2013. Temperature as a potent driver of regional forest drought stress and tree mortality. *Nature Climate Change*, 3, 292-297.

Williams, D. W., R. P. Long, P. M. Wargo, and A. M. Liebhold, 2000. Effects of climate change on forest insect and disease outbreaks. In: Mickler, R. A., R. A. Birdsey, and J. Hom, eds. Responses of northern U.S. forests to environmental change. New York: Springer-Verlag: 455-494.

Williams, M., B.E. Law, P.M. Anthoni, and M.H. Unsworth. 2001. Use of a simulation model and ecosystem flux data to examine carbon-water interactions in ponderosa pine. *Tree Physiology*, 21, 287-298.

Wimberly, M. C., T. A. Spies, C. J. Long, and C. Whitlock. 2000. Simulating Historical Variability in the Amount of Old Forests in the Oregon Coast Range. *Conservation Biology*, 14, 167–180, doi:10.1046/j.1523-1739.2000.98284.x.

Wimberly, M.C., and T.A. Spies. 2001. Influences of environment and disturbance on forest patterns in coastal Oregon watersheds. Ecology, 82, 1443 – 1459.

Woods, A., K. D. Coates, and A. Hamann. 2005. Is an Unprecedented Dothistroma Needle Blight Epidemic Related to Climate Change? *BioScience*, 55 (9), 761-769, doi:10.1641/0006-3568(2005)055[0761:IAUDNB]2.0.CO;2.

Xu, L., A. Samanta, M. H. Costa, S. Ganguly, and R. Nemani. 2011. Widespread decline in greenness of Amazonian vegetation due to the 2010 drought. *Geophysical Research Letters*, 38, L07402, doi: 10.1029/2011GL046824.

Yin, J., J.T. Overpeck, S.M. Griffies, A. Hu, J.L. Russell, and R.J. Stouffer. 2011. Different magnitudes of projected subsurface ocean warming around Greenland and Antarctica. *Nature Geoscience*, 4, 524-528, doi:10.1038/ngeo1189.

Zhang, K., J.S. Kimball, Q.Z. Mu, L.A. Jones, S.J. Goetz, and S.W. Running. 2009. Satellite based analysis of northern ET trends and associated changes in the regional water balance from 1983 to 2005. *Journal of Hydrology, 379*, 92-110.

Zhao, J., D. B. Mainwaring, D. A. Maguire, and A. Kanaskie. 2011. Regional and annual trends in Douglas-fir foliage retention: correlations with climatic variables. *Forest Ecology and Management*, 262, 1872–1886, doi:10.1016/j.foreco.2011.08.008.

Zhao, M., and S.W. Running. 2010. Drought-induced reduction in global terrestrial net primary production from 2000 through 2009. *Science*, 329, 940-943, doi:10.1126/science.1192666.

Zhou, L., and Coauthors. 2014. Widespread decline of Congo rainforest greenness in the past decade. *Nature*, 509, 86-90, doi:10.1038/nature13265.

Zhou, L., Y. Tian, S. Baidya Roy, C. Thorncroft, L. F. Bosart, and Y. Hu. 2012. Impacts of wind farms on land surface temperature. *Nature Climate Change*, 2, 539-543, doi:10.1038/nclimate1505.

Appendices

Appendix A: Supporting information for Chapter 4

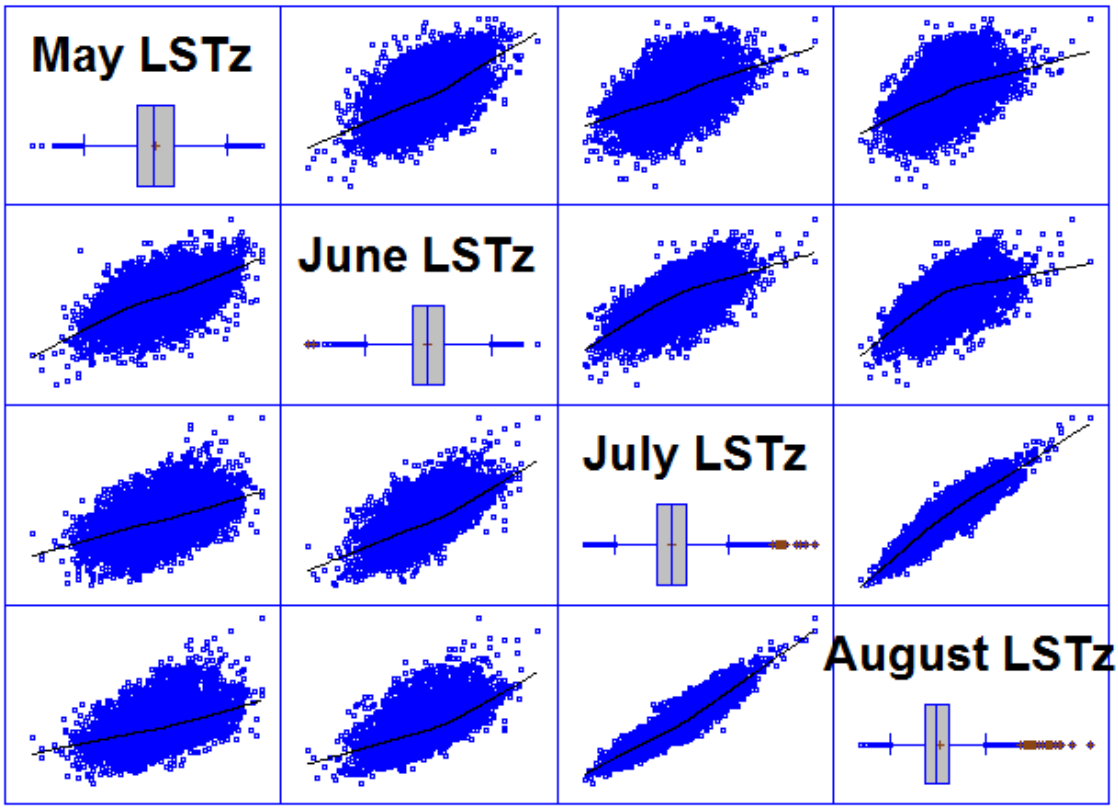

Figure A-4.1. Matrix scatterplots for May – August LSTz data on private lands.

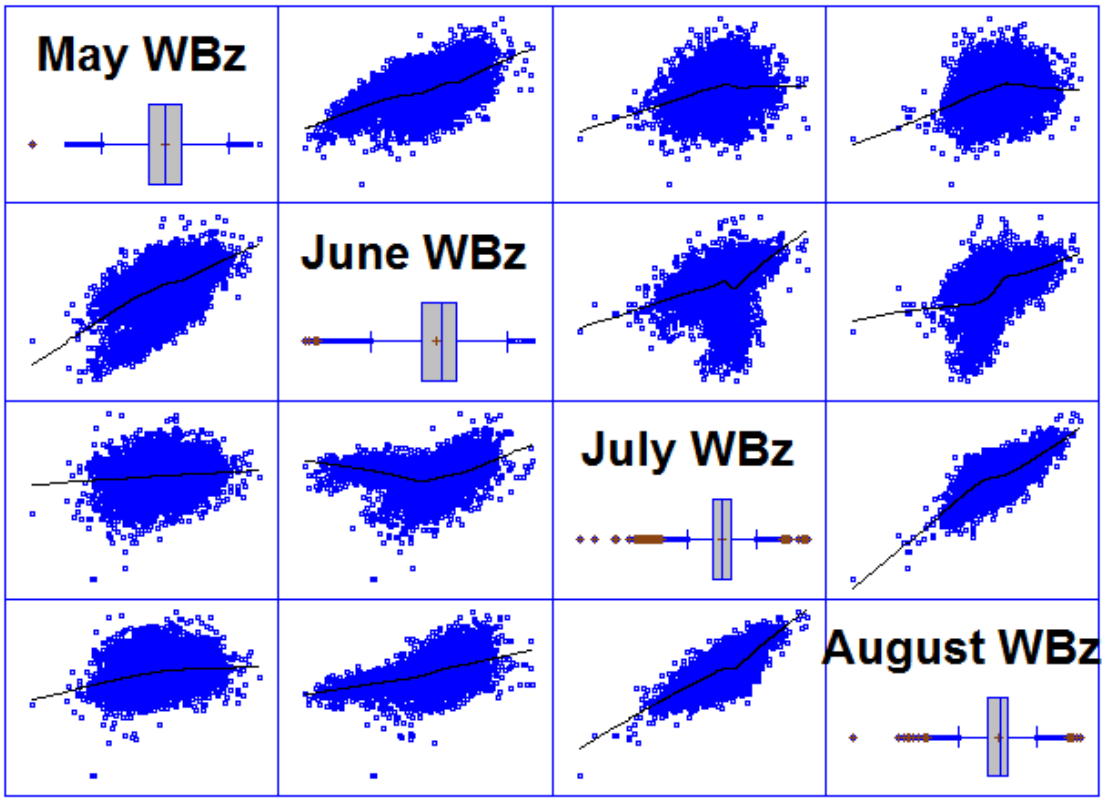

Figure A-4.2. Matrix scatterplots for May – August WBz data on private lands.

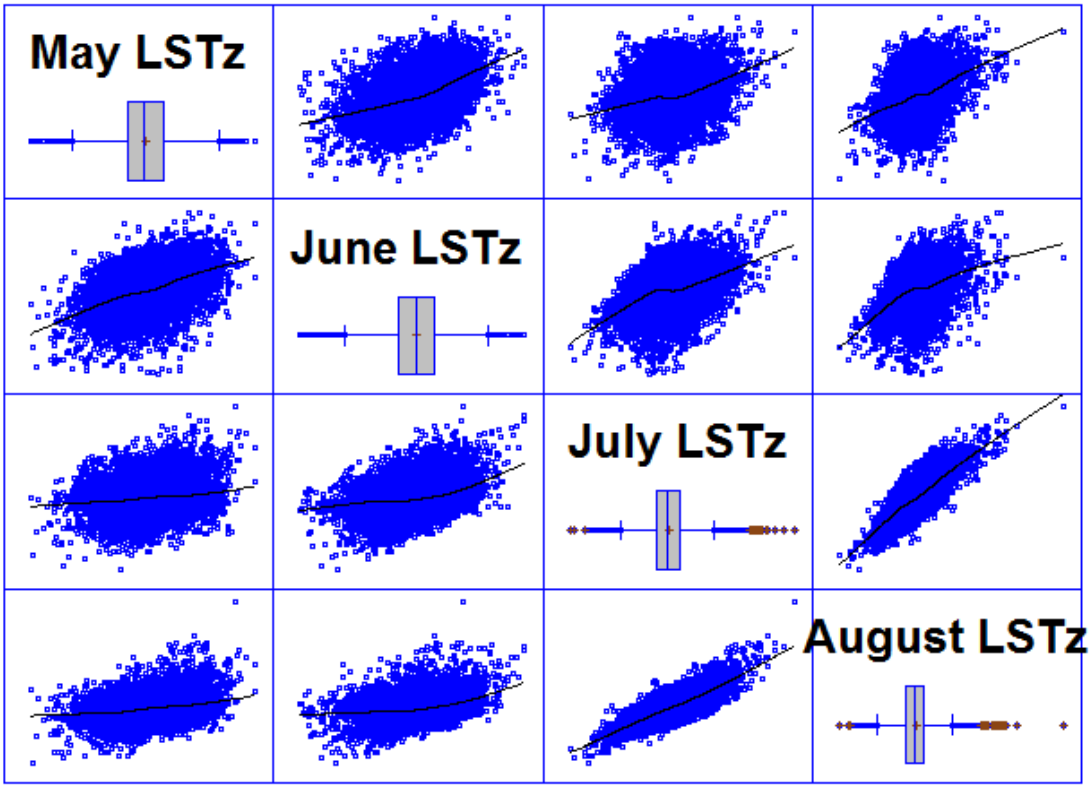

Figure A-4.3. Matrix scatterplots for May – August LSTz data on public lands.

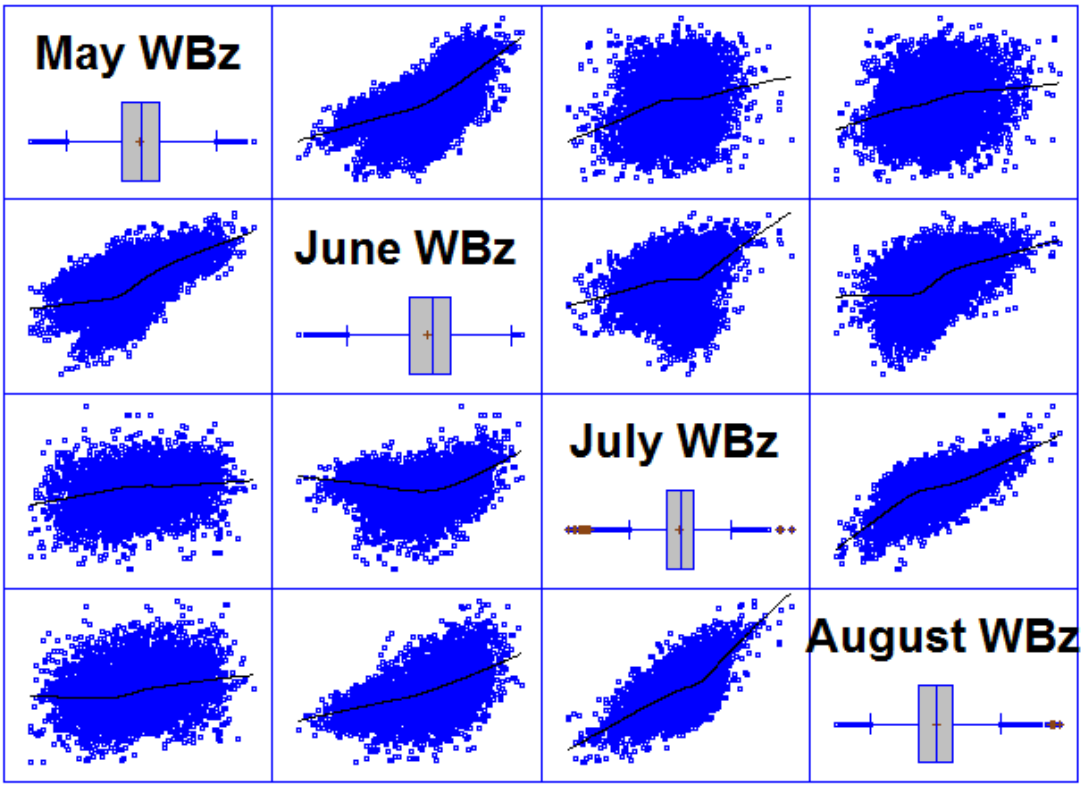

Figure A-4.4. Matrix scatterplots for May – August WBz data on public lands.

Table A-4.1. Correlations for May – August LSTz data on private lands. Also shown in parentheses is the number of pairs of data values used to compute each coefficient. The third number in each location of the table is a P-value which tests the statistical significance of the estimated correlations.

Correlations

	May LSTz	June LSTz	July LSTz	August LSTz
May LSTz		0.5620	0.4512	0.4451
		(10614)	(10614)	(10614)
		0.0000	0.0000	0.0000
June LSTz	0.5620		0.6182	0.5694
	(10614)		(10614)	(10614)
	0.0000		0.0000	0.0000
July LSTz	0.4512	0.6182		0.9043
	(10614)	(10614)		(10614)
	0.0000	0.0000		0.0000
August LSTz	0.4451	0.5694	0.9043	
	(10614)	(10614)	(10614)	
	0.0000	0.0000	0.0000	

Table A-4.2. Correlations for May – August WBz data on private lands.

Correlations

	May WBz	June WBz	July WBz	August WBz
May WBz		0.5123	0.1591	0.2134
		(10614)	(10614)	(10614)
		0.0000	0.0000	0.0000
June WBz	0.5123		0.1388	0.5513
	(10614)		(10614)	(10614)
	0.0000		0.0000	0.0000
July WBz	0.1591	0.1388		0.6365
	(10614)	(10614)		(10614)
	0.0000	0.0000		0.0000
August WBz	0.2134	0.5513	0.6365	
	(10614)	(10614)	(10614)	
	0.0000	0.0000	0.0000	

Table A-4.3. Correlations for May – August LSTz data on public lands.

Correlations

	May LSTz	June LSTz	July LSTz	August LSTz
May LSTz		0.4305	0.2079	0.3083
		(9969)	(9969)	(9969)
		0.0000	0.0000	0.0000
June LSTz	0.4305		0.3011	0.3167
	(9969)		(9969)	(9969)
	0.0000		0.0000	0.0000
July LSTz	0.2079	0.3011		0.7914
	(9969)	(9969)		(9969)
	0.0000	0.0000		0.0000
August LSTz	0.3083	0.3167	0.7914	
	(9969)	(9969)	(9969)	
	0.0000	0.0000	0.0000	

Table A-4.4. Correlations for May – August WBz data on public lands.

Correlations

	May WBz	June WBz	July WBz	August WBz
May WBz		0.6547	0.1792	0.2524
		(9969)	(9969)	(9969)
		0.0000	0.0000	0.0000
June WBz	0.6547		0.1712	0.5083
	(9969)		(9969)	(9969)
	0.0000		0.0000	0.0000
July WBz	0.1792	0.1712		0.6119
	(9969)	(9969)		(9969)
	0.0000	0.0000		0.0000
August WBz	0.2524	0.5083	0.6119	
	(9969)	(9969)	(9969)	
	0.0000	0.0000	0.0000	